universität wien

# DIPLOMARBEIT

Titel der Diplomarbeit

## Surface functionalization of amorphous hydrogenated silicon and polyimide evanescent waveguide based Mach-Zehnder interferometers to realize a biosensing platform


Verfasserin

Eva Melnik


angestrebter akademischer Grad

Magistra der Naturwissenschaften (Mag. rer. nat.)

Wien, 2011

| | |
|---|---|
| Studienkennzahl lt. Studienblatt: | A 419 |
| Studienrichtung lt. Studienblatt: | Chemie |
| Betreuerin / Betreuer: | ao. Univ.-Prof. Mag. Dr. Michael Lämmerhofer |

## Contents

Part IV: Real-time measurements of streptavidin and surface sensing DNA experiments on MZI sensors

## Introduction and definition of the diploma thesis

The need for rapid and selective analysis of ions, organic molecules or biological components in industry, medicine or science is almost infinite. This could also be recognized by the rapid developments in the field of optical biosensors, which promise to fulfill the main requirements for fast, sensitive, low cost and selective multiparameter analysis on robust and small devices.

In the last decades a large number of concepts of optical sensors have been developed such as fiber optical-, resolved fluorescence-, electrochemiluminescence- and displacement flow sensors, as well as planar waveguides based on refractometric sensing, e.g. surface plasmon resonance and integrated optical Mach-Zehnder interferometer. **[1]** Some of the listed optical sensor types have demonstrated their abilities of fast and specific analysis under laboratory conditions, for science issues and in field today. **[2,3,4]** One of the most common is the surface plasmon resonance sensor (SPR), which has been reviewed by J. Homola et al. [**5**]. The used principle relies on the interaction between the evanescent field of surface plasmon polaritons with the immobilized molecular layer. The specific binding of the analyte to the molecular layer causes a shift in the plasmon resonance frequency, which is usually detected over the angle shift.[**6**]

Another refractometric measurement concept is the integrated Mach-Zehnder interferometer (MZI) that exploits evanescent waves.

In this concept laser light is coupled into a single mode waveguide and split equally in a reference- and measurement arm over a Y-junction.

The measurement arm is functionalized with an organic layer that carries the binding sites for the analyte molecules. The interaction of the analyte with the molecular layer leads to an increase of the optical path length, which causes a relative phase shift of the light beam in the measurement branch with respect to the reference arm. When the two light beams of the measurement- and reference arm recombine again at another Y-junction they interfere. The measurement signal is the power of the laser beam after interference. With this method it is possible to measure label-free, with one wavelength and nearly temperature independent the intensity of light proportional to the analyte concentration.

The Austrian Institute of Technology (Health and Environment department, Nano Systems) pursues two different approaches for implementing such MZI sensors, in line with the project PLATON.

The main goal of this diploma thesis is the functionalization of two different material systems of Mach-Zehnder-Interferometer. One of this material systems consist of hydrogenated

amorphous silicon and the other one consists of polyimide. Both material systems are tested for their use as biosensors on the model of the streptavidin/biotin-binding interaction. After the test on the streptavidin/biotin model, biotin tagged DNA strands are immobilized on the surface and the hybridization of the complementary DNA strands gets verified.

**1** S. Ligeler, C. A. Rowe Taitt, *Optical Biosensors*, Elsevier Science B.V., Amsterdam, Netherlands, first edition 2002*

**2** B.H. Schneider, E.L. Dickinson, M.D. Vach, "Highly sensitive optical chip immunoassays in human serum", *Biosensors & Bioelectronics*, 15(2000), p.13–22

**3** S. Busse, M. DePaoli, G. Wenz, "An integreated optical Mach-Zehnder interferometer functionalized by ß-cyclodextrin to monitor binding reactions", *Sensors and Actuators*, 80(2001), p.116-124

**4** L. Lechuga, A. Lenferink, R. Kooyman, "Feasibility of evanescent wave interferometer immunosensors for pesticide detection: chemical aspects", *Sensors and Actuators B*, 1995, 24-25 , p. 762

**5** J. Homola, "Surface Plasmon Resonance Sensors for Detection of Chemical and Biological Species", *Chemical Revies*, 2008, 108(2), p. 462-493*

**6** J. H. Schmid, W. Sinclair, J. García, "Silicon-on-insulator guided mode resonant grating for evanescent field molecular sensing", *Optical Society of America*, 2009, 17(20), p. 18371-18380, p.18732

# Part I: The Mach-Zehnder Interferometer

**Content**

## The Mach-Zehnder Interferometer

The principle of evanescent sensing can be found in various photonic sensors such as ring resonators [**1**], grating based devices [**2**] or Mach-Zehnder interferometers [**3**] (MZIs). These sensor types are based on different photonic key elements, but all consist of a multilayer stack of organic or inorganic films with different refractive indices. In this diploma thesis, functionalization protocols are elaborated for Mach-Zehnder interferometers comprising either polyimide (PI) or amorphous hydrogenated silicon (a-Si:H) waveguide layers in order to allow their use as label-free optical biosensors. The following sections explain the theoretical background of integrated optical waveguiding, the MZI structure, the experimental setup, and the measurement principle. The last section describes the fabrication of the MZI sensors and samples that are used for functionalization tests.

## 1 Theoretical background

The integrated MZIs exploit the concept of optical waveguiding. Optical waveguides – in form of fibers or planar structures – can be found *e.g.* in the field of telecommunication, where they are used to transmit information with light as carrier.

Optical waveguiding relies on the effect of total internal reflection of light. At the interface of a dielectric medium with a high refractive index $n_g$ and a dielectric medium with a lower refractive index $n_c$, a light beam gets totally reflected if the angle of incidence θ in the high index media is:

$$\theta_g < \theta < 90^\circ \tag{1.1}$$

where $\theta_g$ is the critical angle of total internal reflection. For angles of incidence smaller than this critical angle the light gets partly reflected and partly transmitted. In a slab waveguide system, which is the simplest planar waveguide structure, light is guided in a layer with a high refractive index (see Fig. 1), surrounded by cladding layers of lower refractive indices. Depending on the refractive indices and the thickness of the high index layer, there exist certain values of the propagation angle θ, for which the reflections of the guided light interfere constructively and, thus, result in a lossless propagation of light along the waveguide layer. These discrete values of θ can be defined as $\theta_m$, where $m$ is an integer ($m$=0, 1, 2, ... ) and each $\theta_m$ corresponds to a specific light field distribution in the waveguide, which are referred as waveguide modes. The mode with the highest angle has the mode index $m$=0, the modes with the next lower angle corresponds to $m$=1, 2, … and so on. If the angle $\theta_m$ gets smaller than $\theta_g$ for a specific mode number, total internal reflection does not occur anymore

and no more guided modes exist. The number of modes is determined by the waveguide layer height, the refractive indices as well as the wavelength of the light. In Fig. 1 the theoretical light path through the waveguide is shown.

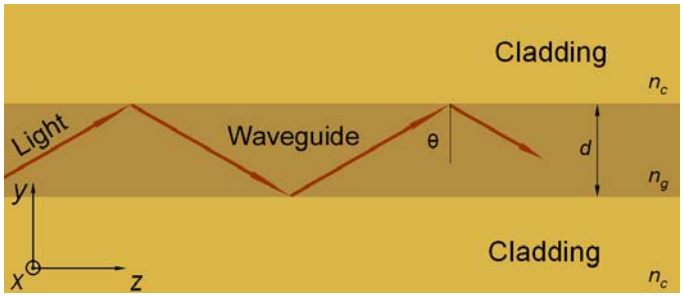


**Figure 1: Theoretical path way through the waveguide with total internal reflection**

In fact, the light is not reflected exactly at the interface, but the light slightly penetrates into the cladding. The light in the cladding layer is the so called evanescent field. The depth of penetration is defined by $1/\gamma_c$, where $\gamma_c$ is the decay constant in the cladding layer. Depending on the depth of penetration, the path length of the light in the propagation direction is influenced (see Fig. 2). This is called the Gooth-Hänchen-shift $Z_c$. The depth of penetration (and so the Gooth-Hänchen-shift) depends on the wavelength, the waveguide thickness and on all involved refractive indices of the layers.

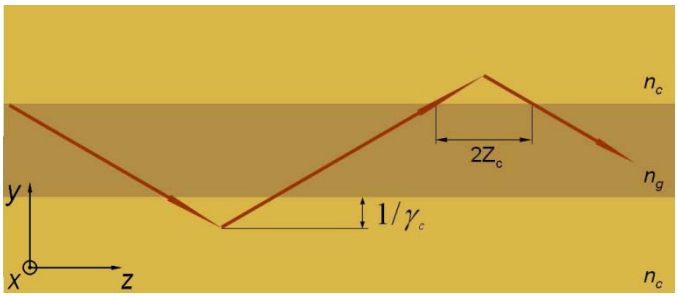


**Figure 2: More accurate ray model with the parameters of depth of penetration ($1/\gamma_c$), difference in light path $2Z_c$ and the evanescent field.**

Figure 2 also illustrates the transport of the optical power in propagation direction. The distribution of the optical power, i.e., the intensity profile within the layer stack is shown in Fig. 3 under the assumption that the refractive indices of the claddings $n_c$ are equal.

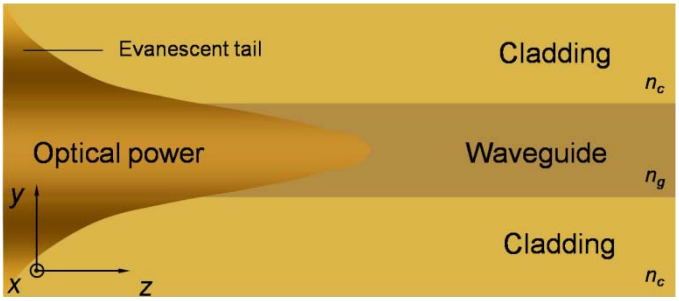


**Figure 3: Illustration of the intensity profile of the propagating light**

One of the most important factors is the effective index $n_{eff}$. The effective index is defined as the average refractive index that is "seen" by the intensity profile of the guided mode. This means that the effective index, but also the intensity profile and the shape of the evanescent field depends on the surrounded refractive indices. In Fig. 3 a symmetric evanescent field is shown. This symmetric behavior changes if the refractive indices of the claddings are not identical [**4**].

## 2 Structure of the Mach-Zehnder interferometer sensors

The Mach-Zehnder interferometer (MZI) is a three dimensional planar optical waveguide structure made of different planar inorganic or organic films, which have different refractive indices that provide a vertical guidance of the light, as explained in the last section, for the slab waveguide. A lateral light guidance is created by patterning of the high index layer. In the so called rib waveguide structure, the high index layer outside the waveguide is thinned. Therefore, the light "sees" a lower effective index outside of the waveguide and is laterally guided by total internal reflection. The cross section of this waveguide structure is shown in Fig. 4 and 5 for the a-Si:H and PI waveguides. The width and height of the waveguide ribs are designed in order to ensure single mode behavior. The rib width is about of 1.8-2.2 µm for the a-Si:H-MZI sensors and 1.8-2.7 µm for the PI – MZI sensors. In the experimental chapters of this diploma thesis we are going to use the definition such as MZI 2000, which corresponds to a MZI based on 2 µm wide rib waveguide.

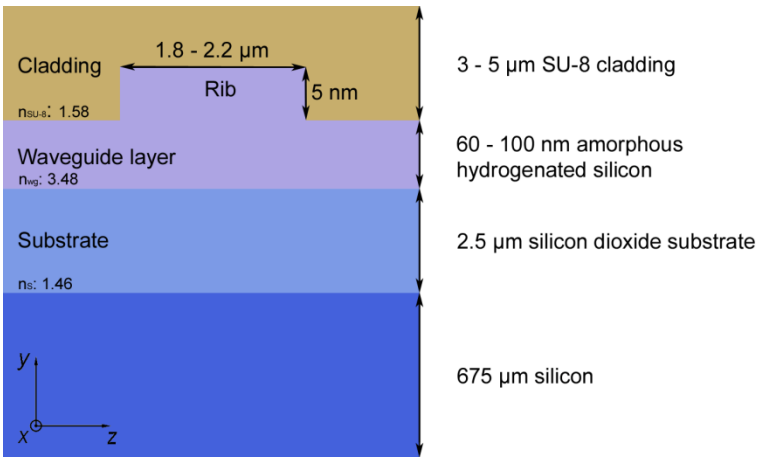


**Figure 4: Cross section of the a-Si:H based MZI and its layer system.**

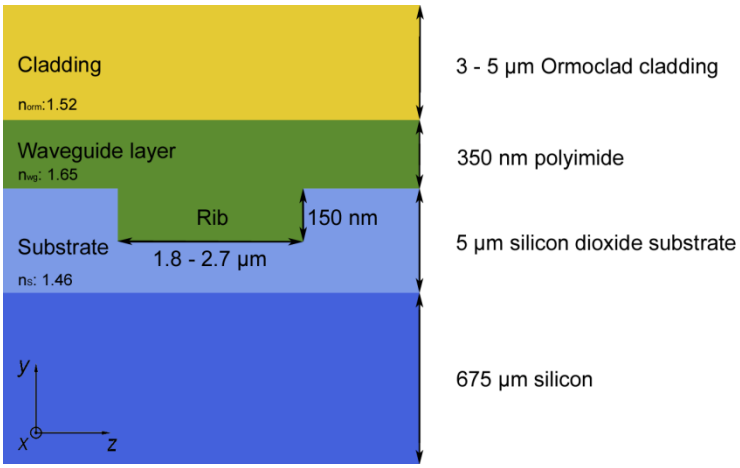


**Figure 5: Cross section of the PI based MZI and its layer system.**

Figure 6 shows a schematic of a MZI sensor and waveguide layout. The top layer (SU-8 or Ormoclad[1]) covers the surface except for the measurement window (10 mm length x 300 µm width). The light is coupled into the MZI at the light input, gets split into two light paths by the Y-junction and is subsequently guided through the sensing and reference arms. At the end, the light in the two arms recombined again by another Y-junction. In combination with a flow cell on the top of the MZI sensor chip, liquids such as buffer or analyte standards can be rinsed over the sensor surface and real time measurements of the effective index change can be monitored via the light output.

[1] Ormoclad is the trade name of this positive photoresist. Ormoclad is produced by the company Micro resists technology, Berlin, Germany.

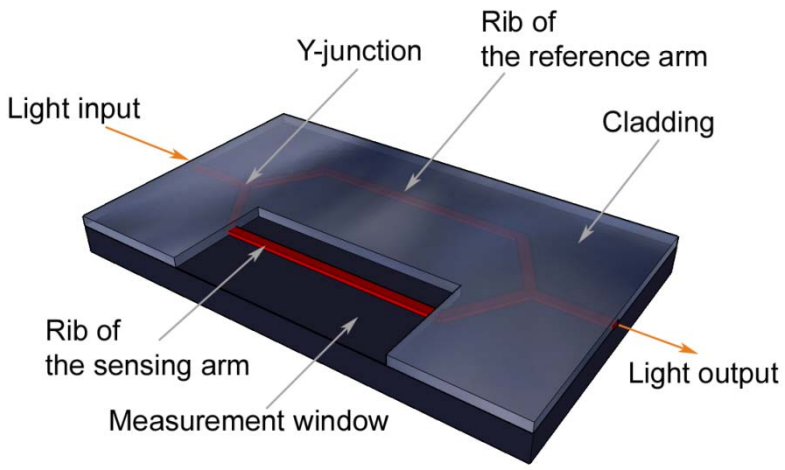


**Figure 6: Schematic of an MZI sensor. The surface is covered with a cladding (SU-8 or Ormoclad) except for the measurement window. The light is coupled into the MZI structure, is split by the Y-junction into the sensing and reference arm, and recombined again at the end of the MZI.**

## 3 Measurement setup

The PI and a-Si:H MZI sensor chips have the same MZI - array structure on the surface, with 56 MZIs and five reference waveguides in between, which are simple straight waveguides for testing purposes that are covered completely with cladding (Ormoclad or SU-8).

The MZI sensor chips (3 cm long, 1.7 cm width and 0.7 mm thick) get fixed on a copper plate via melt mount resin (a polymer with a low melting temperature, developed for sample preparation in microscopy) at 60°C. After cooling, the copper plate with the MZI – sensors on top gets mounted on a sample holder (See Fig. 7). On this sample holder the MZI can be adjusted and a fluidic system can be fixed on the top of the sensor array. The sample holder again is mounted on an optical table. The optical fibers and the microscope for visual alignment of the fibers are fixed on the optical table as well. The optical fibers for in- and out-coupling are first manually aligned to the waveguides by means of a three-axis stage with micrometer screws. Then, the position of the fibers is optimized with respect to maximum transmission employing piezo-driven two-axis auto-alignment stages, which are controlled using a Labview program, version 7.1, from National instruments, Texas, USA. The piezo-driven auto-alignment stages have a mechanical operating range that is limited to a distance of 20 µm.

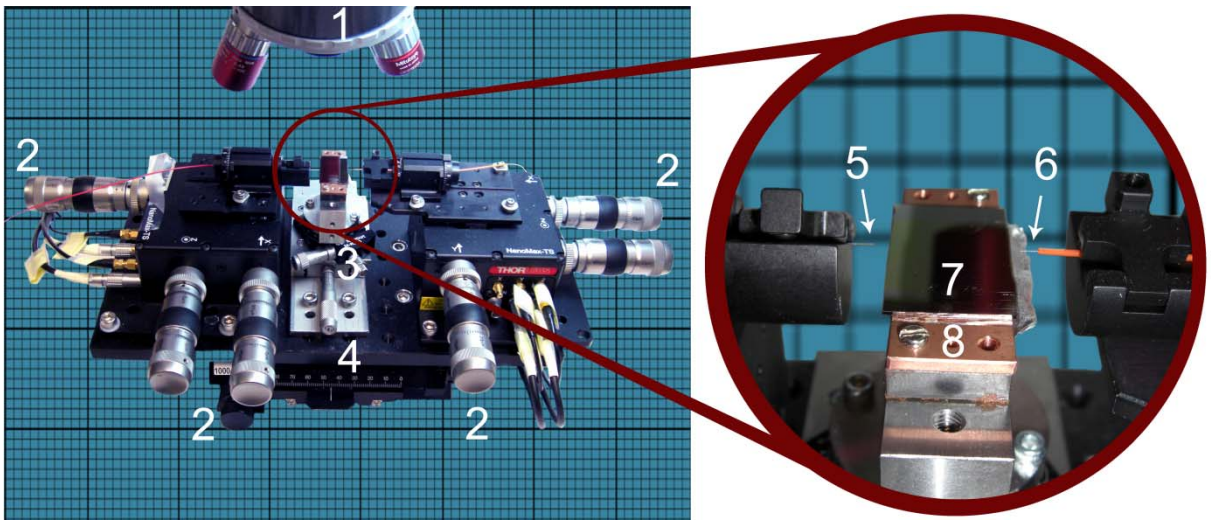


**Figure 7: Measurement setup: 1 microscope, 2 micrometer screws, 3 sample holder, 4 optical table, 5 input fiber, 6 output fiber, 7 MZI senor chip, 8 copper plate**

When the laser source is activated and the manual alignment of the fibers is completed, the autoalignment procedure is activated employing the Labview program. As laser source, an Agilent Light Wave Measurement System 8164A with an 81600B tunable laser module with a center wavelength of 1310 nm is used. The laser provides linear polarized light with a wavelength that can be varied between 1260 to 1360 nm. The light input coupling is done over a polarization maintaining single mode fiber. This fiber can be rotated with respect to the sensor surface which allows the adjustment of the polarization of the incident light. In the experiments, the fiber is rotated in a way that only the TE (transversal electric) waveguide mode is excited in the input waveguide of the MZI. For TE modes, the electric field of the propagating light is parallel to the sensor surface. The transmitted light output is collected by means of a tapered lens single mode fiber (Fig. 8).

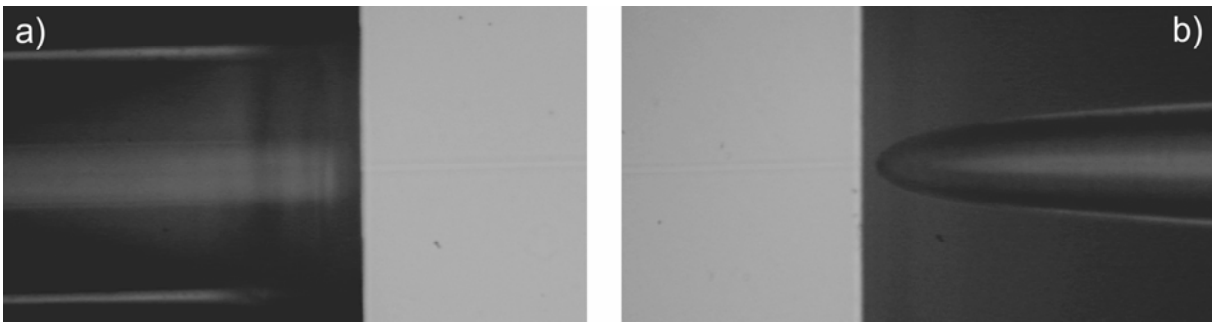


**Figure 8: Optical fibers aligned to the MZI input and output waveguides: a) polarization maintaining single mode fiber for input coupling; b) tapered lens single mode fiber for output coupling.**

For a constant measurement with liquids, a fluidic system is mounted on the sample holder (Fig. 9). The liquid is introduced to the surface via a syringe pump. The volume of the syringe

is 10 ml. The pump speed can be adjusted, but in our experiments we used only speeds of 20 µl/min.

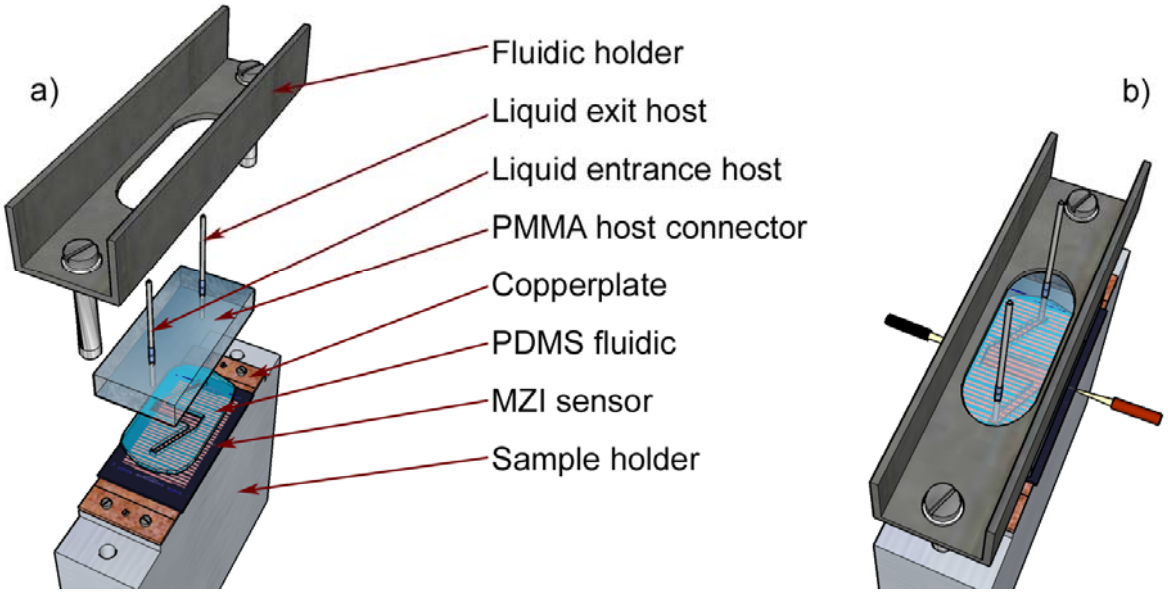


**Figure 9: Schematics of the fluidic system for the measurements with liquids: a) exploded graph of the fluidic system and the order of mounting; b) ready mounted fluidic system and aligned fibers**

## 4 Measurement principle

The Mach-Zehnder interferometer is, as the name suggests, based on an interferometric sensing principle. The laser light enters the input waveguide and gets equally split via the Y-junction. The top cladding layer (SU-8 or Ormoclad) protects the reference arm while the measurement window at the sensing arm allows access to the waveguide (see Fig. 6).

When the effective index in the sensing arm changes (*e.g.* due to the enrichment of analyte molecules on the surface), it leads to a change in the propagation constant and causes a phase shift of the guided mode at the end of the sensing arm with respect to the guided mode in the reference arm. At the end of the MZI, the propagating modes of the two arms are recombined in the second Y-junction. Interference depending on the phase shift leads to a modulation of the transmitted power. This characteristic is described in the Eqn. (4.1), where the ratio $P_{out}/P_{in}$ is the normalized output power, $L$ the length of the measurement window, $k_0$ the wave number in vacuum and $\Delta n_{eff}$ the difference of the effective indices in the reference and the sensing arm.

$$\frac{P_{out}}{P_{in}} = \frac{1}{2}\left[1 + \cos\left(Lk_0\Delta n_{eff}\right)\right] \tag{4.1}$$

In the case of a real measurement the transmitted optical power at the output is measured in dBm. The input powers are 8 and 5 dB for a-Si:H- and PI-MZIs. For a-Si:H-MZI sensors the typical output power is above -30 dBm and for PI-MZI sensors it is above -22 dBm. The insertion loss from the laser source to the photo detector for a-Si:H- and PI-MZIs are better than -22 dB and -18 dB. Another important characteristic of the MZI sensor is the extinction ratio. It is the ratio between the highest and the lowest transmission signal. The extinction ratio is typically about 15 dB for both a-Si:H- and PI-MZI sensors.

## 4.1 Homogenous and surface sensing measurements

In practice, there are two different ways to change the refractive index above the sensing arm of the MZI: a) homogenously – and b) in close vicinity to the surface (see Fig. 10). In the homogenous measurement the effective index in the area of the measurement window is affected by the refractive index of the sample fluid that is rinsed over the sensor, whereas in the surface sensing scenario the interaction of the analyte molecules with the thin sensing layer affects the effective index.

In the case of surface sensing the measurement window is functionalized with specific chemical groups that form the sensing layer. The sensing layer is able to bind the analyte molecules covalently, affinity based or adsorptively to the surface. These chemical interactions lead to an immobilization and enrichment of the analyte on the sensing layer occurs. As consequence, the refractive index of the sensing layer and therefore the effective index of the guided mode changes. The optical power on the output will change in dependence of the concentration of the analyte that attaches to the surface. One important aspect is the light intensity distribution (Fig. 10). The light intensity has its maximum in the waveguide layer and drops exponentially in the surrounding low index cladding layers. In dependence of the refractive index of the neighboring media the light intensity distribution differs. Near the surface of the waveguide layer the light intensity and therefore the interaction with the sensing layer is maximal. Because of this fact, the sensing layer height ($h_{sl}$) affects the theoretically achievable sensitivity. In Fig. 11, the transmitted power of a MZI sensor during a homogenous measurement is shown. In this measurement water was first rinsed via a fluidic system over the sensor surface. Then the water was exchanged against phosphate buffer saline (PBS) 150 mM. The occurring refractive index difference of $\Delta n$=0.005 causes a phase shift of approximately 6π, which translates into a modulation of the transmitted power as becomes apparent in Fig. 11. The signal stabilizes after rinsing with PBS for 1 min. From the transmitted power the phase shift can be calculated by reversing the

sinusodial characteristic of the MZI. The calculated phase shift as function of time is the parameter for the data analysis.

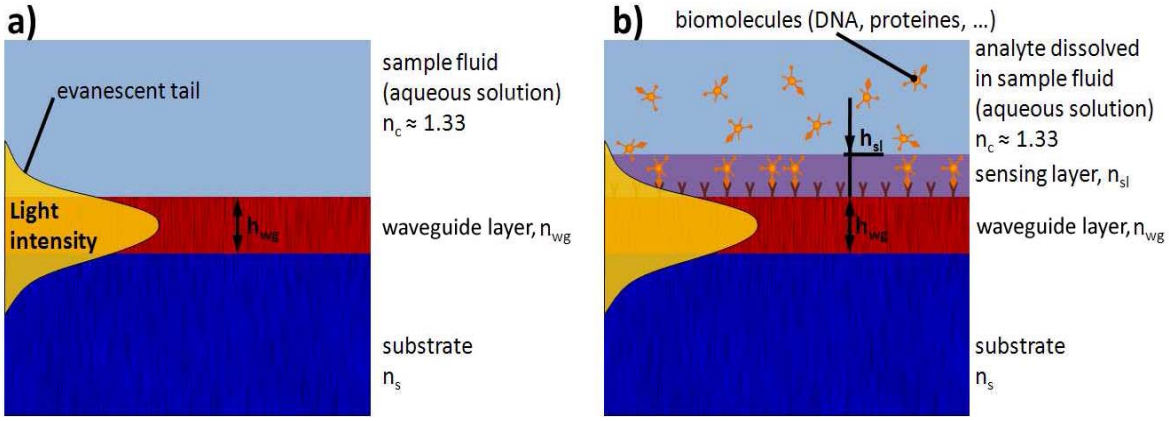


**Figure 10: Side view of the waveguide structure in the measurement window for a) homogeneous and b) surface sensing measurements. In the case of homogeneous sensing, a refractive index change occurs homogeneously in the whole sample fluid covering the measurement window, whereas in the case of surface sensing the refractive index changes only in close vicinity to the waveguide surface because of the interaction of analyte molecules with the sensing layer. The arrowhead and the $h_{sl}$ show the sensing layer height and $h_{wg}$ the height of the waveguide layer.**

In the surface sensing mode the interference signal can be a combination of homogenous and surface sensing signals. This can happen for example, when water is exchanged against the PBS buffer and the PBS buffer additionally contains the analyte that reacts with the surface molecules (see Fig. 11). Then, the induced phase shift results from the refractive index change ($\Delta n$=0.005) from water to PBS buffer and the refractive index change due to the binding of the analyte to the sensing layer.

To prevent such combined signals, which make the data analysis more difficult, it is beneficial that the refractive indices of all fluids involved in the surface sensing measurement are the same. Then only the enrichment of the analyte on the sensing layer influences the transmitted optical power.

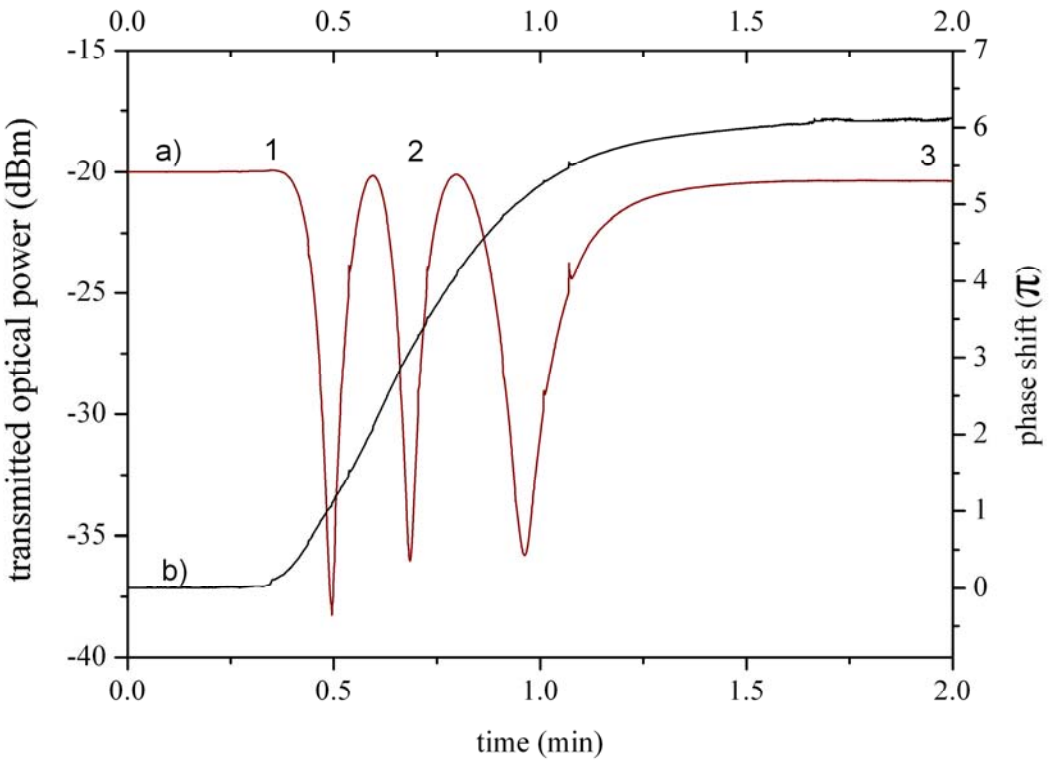


**Figure 11: a) Transmitted optical power during a homogenous measurement on a PI-MZI sensor while exchanging water against phosphate buffer saline (PBS) on the sensor surface: 1. water signal ($n_w$=1.3330); 2. PBS buffer ($n_{PBS}$=1.3381) is rinsed instead of water over the surface of the MZI. The transmitted optical power shows an interference that is caused by the refractive index change ($\Delta n$=[$n_{PBS}$ – $n_w$]= 0.0051); 3. stable response while rinsing with PBS buffer; b) calculated phase shift as function of time.**

## 4.2 Wavelength scan

The wavelength dependent transmission characteristic provides additional information about the sensor. The sample is covered with one media. Then, the transmitted optical power of the MZI is recorded while the laser light source sweeps the wavelength from a shorter to a longer value. Due to the fact that the effective indices of the guided modes in the reference and in the sensing arm depend differently on the wavelength, a relative phase shift between both arms is induced and leads to a characteristic modulation of the optical output signal. Figure 12 shows an example of such a wavelength dependent transmission characteristic. The graph shows that a change of the wavelength characteristic of the sensor is similar to that of the time dependent measurement. However, the wavelength scan does not necessitate a refractive index change in the vicinity of the sensing arm and can be performed at any stage of the sample preparation. For this reason it is beneficial to check the sensor before a homogenous or surface sensing

experiment using a wavelength scan, *e.g.* after the functionalization procedure, in order to ensure sufficient senor performance. A special characteristic of the wavelength scan profile is the number of periods. It depends on the waveguide and sensor geometry as well as on the properties of the sensitive layer. In the case of immobilization of an analyte, *e.g.* a protein, the sensing layer height and/or refractive index changes and the number of periods changes. This fact allows using the measurement strategy of continuous wavelength scans as an alternative to the recording of the transmitted power. Measurements applying continuous wavelength scans for the purpose of demonstrating a surface sensing device are more elaborate and are not used in this diploma thesis [**5**,**6**]. However, wavelength scans are used to monitor the sensor function and the changes on the surface after different functionalization steps.

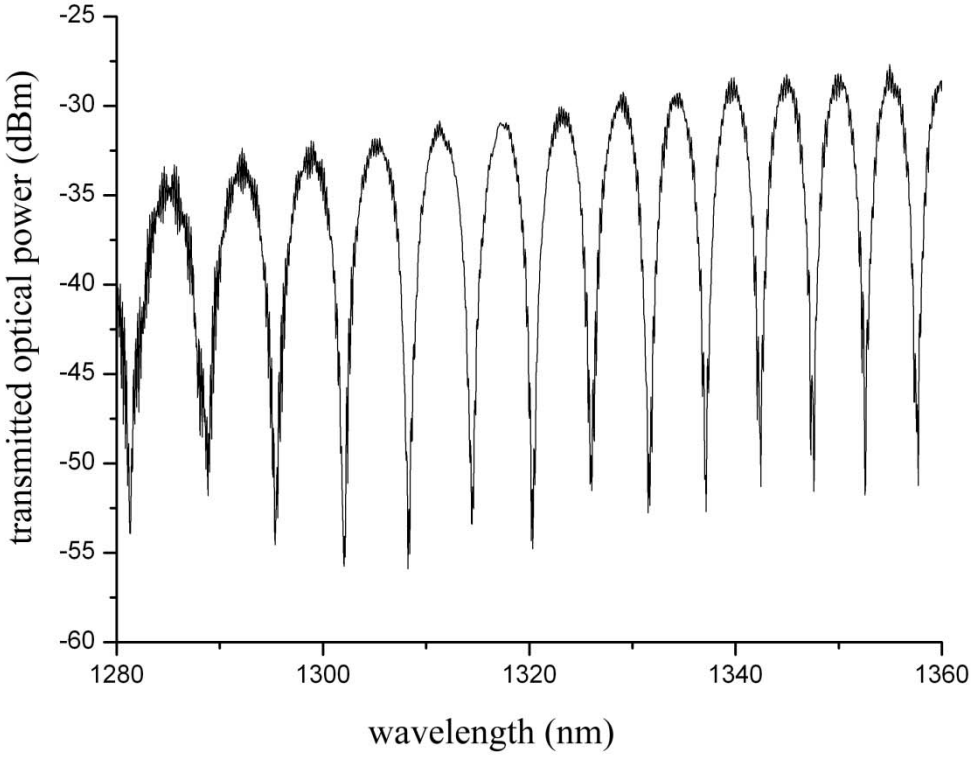


**Figure 12: Wavelength scan for a-Si:H-MZI sensor 1800 in air. The transmitted optical power is between -30 and -55 dBm, with an extinction ratio of about 25 dB. In this specific wavelength scan, wavelengths below 1300 nm show a noisy profile and are excluded for further measurements. A wavelength between 1300 and 1350 nm can be chosen for a homogenous or surface sensing measurements.**

# 5 Sensitivity

For surface sensing applications it is necessary to know the theoretically achievable surface sensitivity for a Mach-Zehnder interferometer. This theoretically achievable surface sensitivity $S_p$ can be calculated employing the definition derived by Parriaux et al. [**7**]. This definition leads to a theoretical sensitivity, which depends on the design of the waveguide geometry, the wavelength, and the refractive indices of the materials. The surface sensitivity $S_p$ can be used to compare different waveguide designs such as a-Si:H- and PI-MZI sensors. For a real surface sensing measurement, the theoretical surface sensitivity is not completely sufficient to evaluate the sensor, because also chemical parameters have to be considered. Therefore, the definition of the empirically obtained chemical surface sensitivity has to be established.

## 5.1 Theoretical surface sensitivity

The effective index is influenced by the waveguide parameters such as refractive indices of the layers, the wavelength, and the layer thicknesses. The following diagrams are the results of calculations highlighting the importance of these parameters.
Table 1 summarizes values used for these calculations.

**Table 1: parameters for the calculation**

| | |
|---|---|
| **thickness of the sensing layer, $h_{sl}$** | 10 nm |
| **refractive index of the sensing layer, $n_{sl}$** | 1.50 |
| **refractive index sample fluid, $n_l$** | 1.33 |
| **refractive index of the substrate $SiO_2$, $n_s$** | 1.46 |

Figure 13 and 14 show the maximum theoretically achievable surface sensitivity of a three layer slab system as a function of the refractive index of the waveguide layer and the corresponding optimized waveguide layer thicknesses, calculated with a *Mathematica* script [**8**]. The theoretical sensitivity increases with the refractive index of the waveguide layer ($n_{wg}$). The optimum thickness of the waveguide layer depends on the wavelength and the refractive index of the waveguide structure. For instance, for the a-Si:H-MZI sensors with $n_{wg}$ = 3.48, the optimum thickness of the waveguide layer is 50 nm and for PI-MZI sensors with $n_{wg}$ = 1.65 the optimum thickness of the waveguide layer is 350 nm, assuming a wavelength of 1310 nm (see Fig. 14).

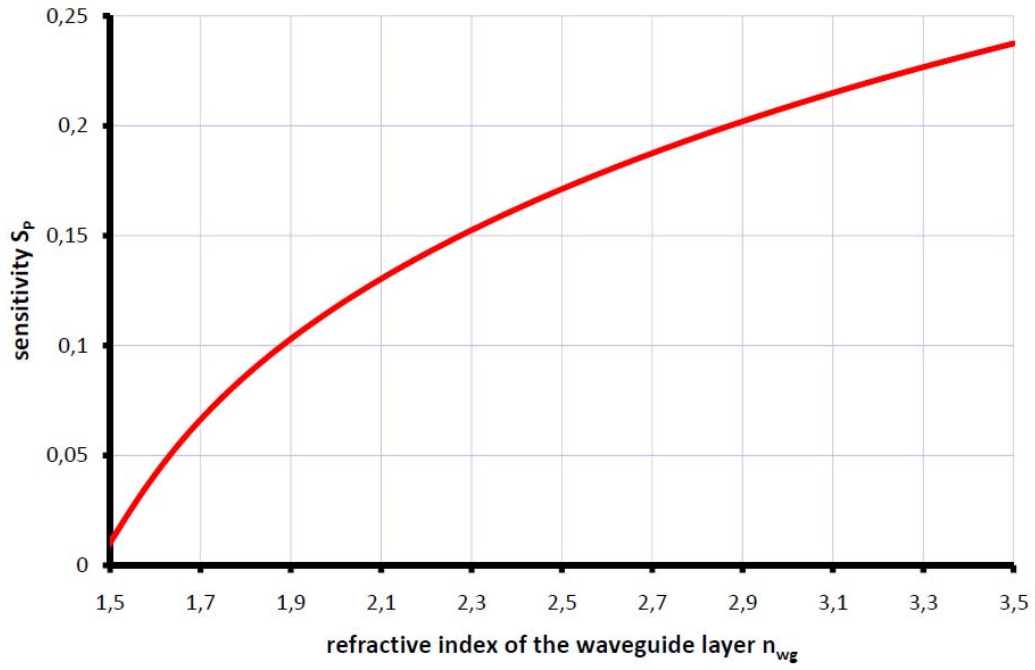


**Figure 13: Dependence of the theoretical sensitivity on the refractive index of the waveguide layer**

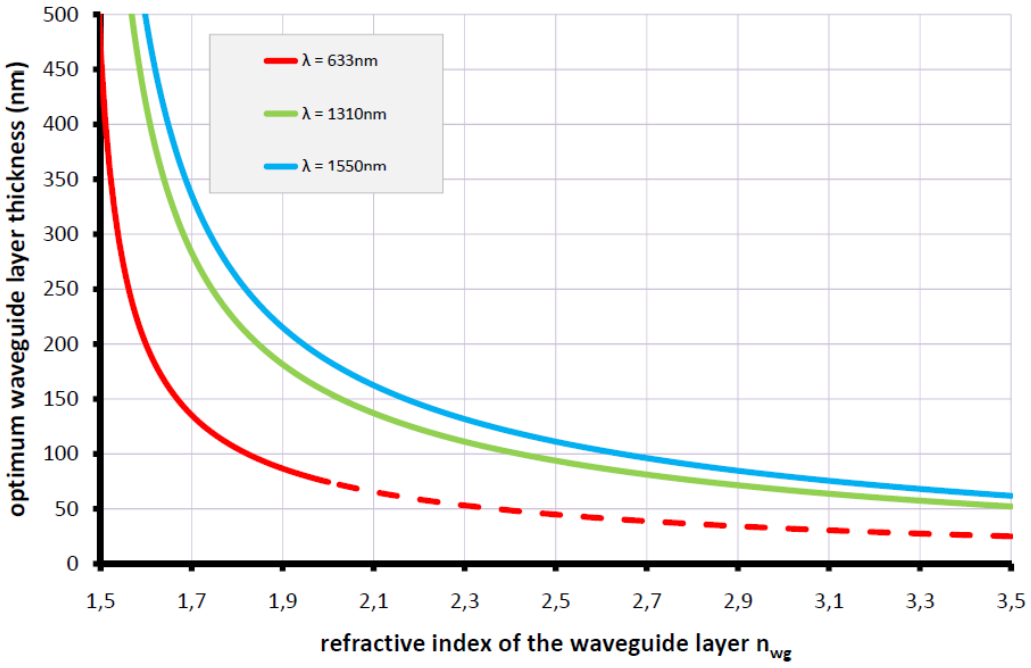


**Figure 14: Optimum waveguide layer thickness as function of the refractive index of the waveguide layer $n_{wg}$**

The figure of merit for the design of sensor devices is the maximum phase shift that can be induced per window length and refractive index unit (RIU) change of the sensing layer for a given waveguide geometry. Figure 15 plots this maximum phase shift in dependence of the refractive index of the waveguide layer and the input wavelength.

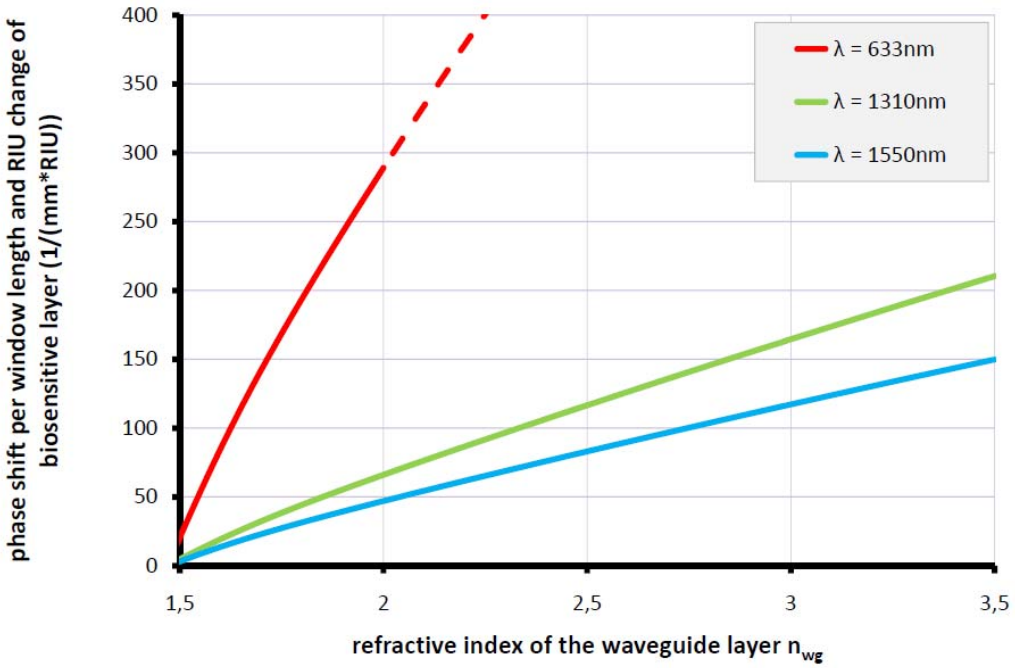


**Figure 15: Dependence of the maximum achievable phase shift per window length and refractive index unit (RIU) on the refractive index of the waveguiding layer calculated for TE-polarization.**

Hence, the refractive index change (RIC) necessary to gain a phase shift of π, for a-Si:H- and PI-MZI sensors with a measurement window length of 10 mm can be calculated using the following equation:

$$\mathrm{RIC} = \pi / (\mathrm{PWR} * L), \tag{5.1}$$

where $L$ is the measurement window length, PWR is the phase shift per window length and RIC, which is the refractive index change of the biosensing layer. For instance when the MZI is part of an a-Si:H-MZI sensor array, the refractive index of the waveguide layer $n_{wg}$ is 3.48. Assuming an input wavelength of 1310 nm the PWR is 210. Calculation with (5.1) results in a phase shift of π when the refractive index change in the sensing layer is 0.0014. In other words, when the analyte causes a refractive index change of 0.0014 in the sensing layer, the analyte generates a phase shift of π, which can be measured over the modulated output signal.

## 5.2 Chemical surface sensitivity

The described theoretical surface sensitivity $S_p$ predicts that a-Si:H-MZI sensors show an 8-times better sensitivity than the PI-MZI sensor. This is true under the assumption that the chemical aspects are identical on PI as on a-Si:H surfaces. One aspect is *e.g* the population density of the receptor molecules on the surface. This population density depends on various

characteristics of the substrate such as the reaction properties and is different for PI and a-Si:H waveguide layers.

The chemical sensor sensitivity $S_c$ includes this aspect and is empirically derived from the slope of a calibration curve under standard conditions. The slope of a calibration curve (and the chemical sensitivity) is influenced by several physical parameters such as the temperature and the pressure (*e.g.* in the flow chamber), but also by chemical parameters such as the kinetic behavior of the chemical interaction and the population density of the receptor molecules on the surface. Here, another important definition, the dynamic range, has to be mentioned. The concentration of the analyte on the surface is limited by the receptor molecules available on the surface and/or by the steric hindrances caused by the volume of the analyte. This limitation causes a flattening of the calibration curve above a certain saturation concentration of the analyte. The linear part of the calibration curve is called the linear range and the dynamic range is the concentration range where a change in the concentration lead to an increase (linear or non linear) of the signal. The chemical sensitivity is analyzed in the linear range.

The achieved chemical surface sensitivities of a-Si:H- and PI-MZI sensors are discussed in part IV, where streptavidin is measured in different concentrations.

# 6 Sample preparation

Besides the MZI sensor measurements various other methods are used in order to optimize the functionalization for streptavidin and DNA hybridization. The necessary samples for the other methods (referred to as control samples) do not comprise waveguide structures but consist of silica covered silicon wavers that are coated with the same material as the waveguide layer.

In some cases also cladding control samples are used, which are partly covered with SU-8 or Ormoclad. The MZIs and the control samples are manufactured in the cleanroom of the Technical University of Vienna. The next chapter describes the sample preparation.

## 6.1 Fabrication of hydrogenated amorphous silicon waveguide based MZI sensors

Table 2 lists the preparation steps for a-Si:H-MZI sensors. In the following experiments we also use so called a-Si:H control samples. These a-Si:H control samples vary in size (1x1 cm or 2x2 cm) and consist of silica covered (5µm) silicon wafers on which the waveguide layer material is deposited. The preparation is similar to the a-Si:H-MZI fabrication but here only

the protocol steps 1-3 of Table 2 are performed. For the cladding control samples also step 8 is included.

**Table 2: Preparation steps of a-Si:H-MZI sensors**

| Nr. | Steps | Description | Time [min] | Time [sec] |
|---|---|---|---|---|
| **1** | Cleaving | Cleaving of the silica (2.5 µm) covered silicon waver | | |
| **2** | Cleaning | Washing in acetone/ultrasonic bath | 4 | |
| | | Washing in acetone | 2 | |
| | | Washing in isopropyl alcohol | 1 | |
| **3** | Plasma enhanced chemical vapor deposition of hydrogenated amorphous silicon (PECVD of a-Si:H) | For a resulting a-Si:H layer of approximately 100 nm: 100 sccm, $SiH_4$, Pressure: 0.5 Torr, Power: 10 W, Temperature: 250 °C | 12 | |
| **4** | Lithography | Spin-coating of HMDS at 7500 rpm | | 10 |
| | | Spin-coating of MIR701 photoresist at 7500rpm | | 35 |
| | | Soft bake: 110°C | | 60 |
| | | Exposure to UV-light through photomask with waveguide layout | | 5.5 |
| **5** | a-Si:H etching - RIE | 10 sccm Ar, Pressure: 1 mTorr, Power: 100 W | 10 | |
| **6** | Resist removal | Washing in acetone/ultrasonic bath | 4 | |
| | | Washing in EBR solvent (special solvent to remove the MIR701 photoresist) | 4 | |
| | | Washing in acetone | 2 | |
| | | Washing in isopropyl alcohol | 1 | |
| **7** | Smoothing of a-Si:H surface - RIE | 10 sccm Argon, 1 mTorr, Power: 100 W | 15 | |
| **8** | SU-8 cladding | Spin-coating of Ti-Prime at 3000 rpm | | 15 |
| | | Spin-coating of SU-8 2005 at 3000 rpm | | 30 |
| | | Softbake, 95°C | 1 | |
| | | Exposure to UV-Light | | 12 |
| | | Post exposure bake, 95°C | 2 | |
| | | Developing in SU-8 developer | | 40 |
| | | Rinsing in isopropyl alcohol | | 30 |
| | | Hard bake, 150°C | 10 | |

Most important for this diploma thesis are the surface properties, which depend on the fabrication process. Step 3, the plasma enhanced chemical vapor deposition (PECVD) [**9**], defines the functional groups on the surface. In this step monosilane ($SiH_4$) gas is used to deposit silicon on the surface. It creates an amorphous Si-H surface, which is more resistant against the reaction with oxygen than crystalline silicon. Because of this fact it can be assumed that on a fresh prepared hydrogenated amorphous silicon surface, the Si-H bound is the dominant chemical group. After a time of about one day a noticeable oxide layer begins to grow exponentially until saturation takes place [**10**].

## 6.2 Fabrication of polyimide waveguide based MZI sensors

Table 3 lists the preparation steps for PI-MZI sensors. In the following experiments we also use so-called PI control samples. These PI control samples vary in size (1x1 cm or 2x2 cm) and consist of a silica covered (5µm) silicon wafer on which the waveguide layer material is spin-coated. The preparation is similar to the PI-MZI procedure but only the protocol steps 1, 2 and 6 of Table 3 are performed. For the cladding control samples also step 7 is included.

**Table 3: Preparation steps of polyimide waveguides**

| Nr. | Step | Description | Time [min] | Time [sec] |
|---|---|---|---|---|
| **1** | Cleaving | Cleaving of the silica (5 µm) covered silicon waver | | |
| **2** | Cleaning | Washing in acetone/ ultrasonic bath | 4 | |
| | | Washing in acetone | 2 | |
| | | Washing in isopropyl alcohol (ISO) | 1 | |
| **3** | Lithography | Spin coating of HMDS at 7500 rpm | | 35 |
| | | Spin coating of MIR701 photoresist at 7500 rpm | | |
| | | soft bake: 110°C | 60 | |
| | | exposure to UV-light | | 5,5 |
| **4** | Etching - RIE | 10 sccm Argon, 20 sccm $SF_6$, Pressure: 50 mTorr, Power: 50 W, | 10 | |
| **5** | Resist removal | Washing in acetone | 4 | |
| | | Washing in acetone | 2 | |
| | | Washing in isopropyl alcohol | 1 | |
| **6** | Polyimide spin-coating | Spin-coating of PI at 5500 rpm | | 30 |
| | | Soft bake: 110°C | 1 | |
| | | Exposure to UV-light | | 30 |
| | | Hard bake, 200°C | 60 | |
| **7** | Ormoclad cladding | Oxygen plasma: 0.7 Torr, temperature: 20°C, power: 300W | | 30 |
| | | Ormoclad spinning at 3000 rpm | | 30 |
| | | Soft bake, 100-120°C | 2 | |
| | | Exposure to UV-light | | 90 |
| | | Post exposure bake, 120°C | 5 | |
| | | Developing in OrmoDev solution | | 40 |
| | | Rinsing in isopropyl alcohol | | 20 |
| | | Hard bake, 150°C | 180 | |

**1** De Vos K, Bartolozzi I, Schacht E, Bienstman P, Baets R, (2007) Silicon-on-Insulator microring resonator for sensitive and label-free biosensing. Opt. Express 15(12):7610-7615.

**2** Waldhäusl R, Schnabel B, Dannberg P, Kley E, Bräuer A., Karthe W, (1997) Efficient coupling into polymer waveguides by gratings. Appl. Opt. 36(36):9383-9390

**3** Heideman RG, Kooyman RPH, Greve J (1993) Performance of a highly sensitive optical waveguide Mach-Zehnder interferometer immunosensor. Sens. Actuators. B Chem. 10(3):209-217

**4** Muellner P (2006), Strukturoptimierung eines Mach-Zehnder interferometrischen Biosensors. Diploma Thesis. University of Vienna, 109 BL

**5** Xu DX, Densmore A, Delâge A (2008) Folded cavity SOI microring sensors for high and real time measurement of biomolecular binding. Optical Society of sensitivity America 16(19):1517-15148

**6** Iqbal M, Gleeson M, Spaugh B, Tybor F, Gunn W, Hochberg M, Baehr-Jones T, Bailey R, Gunn LC (2010) Label-free biosensor arrays based on silicon ring resonators and high-speed optical scanning instrumentation. IEEE Journal of selected topics in quantum electronics 16(3):654-661

**7** Parriaux O, Veldhuis G (1998) Normalized analysis for the sensitivity optimization of integrated optical evanescent-wave sensors. IEEE Journal of Lightwave Technology 16(4):573–582

**8** Bruck R (2010) High index difference polymer waveguide Mach-Zehnder interferometer biosensor, compatible with injection molding and spin coating. Dissertation. University of Vienna

**9** Rassoly A., Herold KE, (2009) *Biosensor and Biodetctions*, Methods and Protocols. Humana Press, USA, Vol. 1, p. 365

**10** Ponpon J P, Bourdon B (1982) Oxidation of glow discharge a-Si:H. Solid-State Electronics., 25(9):875-876

# Part II: Surface Characterization Methods

## Content

## Surface Characterization Methods

The surface characterization is one important factor for the optimization of the functionalization chemistry on the MZI sensor arrays.

For this application it has to be ensured that the thin waveguide layers (a-Si:H or PI) do not get thinned or damaged by the chemical treatment and also the cladding has to be chemically resist to the employed reagents and solvents. Therefore, fast verifications with the microscope and the Alfa-Step are made and then, when a protocol has shown good results, the atomic force microscope (AFM) is used to gain the important parameters of surface roughness and microtopography.

To optimize the functionalization with different chemical groups (carboxyl-, amine-, sulfhydryl group), specific fluorescence markers have been used in this diploma work. In combination with a fluorescence scanner the optimization is done by the analyses of the fluorescence intensity. In some cases also the surface concentration (population density) of the immobilized fluorescence markers can be achieved via calibration curves. The information about the surface near groups and their elementary composition can be provided by X-ray-photoelectron spectroscopy (XPS). The XPS spectra do not only validate the successful binding of a molecule to the target substrate, but can also give information about possible reaction ways and – rates.

The best examples for the use of the described techniques are given in the publications of Drovel **[1]** and Pippig **[2]** et al.

In this chapter the various surface characterization methods for surface analysis are described shortly.

## 1 Microscope tests

The fluorescence microscope type DMLM from Leica Microsystems has been used to make pictures (via camera on the top) of the untreated and treated surfaces to prove on chemical resistance of the layers. This microscope has also the capability to perform fluorescence tests. Therefore, a Hg-vapor discharge lamp is used for excitation. The light is filtered by a filter cube to a specific wavelength range. This filter cube also filters the emitted light of the specimen and guides it to the camera on the top of the microscope. The fluorescence tool is used for fast tests, whether fluorescence occurs. The occurrence of fluorescence on the specimen shows if a binding of a fluorescence marker to a functionalized substrate takes place.

## 2 Alpha-Step

The Alpha-Step IQ surface profiler from the company KLA Tencore (USA), has been used to control the cladding height during critical steps in the functionalization. The Alpha-Step is a computerized surface profiler that drives with a needle in one direction over the surface. The received data give the information about the edge height (height of the cladding measured on the edge to the measurement window). For the measurements always the same settings, shown in Table 1, have been used.

**Table 1: Settings of Alpha-Step**

| settings | Value | Unite |
|---|---|---|
| Scan length | 100 | µm |
| Scan speed | 2 | µm/s |
| Sampling rate | 50 | Hz |
| Sensor range | 20 | µm/1.19 pm |

## 3 Characterization with atomic force microscopy

The Pico Plus atomic force microscope (AFM) from Molecular Imaging, Tempe, USA, is used to analyze the control samples after several steps of an optimized functionalization protocol. Therefore, the measurements have been performed in tapping mode, under air, with small measurement area (1 $\mu m^2$), using NANOSENSORS™ AFM tips, Type: PPP-NCHR-50 (4.0 ± 1 µm wide, 125 ± 10 µm length, tip radius < 10 nm).

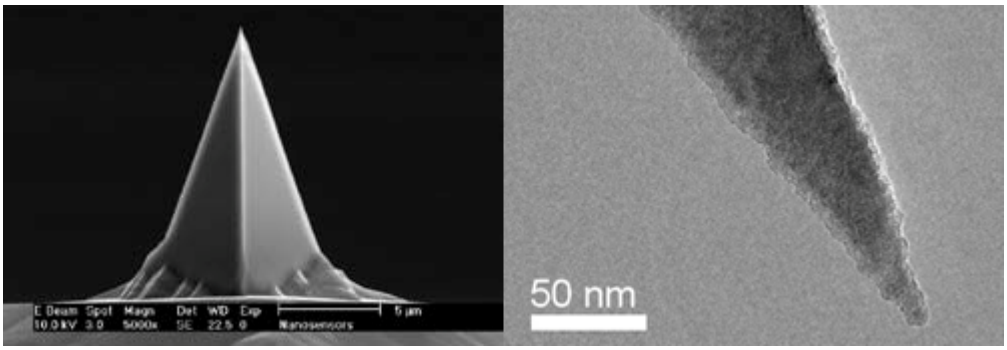


**Figure 1: AFM tip, Type: PPP-NCHR-50 (4.0 ± 1 µm wide, 125 ± 10 µm length, tip radius < 10 nm)[1]**

Instead of the Alpha-Step linear profile, the AFM gives the surface microtopography of a defined area (1 $\mu m^2$). With this profile imaging the surface parameters, such as surface roughness and microtopography, can be provided in tapping mode, which is chosen to reduce

[1] Pictures of the AFM tipe Type: PPP-NCHR-50 taken from the producer´s homepage of NanoWorld AG: http://www.nanosensors.com/PPP-NCHR.htm, 08.11.2010.

the lateral force acting.[**3**] As roughness parameter the arithmetic mean value ($R_a$) is used. The formula for its calculation is given as:

$$R_a = \frac{1}{L_c}\int_0^{L_C} |z_i(x)|\, dx;\; R_a = \frac{1}{N_P}\sum_{1=l}^{N_P} |z_i(x)| \tag{3.1}$$

Where $L_c$ is the cut off length definite over the scan area $A$ ($L_x$ x $L_y$), $N_P$ is the number of the discrete measurement points of $z_i(x)$. The $z(x)$ results form a least square fitted line and give the height profile, without the slope or nominal shape of the entire profile.

## 4 Fluorescence Scan

In this work the ArrayPro® TECAN fluorescence scanner (Media Cybernetics, Bethesda, USA) with 633 nm or 532 nm excitation wavelength and 692 nm or 575 nm emission filter has been used. The optimization of the functionalization protocols has been done via measurements of the fluorescence intensity, supported by the open source software ImageJ 1.43u, developed by the National Institute of Health, USA. In some cases also the population density of the fluorescence markers on the surface has been determined by a calibration curve. Therefore, different concentrations of the respective fluorescence marker have been spotted on untreated control samples and the spots have been dried at room temperature in the dark to create a solid standard array.

In theory, fluorescence occurs after excitation by high energy light in definite wavelength range, at which electrons are excited to the next lowest singlet state. From this state the electrons return into the ground state by emission of light with a higher defined wavelength, which is characteristic and can be measured. Also other processes may appear after excitation, such as internal conversion, intersystem crossing (important for phosphorescence) and quenching (excitation energy would be converted into oscillating energy and no light emission occurs). However, these processes will not be further discussed in this diploma thesis. More important is the fact, that the intensity of the emission light $I$ depends on the intensity of the excitation light $I_0$. This correlation is shown in the following equation:

$$I = QI_0\varepsilon dc \tag{4.1}$$

Where Q is defined by

$$Q = \frac{Number\ of\ emitted\ photons}{Number\ of\ absorbed\ photons} \tag{4.2}$$

and $\varepsilon$ is the molar extinction coefficient, $c$ the concentration of the molecules, $d$ is a geometrical parameter. In this TECAN fluorescence scanner the intensity of the measurement

signal is not adjusted via the excitation light, but via the voltage in the photomultiplier tube. This photomultiplier uses the photoelectric effect to create primary electrons over the light intake. The so called dynodes in the tube are arranged in that way that the produced electrons get accelerated and multiplied. The intensity of the signal can be adjusted by the voltage in between the dynodes [**4**]. At the end the electrons reach the anode and the current of the incoming electrons is converted into a measurement signal. The voltage between the dynodes can be changed over the PMT (Photomultiplier tube amplification) value between 0 and 250, whereby a values between 100 and 200 are mostly sufficient.

## 5 Characterization with XPS

X-ray photoelectron spectra (XPS) are measured before and after the various steps of the optimized functionalization protocols for PI and a-Si:H control samples (1x1 cm) with the Phoibos-Hsa3500 instrument from SPECS Surface Nano Analysis GmbH, Berlin, Germany, using Magnesium X-ray source with 1253 eV emission line. The individual peaks from the XPS spectra have been analyzed and deconvoluted with the software CasaXPS Version 2.3.15., to gain information about the composition and the bonding status of the atoms on the surface. The used XPS setup contains a sampling system, two different X-ray sources (Mg and Al), an electronic focus system, a spectrometer and multi channel electron detector. (See Fig. 2)

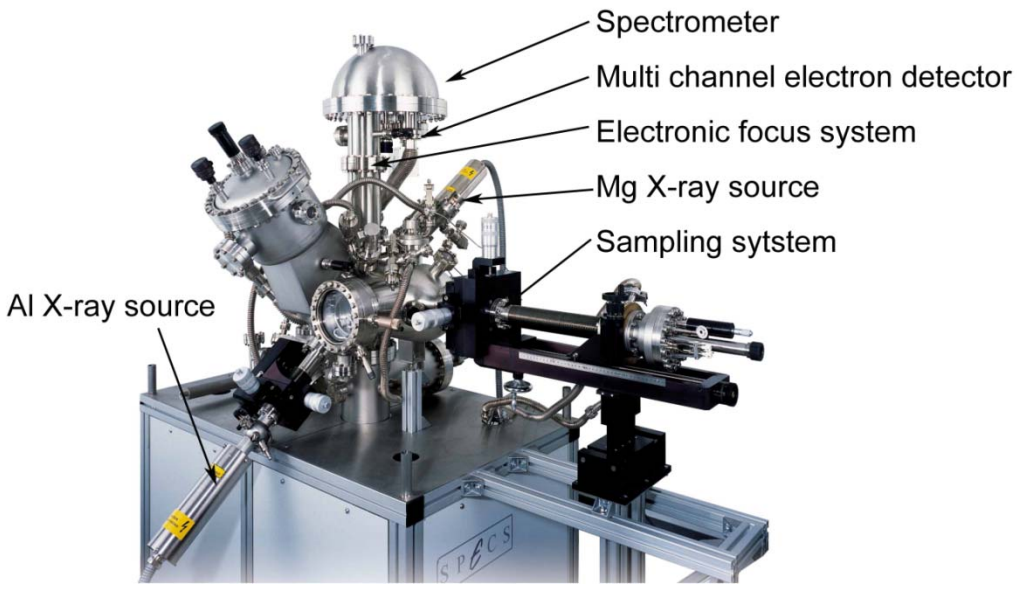


**Figure 2: Phoibos-Hsa3500 instrument from SPECS Surface Nano Analysis GmbH, Berlin, Germany. Picture is taken from the SPECS catalogue of "customized systems for surface analysis"[2]**

[2] Picture is taken from the SPECS catalogue of "customized systems for surface analysis": Available from the internet: http://www.specs.de/cms/front_content.php?idcat=226 09.11.2010

The measurement principle of the XPS belongs to an emission of electrons caused by the X-ray photons of the energy hν. The emitted photoelectrons enter the electronic focus system that stands in a definite angle to the surface. This angle is called take off angle θ and can be adjusted over the horizontal position of the sample table.

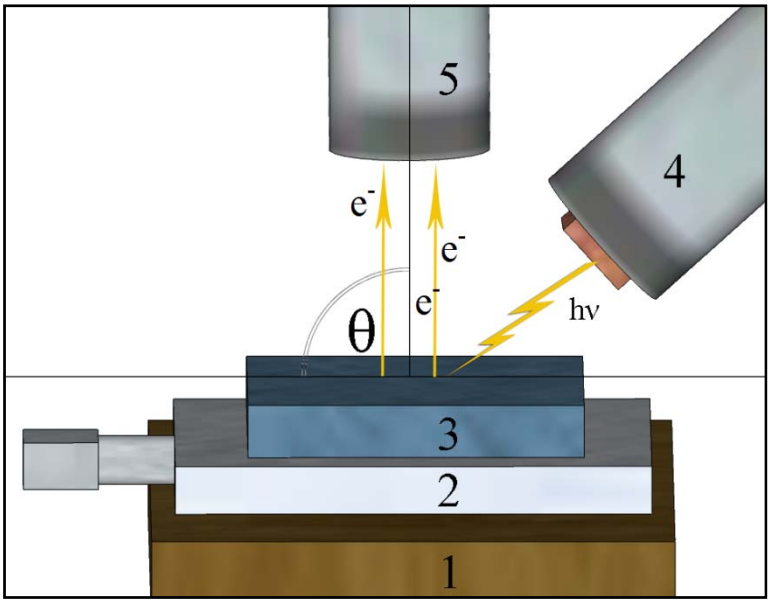


**Figure 3: Sample setup: 1 sample table, 2 sample holder, 3 sample, 4 Mg X-ray source, 5 electronic focus system. The Mg X-ray source excites the electrons of the sample in a depth < 10 nm. The emitted electrons enter the electronic focus system that stands in a definite take off angle θ to the surface. In this picture, the electronic focus system stands normal (0°) to the sample surface.**

The emitted photoelectrons are separated according to their kinetic energy and are analyzed in the multichannel detector. The intensity of the resulting spectra are influenced by the detector age. If a detector is in use for a longer period of time, then more and more residues are left in the multichannel detector and the spectra intensity decreases, because of this aging effect.
For analyses of spectra the binding energy $E_B$ or the kinetic energy $E_k$ of the electron is important to assign the electron to an orbital of an element of the periodic table (*e.g.* C1s) or a specific binding (*e.g.* C-C). The $E_B$ depends on the kinetic energy of the photoelectron $E_k$, as well as on the photon energy $h\nu$ and the spectrometer work function $W$.

$$E_B = h\nu + E_k + W \tag{5.1}$$

The values of $h\nu$ and $W$ are known for an existing XPS setup and the $E_B$ (or $E_k$) vs signal intensity can be shown as spectrum. (See Fig. 4)
The XPS spectra are analyzed and deconvoluted with the software CasaXPS Version 2.3.15. Therefore, the spectra get calibrated on the Carbon C 1s peak, which peak maxima is fixed at 284 eV binding energy $E_B$. With the software CasaXPS Version 2.3.15, the atom peaks can

be identified by their binding energy ($E_B$) and by the software integrated data base (*e.g.* peak maxima 531 eV, belongs to oxygen O 1s). Furthermore, a peak deconvolution could be done with this software, to earn the subpeak´s maxima and shape. The deconvoluted subpeaks have to be literature supported assign to their according binding status. So can, for example, the carbon subpeak at 287 eV ($E_B$) on polyimide substrate assign to the carbonyl binding status (C=O) supported by the literature of Flitsch et al. **[**5**]**.

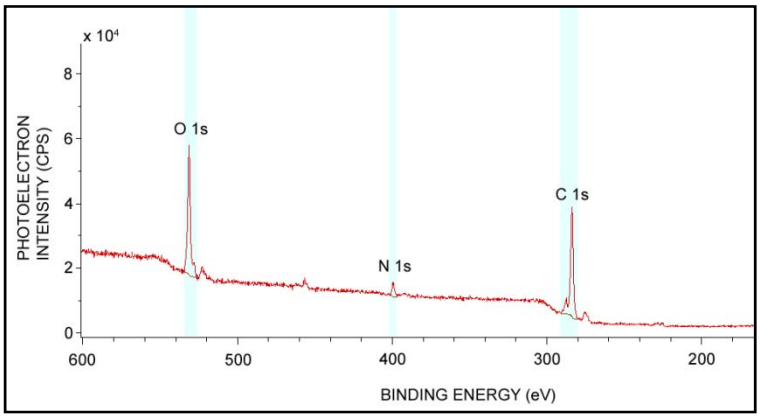


**Figure 4: XPS spectrum of polyimide control sample measured with the Phoibos-Hsa3500 instrument with Mg X-ray source.**

The measurement is performed in ultra high vacuum ($10^{-8}$-$10^{-10}$ mbar), to avoid an influence of the gas molecules (*e.g.* noise in the measurement signal caused by collisions, or a gas monolayer on the sample surface). The sample is grounded over the sample table to preclude charging.

The generation of X-rays is achieved bhigh energy electron bombardment of an anode material. This process produces heat, which needs a cooling system of the X-ray source.

As X-ray anode material magnesium (Mg) or aluminium (Al) can be used which provides photons of the energy 1253.6 and 1486.6 eV, respectively. In the resent work we used only the Mg X – ray source. The attenuation length ($\lambda_a$) depends on the kinetic energy of the photoelectron and material properties. The formula for the calculation of the attenuation length for organic ($\lambda_{org}$) substrates depends on the density ($\rho$), meanwhile in the formula for the attenuation length of inorganic ($\lambda_{ino}$) substrates the volume parameter ($a^3$) of an atom is integrated:

$$\lambda_{org} = \frac{49}{\rho\, E_k^2} + 0.11\, \frac{E_k^{1/2}}{\rho} \tag{5.2}$$

$$\lambda_{ino} = \frac{2170\, a}{E_k^2} + 0.72\, a^{\frac{3}{2}}\, E_k^{1/2} \tag{5.3}$$

The intensity of an electron emitted from the surface depth greater than *d* is given by the Beer-Lambert relationship in dependence of the take-off angle θ:

$$I = I_0 \exp\left(-d/\lambda_a \cos\theta\right) \tag{5.4}$$

The analysis depth d, from which an electron can be detected, is smaller than 10 nm. By use of Eqn. (5.4) it is possible to make a depth profile of the sample by angle resolved measurements. [**6**]

In Fig. 5 the dependence of the take-off-angle and the analysis depth is graphically illustrated. With decreasing the electron take-off angle the sampling depth gets longer.

This means a high electron take-off angle (*e.g.* 75°) gives information about the composition at the surface, meanwhile a low electron take-off angle (0°, detector stands normal to the surface) give the composition of the bulk phase. [**7**]

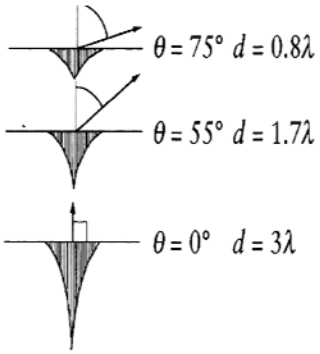


**Figure 5: Dependence of the sampling depth from the take-off angle θ [8]**

The equation (5.4) is true for a homogenous sample substrate. In the case of functionalization, we create an organic film on the surface, and the sample must be seen as substrate with a thin surface layer. For the substrate and the surface layer, own attenuation lengths (and own analysis depths, d) exist and the formula of the intensity behaviour of the emitted electron has to expanded.

In the recently found literature the main challenge for a multilayer system of thin films (<10 nm) is the determination of the attenuation length. However, the Eqn. (5.2) and (5.3) are very precise and represent approximations. For exact results, the formulas must be adjusted for every material and surface layer system, but if this is considered, also the over layer thickness can be determined. Examples for the determination of the surface layer thickness are given in the publication of Labinis et. al, where monolayers of n-alkanethiols [**9**] and in the

publication of Seah et. al. where an ultra thin silicon oxide layer on a silicon substrate [**10**] were characterized.

The information about the composition of the surface is more easy to gain from the spectra and the peak area. These data have to be converted into atomic %.

Therefore, the peak area ($A_P$) is divided by the relative sensitivity factor (R.S.F) of the system and then the quotient is calculated in percent.

$$[Atomic\ \%] = \left\{\left(\frac{A_P}{R.S.F}\right) / \sum\left(\frac{A_P}{R.S.F}\right)\right\} \times 100 \tag{5.5}$$

**1** Dorvel B, Reddy Jr. B, Block I, Mathias P, Clare SE (2010) Vapor-Phase deposition of monofunctional
alkoxysilanes for sub-nanometer-level biointerfacing on silicon oxide surfaces. Adv. Funct. Mater. 20:87–95

**2** Pippig F, Holländer A (2010) Hydrogel nanofilms for biomedical applications: synthesis via polycondensation reactions. Macromol. Biosci. 10:1093–1105

**3** Brune D, Hellborg R, Whitelow HJ (1997) Surface Characterization. Wiley-VCH, Weinheim. p. 94f

**4** Holbrow CH, Lloyd JN, Amato JC (1999) Modern introductory physics. Springer, New York, p. 413ff

**5** Flitsch R, Shih Y (1990) A study of modified polyimide surfaces as related to adhesion. J. Vac. Sci. Technol. A 8(3):2379-2381

**6** Watts JF, Wolstenholme J (2003) An introduction to surface analysis by XPS and AES. Wiley,Weinheim, 2003, p. 11ff

**7** Watts JF, Wolstenholme J (2003) An introduction to surface analysis by XPS and AES. Wiley,Weinheim, 2003 p. 80ff

**8** Brune D, Hellborg R, Whitelow HJ (1997) Surface Characterization. Wiley-VCH, Weinheim. p. 303f

**9** Laibinis PE, Bain CD, Whitesides GM (1991) Attenuation of Photoelectrons in Monolayers of n-Alkanethiols Adsorbed on Copper,Silver, and Gold. *J. Phys. Chem. 95:*7017-7021

**10** Seah MP, Spencer SJ (2005) Ultrathin SiO2 on Si. VII. Angular accuracy in XPS and an accurate attenuation length. Surface and interface analysis 37: 731–736

# Part III: Functionalization of polyimide and hydrogenated amorphous silicon

# Content

## Functionalization of polyimide and hydrogenated amorphous silicon

In the last two parts the Mach-Zehnder interferometer (MZI) and the surface characterization methods were described.

In this part first the surface chemistry of polyimide (PI) and hydrogenated amorphous silicon (a-Si:H) are discussed and characterized with the X-ray photoelectron spectrometer (XPS) to understand the reaction properties on these waveguide layers. Also the claddings (Ormoclad and SU-8) are discussed shortly to understand their chemical resistivity.

In the following section, a short overview of relevant functionalization protocols from literature for hydrogenated amorphous silicon and polyimide is given. Also literatures for the streptavidin immobilization and ways to realize a platform for DNA hybridization experiments are cited shortly.

According to this knowledge clad control samples have been tested regarding on their chemical resistivity, which build an own section in this part. The information about chemical resistivity are performed by treating the layer systems (waveguide layer plus cladding) with different solvents and chemical, and this information is important to guarantee that the thin MZI layers and claddings do not get damaged or etched.

Furthermore the chemical resistivity of the layers is rarely discussed in the literature, and the resistivity tests build a good background for the following time-consuming and expensive functionalization tests.

The primary aim of these functionalization tests is the immobilization of streptavidin, to realize a streptavidin biosensor and secondary to perform a platform for DNA hybridization experiments. Therefore the waveguide layers (PI and a-Si:H) have been functionalized with different chemical groups, namely carboxyl-, amino- and sulfhydryl groups, to provide flexibility in terms of the possible reaction ways on the surfaces. From this pool of functional groups on the surface, the sulfhydryl way has then been chosen to optimize the immobilization of streptavidin on the surfaces. To monitor the optimization of the functionalization, and the streptavidin immobilization different fluorescence labels have been bound to the surface, the intensities of which have been monitored by the TECAN fluorescence scanner.

To ensure that the chemical treatment of the different functionalization steps until streptavidin immobilization do not damage the waveguide layers, the atomic force microscopy (AFM) is used to characterize the surface roughness and microtopography before and after several steps of the functionalization protocols for PI and a-Si:H substrates. The X-ray photoelectron spectrometer gives additional information about the chemical changes on the surfaces like the atom composition and binding status, and support the theory of the functionalization.

At the end of this part an optimized protocol for the functionalization of a-Si:H- and PI-MZI to yield streptavidin biosensors is established.

# 1 Hydrogenated amorphous silicon –MZI sensors

The interaction between the analyte and the a-Si:H-MZI sensor takes place over the sensitive layer, which has sensing molecules covalently bound to the waveguide layer. In this section the chemistry of the a-Si:H waveguide layer is explained, to understand how the covalent bonding of the sensing layer molecules can be achieved on the hydrogenated amorphous silicon (a-Si:H). Furthermore, also the chemistry of the SU-8 cladding is explained shortly in conjugation with the chemical resistance.

## 1.1 Chemistry of hydrogenated amorphous silicon waveguide layer

Silicon is a widely used material because of the optical, thermal and electrical (semiconductor) properties. There exist two commercial forms of silicon: crystal and amorphous silicon. The crystal silicon is organized in long range order, while the amorphous silicon is organized in short range order and has a less chemical stability because of the additional contact areas on the grain boundaries. Beside the important optical characteristics, amorphous silicon is in comparison to crystalline silica a strongly reduced thermal carrier under biocompatible conditions [**1**]. There exists a special form of amorphous silicon, called hydrogenated amorphous silicon (a-Si:H) that can be deposited by using the standard plasma-enhanced chemical vapor deposition (PECVD) with monosilane gas ($SiH_4$) diluted in inert gas (*e.g.* carbon dioxide). It can be deposited on wide areas and afterwards it can be structurally modified on nanoscale. The network structure of the a-Si:H depends on the parameters of the PECVD such as temperature, pressure and concentration of the mono silane.

In theory there exists only silicon hydrogen bonds (Si-H) on the via PEVCD freshly prepared a-Si:H surface. These Si-H bounds are more resistant against the reaction with oxygen than *e.g.* crystalline silicon. In literature it is described that the oxygen layer is detectable on an a-Si:H surface after one day (24 h) and then grows exponentially until a saturation gets achieved. Because of this fact it can be suggested that on fresh prepared hydrogenated amorphous silicon surface, the Si-H bond is the dominant chemical group.[**2**]

To prove this theory and to get an idea of the surface composition, two samples (from different fabrication days) were measured with the XPS by an take-off angle of 0° to gain information of the bulk phase.

The first sample is a freshly prepared a-Si:H control sample [1], the second one is a-Si:H control sample that has been stored for three weeks under air at room temperature. The XPS spectra are shown in Fig. 1.

**Table 1: XPS results of the freshly prepared a-Si:H control sample**

| Elements | Position (eV) | Area | R.S.F | Atom% |
|---|---|---|---|---|
| **F 1s** | 685.88 | 4977.20 | 4.26 | 1.14 |
| **O 1s** | 532.13 | 43913.50 | 2.85 | 15.03 |
| **N 1s** | 396.88 | 38716.90 | 1.77 | 21.34 |
| **C 1s** | 284.38 | 6298.80 | 1.00 | 6.15 |
| **Si 2p** | 99.88 | 49958.00 | 0.87 | 56.34 |

**Table 2: XPS results of the a-Si:H control sample after 3 weeks storage under air**

| Elements | Position (eV) | Area | R.S.F | Atom% |
|---|---|---|---|---|
| **O 1s** | 531.54 | 54623.00 | 2.85 | 26.70 |
| **N 1s** | 396.29 | 16197.70 | 1.00 | 22.57 |
| **C 1s** | 283.79 | 6382.30 | 1.00 | 8.89 |
| **Si 2p** | 99.04 | 25974.90 | 0.87 | 41.84 |

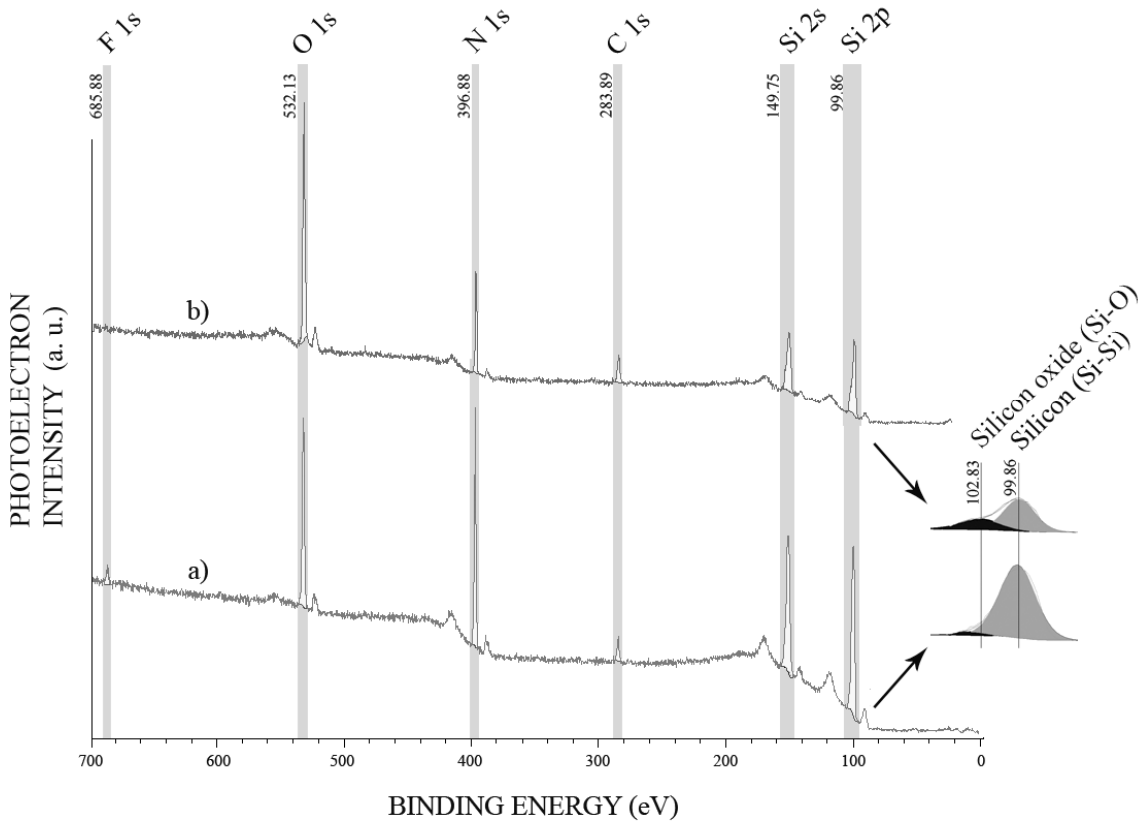


**Figure 1: XPS spectra measured with a take-off angle of 0° (bulk substrate) of a-Si:H samples: a) freshly prepared a-Si:H control sample. Silicon peak: 2.5% silicon oxide (Si-O) and 97.5% silicon (Si-Si); b) a-Si:H control sample after 3 weeks storage under air and room temperature. Silicon peak: 28.3% silicon oxide (Si-O) and 71.7% silicon**

The freshly prepared a-Si:H sample shows the element peaks of fluorine (685.89), oxygen (532.13), nitrogen (396.88), carbon (283.89) and silicon (149.75 and 99.86). The peaks of

[1] The freshly prepared sample is measured 12 h after preparation.

carbon and fluorine in the spectrum may result from the residues of the cleaning gas (tetrafluoromethane, $CF_4$) of the PECVD. Furthermore a contamination with nitrogen could be found in the spectra. This may result from the PECVD system, which is also used to create nitrites with ammonia gas. The nitrogen and the oxygen content of the a-Si:H sample is with 21% and 15% quite high (see Table 1). The a-Si:H control sample, which is stored for three weeks under air at room temperature and is produced on a different fabrication day, shows similar peaks, only the fluorine peak is not detectable. The oxygen content on the surface is now higher (26%) and the silicon peak splits in a duplet, which indicates the presence of silicon oxides in the surface near reagions.

For the functionalization we can assume that the a-Si:H layer does not only contain Si-H bonds on the surface because of the sum of other elements in the bulk phase. In summary it can be concluded that the Si-H bonds exists on the surface, but their concentration depends on the PECVD process (and also on the fabrication day) and duration of storage of sample in air. Then the surface silicon converted into silicon oxide, which can be detected in the XPS spectra over the silicon duplet.

## 1.2 Chemistry of the SU-8 cladding

The SU-8 for the cladding is purchased from the company MicroChem, Boston, USA. It is an epoxide resin that polymerizes under UV-light exposure. The mechanical, electrical and adhesive properties are descriped by the producer MicroChem [**3**] and a protocol gives an overview over the possibilities to create microstructures [**4**]. Regarding the chemical resistance there is published that the SU-8 is resistant against the reaction with acids and bases, but no detailed information is given. There exist several protocols that describe the conditions for the etching SU-8 layers. It is shown that with a mixture of sulfuric acid and hydroxyl peroxide (piranha clean) [**5**] SU-8 can be removed, and with oxygen plasma the SU-8 can be etched [**6**]. For functionalization this information is used to undergo a controlled damage of the cladding layer.

# 2 Polyimide-MZI sensor

The interaction between the analyte and the PI-MZI sensor takes place over the sensitive layer on which molecules are covalently bound to the waveguide layer. In this section the chemistry of the PI waveguide layer is explained, to understand how the covalent bond of the sensing

layer molecules can be achieved. Furthermore also the chemistry of the Ormoclad cladding is explained shortly in conjugation with the chemical resistance.

## 2.1 Chemistry of Polyimide waveguide layer

Polyimide is widely used in the electronics industry and as coating material because of its thermal stability, low density, excellent insulation properties, lithographic sensitivity and chemical purity. Strictly speaking one has to distinguish between poylimides and copolyimides. Copolyimides have a more complex structure resulting from two or more diamine reactants instead of one in the case of polyimide. These diamines react with the dianhydride to form the polymer chain. However, both types are commonly referred to as polyimide. In the further discussion the common term is used. For this diploma thesis the photosensitive Pyralin® PI-2771 copolyimide siloxane precursor solution (purchased form HD Micro Systems, Neu-Isenburg, Germany) is used. Pyralin® PI-2771 is a copolyimide consisting of benzophenone tetracarboxylic dianhydride (BTDA), which forms the polyimide moiety with the types of diamines oxydianiline, m-phenylenediamine [**7**,**8**] and a diamine siloxane. The main functional groups in the polyimide structure are imide and carbonyl groups. The siloxane build own substructures [**9**]. The exact molecular formula, the numbers of the substructure (n,m,o) as well as the number and shape of the siloxane units are not given by the producer of the Pyraline® PI-2771. With the information of the different literatures a molecular formula like it is shown in Fig. 2 can be assumed.

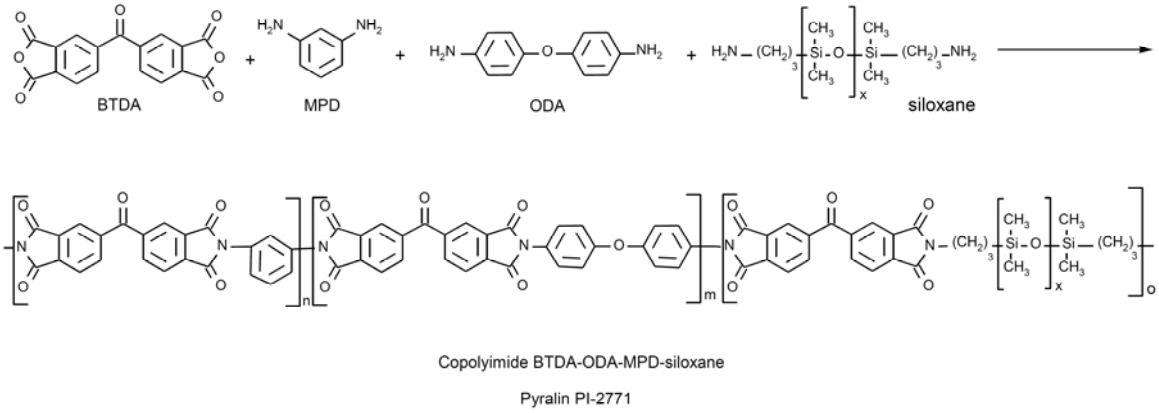


**Figure 2: Possible molecular constituents of Pyralin® PI-2771 and the syntheses form benzophenone tetracarboxylic dianhydride (BTDA) with oxydianiline (ODA), m-phenylene diamine (MPD) and the diamine siloxane. The exact molecular structure and the numbers of the substructures n, m, o and x of the copolyimide siloxane is not given by the producer (HD Mircosystems) of Pyralin® PI-2771.**

To get an idea of the composition, two samples (from different fabrication days) were measured with the XPS. Figure 3 shows the XPS spectra of a freshly prepared PI control sample and a PI control sample, which has been stored for three weeks under vacuum. The freshly prepared PI[2] and the stored PI control sample show both the element peaks of oxygen (532.11 eV), nitrogen (399.39 eV), carbon (284.00 eV) and silicon (149.75 and 100.86 eV). The elemental composition of both samples is almost equal (see Table 3 and 4). Only the carbon and silica content is differs by about 4%.

**Table 3: XPS results from the freshly prepared PI control sample**

| Elements | Position | Area | R.S.F | Atom% |
|---|---|---|---|---|
| **O 1s** | 531.11 | 59647.20 | 2.85 | 18.96 |
| **N 1s** | 399.39 | 8266.00 | 1.77 | 4.23 |
| **C 1s** | 284.00 | 75497.40 | 1.00 | 68.40 |
| **Si 2p** | 100.86 | 8034.10 | 0.87 | 8.51 |

**Table 4: XPS results from the PI control stored 3 weeks under vacuum**

| Elements | Position | Area | R.S.F | Atom% |
|---|---|---|---|---|
| **O 1s** | 531.11 | 28441.20 | 2.85 | 18.63 |
| **N 1s** | 399.39 | 3695.80 | 1.77 | 3.90 |
| **C 1s** | 284.00 | 34527.10 | 1.00 | 64.49 |
| **Si 2p** | 100.86 | 6010.00 | 0.87 | 12.98 |

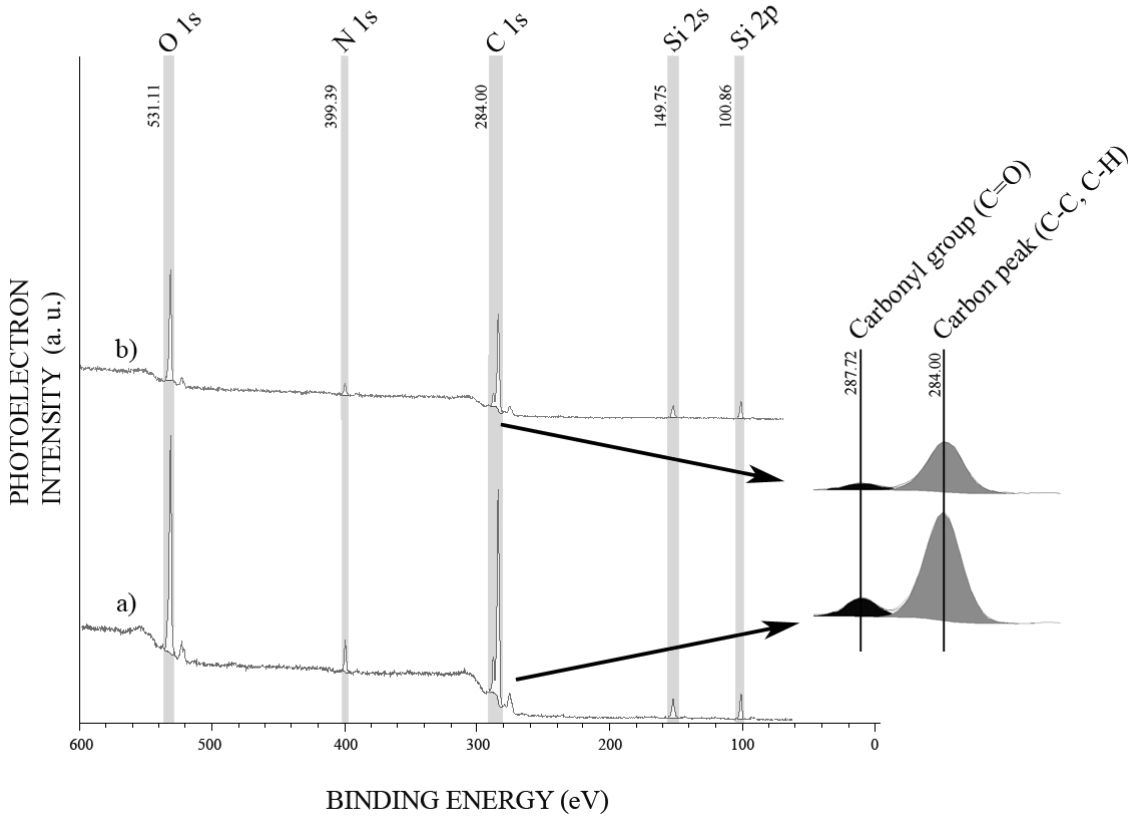


**Figure 3: The XPS spectra of the PI control samples are measured with a take-off angle of 0° (bulk substrate): The intensity differences of the XPS spectra a) and b) are caused by detector aging. a) freshly prepared PI control sample. C 1s peak: 13% Carbonyl (C=O), 87% Carbon (C-C, C-H); b) PI control sample after 3 weeks storage in vacuum and room temperature. C 1s peak: 12% Carbonyl (C=O), 88% Carbon (C-C, C-H)**

[2] The freshly prepared sample is measured 12 h after preparation.

To validate the molecular formula of the polymerized Pyralin® PI-2771 in Fig. 2 the XPS results of the freshly prepared sample are used for the modulation of the numbers from the substructures *n*, *m*, *o*, *x*. [**10**] (See Table 3 and Fig. 2) Therefore the below listed formulas (Eqn. 2.1-2.5) are used to calculate the theoretical content of oxygen [O%], nitrogen [N%], carbon [C%] and silicon [Si%] by modulation of the values of *n*, *m*, *o* and *x*. The sum of the atoms ($S_n$, $S_m$, $S_o$) are build for each substructure and then the overall sum of all atoms (S) in one molecular unite is calculated. The modulated numbers of the substructures are $n = 1$, $m = 1$, $o = 2$ and $x = 7$ and give a composition of the atoms with [O%] = 18.5, [N%] = 4.2, [C%] = 68.8 and [Si%] = 8.5 almost equal to the composition of the freshly prepared PI control sample measured by the XPS. (See Table 3)

$$n * \{\sum(\mathrm{O_n}) + \sum(N_n) + \sum(C_n)\} = S_n \quad (2.1)$$

$$m * \{\sum(\mathrm{O_m}) + \sum(N_m) + \sum(C_m)\} = S_m \quad (2.2)$$

$$o * \{\sum(\mathrm{O_o}) + \sum(N_o) + \sum(C_o) + \sum(Si_o) + x * (\sum(Si_x) + \sum(C_x) + \sum(O_x))\} = S_o \quad (2.3)$$

$$S = S_n + S_m + S_o \quad (2.4)$$

$$[\mathrm{O\%}] = 100\, x\, \frac{\sum(\mathrm{O})}{S};\ [\mathrm{N\%}] = 100\, x\, \frac{\sum(\mathrm{N})}{S};\ [\mathrm{C\%}] = 100\, x\, \frac{\sum(\mathrm{C})}{S};\ [\mathrm{Si\%}] = 100\, x\, \frac{\sum(\mathrm{Si})}{S} \quad (2.5)$$

For the functionalization of polyimide we can say, that the major chemical group in the molecular unit of PI are the carbonyl (C=O) and imide (>N-C=O) groups. The chemical purity of the two different PI samples is good and no residues can be detected. Also the storage in vacuum seems to be a good strategy to keep the sample composition almost constant.

## 2.2 Chemistry of the Ormoclad cladding

The Ormoclad, used for the cladding, is purchased from the company Micro resists technology GmbH, Berlin, Germany. Ormoclad is the trade name of this inorganic-organic hybrid polymer and is a positive photoresist from the ORMOCER® product line.

The mechanical, electrical and adhesive properties, as well as a protocol for the processing are descriped by the Micro Resists Technology GmbH [**11**]. Information about the chemical resistance are rarely published, but it is shown that with piranha clean Ormoclad can be removed from the surface, and with oxygen plasma the Ormoclad gets etched or damaged [**12**]. For functionalization this information is used to undergo a controlled damage of the cladding layer.

# 3 Functionalization literature

In this work the surfaces are functionalized with different chemical groups. This should be achieved to bind receptors for the analyte interaction covalently to the waveguide layers. The aim in this work was primary the immobilization of streptavidin and secondary the binding of biotin tagged DNA strands to the streptavidin surface, for real-time hybridization experiments on MZI sensors. Therefore, relevant literature is listed in this section for the functionalization of PI and a-Si:H substrates, and for streptavidin immobilization in conjugation with DNA hybridization experiments.

## 3.1 Literature for the functionalization of amorphous hydrogenated silicon

The a-Si:H surface provides silicon hydrogen bonds (Si-H) on the surface. These bonds can be used for a direct reaction with an alkene or alkine groups of different reactants. [**1**,**13**,**14**]
The main method is to create first a fresh Si-H surface by removing the silicon oxide with hydrofluoric acid or ammonium fluoride. Afterwards the freshly prepared Si-H surfaces are transferred into an organic solvent, in which the reactant is solved. The reaction gets started by heat or UV light exposure. With this direct functionalization strategy the Si-H groups of the a-Si:H can react UV-light supported with the reactant undecylenic acid to creat carboxyl groups on the surface. [**15**]
Besides the direct reaction with the Si-H bounds, the surface can be activated by forming hydroxyl groups on the silicon surface. This can be done for several substrates such as glass, silica or silicon by basic and/or acid treatments. [**16**]
The formation of hydroxyl groups on amorphous silicon is similar to the crystalline silicon. This behavior was reviewed by Zhuravlev et. al. The author published in this work the surface concentration values of surface bound water, hydroxyl groups and their internal analogs. The concentration values were obtained by thermo gravimetric analysis. The author showed that the concentration of the hydroxyl groups on amorphous silicon is about 4.9 OH $nm^{-2}$ (arithmetical mean). This equate to 8 µmol/$m^2$ (or ~8000 fmol/$mm^2$) hydroxyl groups on the planar amorphous silicon the surface [**17**].
To create such hydroxyl groups, tests with the sodium hydroxide, like it is done for silica materials [**18**], seems to be a good choice.
Another way to generate hydroxyl groups on the a-Si:H surface is the use of oxygen plasma followed by water, acid or basic treatment. To do so, first the a-Si:H surfaces get oxygenized and then samples are dipped into the corresponding liquids [**19**].

By generation of the hydroxyl groups on the surface, the way to the so called silane surface chemistry is opend.

The silane chemistry is the main strategy for functionalization of silicon based surfaces and is representatively reviewed in the book *Bioconjugate Techniques* [**20**].

The silane coupling agents, which bind to the hydroxyl groups, consist of a silicon atom that is tetragonal substituted. Three of these substituents (linkage group) are hydrolysable and responsible for the binding to the surface (or between the silanes) and one of these substituents is an alkyl chain, which may carry the functional group (*e.g.* amine group).

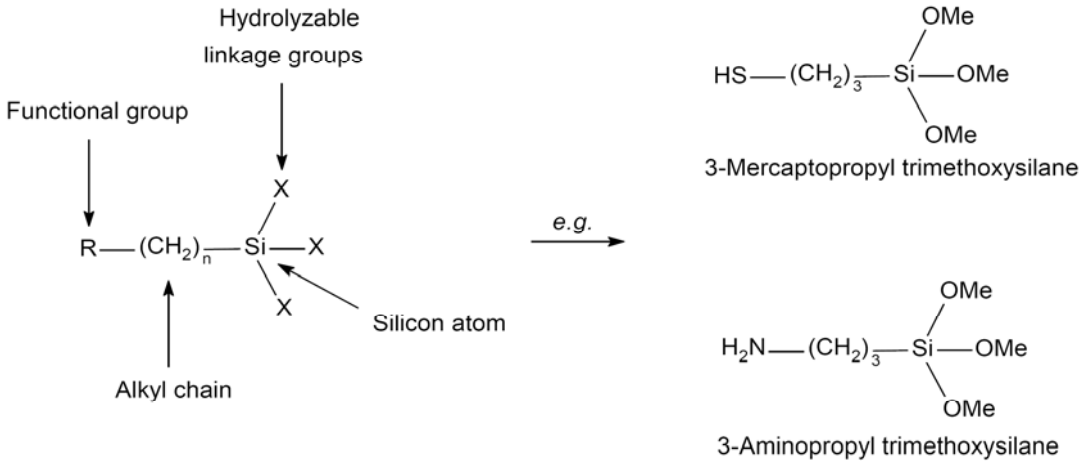


**Figure 4: Silane coupling agent and the subunits. The two examples, 3-Mercaptopropyl trimethoxysilane (MPTMS) and 3-Aminopropyl trimethoxysilane (APTMS), will be used in the functionalization tests.**

The most common linkage groups are the chloro- and alkoxysilanes. The alkoxy silanes are available as mono-, di- or trialkoxy silanes, which are able to hydrolyse and form the reactive silanols. In the case of trialkoxy silanes the silanols build under acid aqueous conditions a polymer linkage before they assemble on the surface. By this behavior a high surface density of functional groups can be achieved [**21**]. (See Fig. 5)

The functionalization with silanes can also be done in organic solvents like toluene [**22**, **23**,**24**], tetrahydrofuran (THF) [**25**] or chloroform [**26**] and with different basic or acid catalysts to accelerate the condensation to the surface. The silane chemistry under organic or aqueous conditions can be used in functionalization tests for the functionalization with two different trialkoxy silanes, namely the 3-Mercaptopropyl trimethoxysilane (MPTMS) and 3-Aminopropyl trimethoxysilane (APTMS) (see Fig. 4).

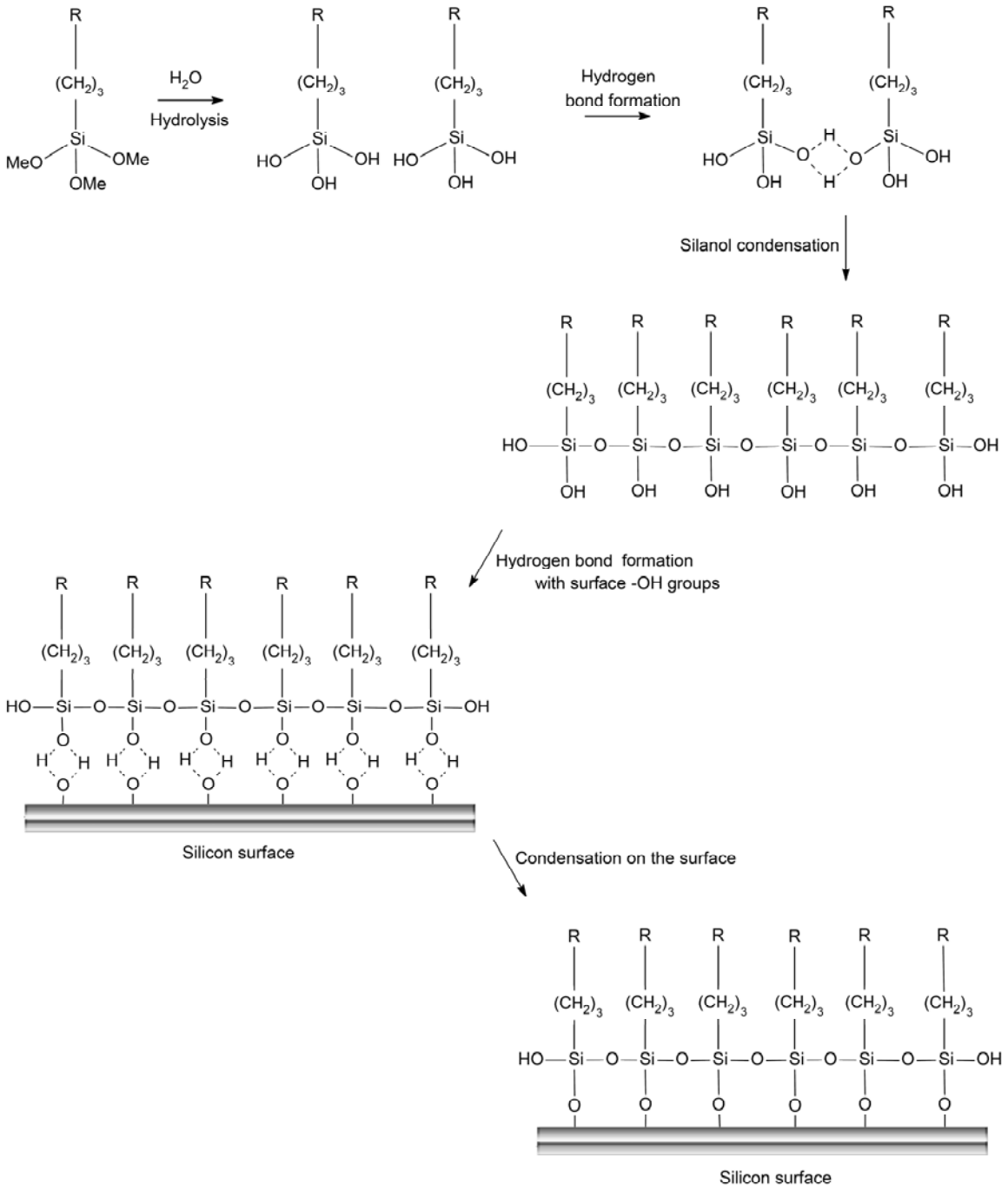


**Figure 5: Reaction way of trialkoxy silanes under aqueous conditions. The first step is the hydrolysis of the linkage groups, followed by hydrogen bond formation and silanol condensation. The polymer linked silanols bind covalently, via hydrogen bond formation with the surface -OH groups, to the silicon surface.**

## 3.2 Literature for the functionalization of polyimide

As it is shown in the section 2.1 *Chemistry of Polyimide*, the Pyralin®PI-2771 thin film contains carbonyl and imide groups. These groups can be used for different direct reaction strategies on the surface. One of this strategies is the aminolytic ring opening reaction [**27**], where the nitrogen in the imide gets under heat exchanged against another amine in the reactant. This strategy can also be used to produce cyclodextrin functionalized polyimide membranes [**28**]. There are carbonyl groups in Pyralin®PI-2771 which stems from the benzophenone subunits. These carbonyl groups can be activated by UV light (~300 nm). Via formation of a triplet state intermediate of the carbonyl groups in the benzophenone subunit, it may react with reactive hydrogen containing components (*e.g.* H-C, H-N) [**29**]. Besides the benzophenone carbonyl groups also the C=C and C–H bonds in a polymer structure can be derivatized by a photoreaction with the photoactivatable aryl azides under UV exposure (~350-370 nm), but this reaction is not specifical for polyimide substrates [**30**]. Instead of a direct reaction strategy, the PI substrate can be activated by alkaline hydrolysis [**31**,**32**,**33**]. (See Fig. 6)

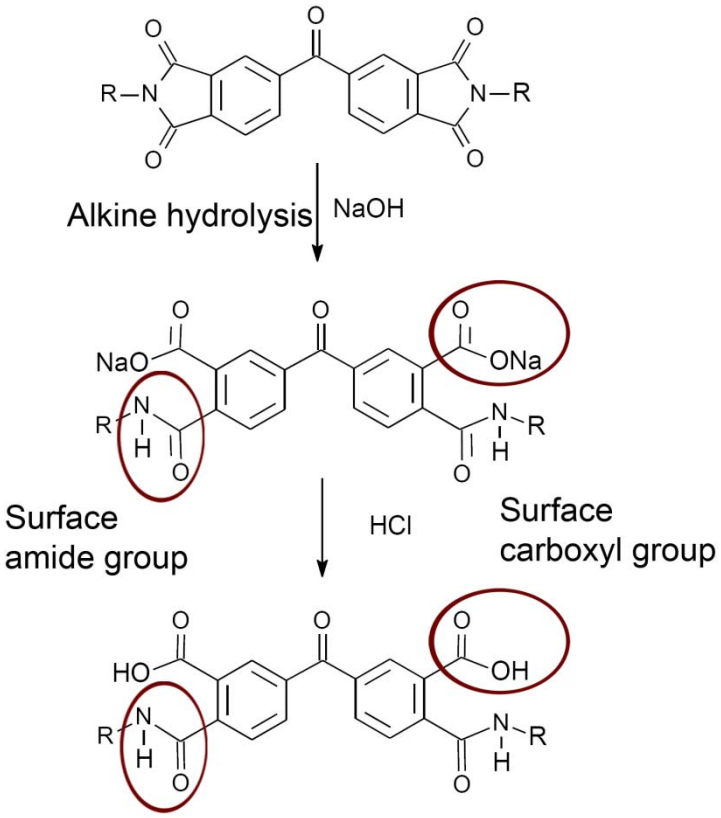


**Figure 6: Reaction scheme of the reaction way of alkaline hydrolysis under aqueous conditions with sodium hydroxide (NaOH) and the reaction to surface carboxyl and amide groups after treatment with hydrochloric acid (HCl)**

By the alkaline hydrolysis the imide ring gets attacked by the hydroxide ions and the reaction leads to surface amides and carboxylic acids. Via the generated carboxyl groups various reactions with hydrazines, epoxides, amines, alcohols and aminosilans are possible [**34**]. Also the derivatization of the surface carboxylic groups by activation with *N*-(3-dimethylaminopropyl)-*N* ethylcarbodiimide (EDC) followed by reaction with diamine is well known [**35**,**36**].

For the activation of the PI surface also the oxygen plasma can be used. The effects on polyimide of atomic oxygen [**37**], oxygen plasma exposure [**38**] and reactive ion etching [**39**] are well described in literature and shows possible reaction ways that lead to surface peroxides [**39**], and hydroxyl groups [**40**] after dipping the activated surface into water.

These reactive groups can serve as binding sites for silanes, like it is described in the last subsection (3.1 *Literature for amorphous hydrogenated silicon*). A test with two different silanes 3-Mercaptopropyl trimethoxysilane (MPTMS) and 3-Aminopropyl trimethoxysilane (APTMS) in aqueous and organic solvents has been done performed to prove this theory.

## 3.3 Literature for streptavidin immobilization

Avidin is a biotin binding glycoprotein isolated from egg white and biotin itself a water soluble vitamin. Avidin can bind four biotins per protein unit. Streptavidin is the analogue without the carbohydrates, but with the same biotin binding capacity. The lack of carbohydrates makes streptavidin less soluble in water than avidin, but reduces the unspecific interactions *e.g.* to a sensor surface [**41**].

The binding of the streptavidin to the sensor surfaces can be achieved covalently or affinity based. In the case of a covalent binding to the surface, the protein can be immobilized via amine coupling methods, where free amino groups (*e.g*. in the amino acid lysine) in the protein react with aldehydes or carboxyl groups on the surface [**42**]. A further possibility is to functionalize the streptavidin with hydrazine and then bind the protein to a with carbonyl functionalized surface [**43**].

In case of the affinity binding of streptavidin to the surface, the surface gets functionalized with biotin. Two biotin molecules can then bind affinity based to two of the four biotin binding pockets in the streptavidin structure, and immobilize the protein. The interaction between biotin and (strept)avidin is well documented by Green et. al. [**44**].

For new biosensors the biotin streptavidin interaction is common to prove the sensitivity of the device [**19**,**45**], because of the high mass of the streptavidin (60 kDa), that serves as

analyte, and the strong affinity bond between biotin and streptavidin (association constant $K_a \approx 10^{15}$ L mol$^{-1}$).

On the streptavidin covered surface, biotin tagged single strand DNA can be bound to the free biotin binding sites. The single DNA strands on the surface are able to hybridize with the complementary DNA strands and so hybridization experiments can be provided.

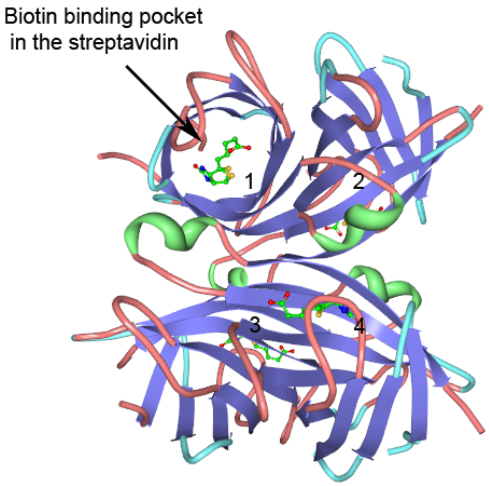


**Figure 7: Tetrameric structure of the streptavidin protein. It consists of four different subunits. Each subunit can bind one biotin molecule. One binding pocket is shown with an intercalated biotin molecule** [**46**].

For this DNA hybridization experiments the streptavidin should be affinity bound to the surface, because this strategy lead to a better orientation of the streptavidin on the surface. Furthermore, this induces a better binding rate and orientation of the biotin tagged DNA stands on the streptavidin layer and influences thereby positively the hybridization rate. The affinity bound streptavidin binds on average 1.5 biotin tagged DNA strands per unit and the hybridization rate is nearly 1:1 [**47**].

According to this knowledge, streptavidin should be immobilized by affinity principle on the PI and a-Si:H surface, for real-time streptavidin measurements and for DNA hybridization experiments by MZI. Therefore, the surface has to be functionalized first with biotin.

There exist several biotin containing reactants with polyethylene glycol (PEG) spacer groups [**48**]. The PEG spacers make the surface hydrophilic and reduce unspecific interactions with the sensor surface. In case of a covalent binding of PEGs to the surface, they remain stable under various conditions and give a good reproducibility of the measurements [**49**].The good bio-compatibility of PEGs has lead to many different kinds of PEG based reagents with different receptors for biomolecules [**50**], such as a biotin receptor for streptavidin binding. The PEG based reagents are available in different lengths *e.g.* $PEG_2$ and $PEG_3$ with 2.9 and 3.6 nm chain length. By the variation of the PEG spacer length, also 3D matrixes can be

simulated on the sensor surface, which increase the maximal possible analyte concentration on the surface. [**51**] To guarantee access of the immobilized biotin to reach one of the four binding pockets in the streptavidin (binding pocket length 0.9 nm), a $PEG_2$ with 2.9 nm is useful [**52**].

Thus, the PI and a-Si:H surfaces have to be functionalized with $PEG_2$-biotin. If activation of the surface with amine or sulfhydryl groups is achieved, then the common reagents N-hydroxysuccinimide (NHS)- or maleimide-$PEG_2$-biotin can be used to biotinylate the surface (see Fig. 8).

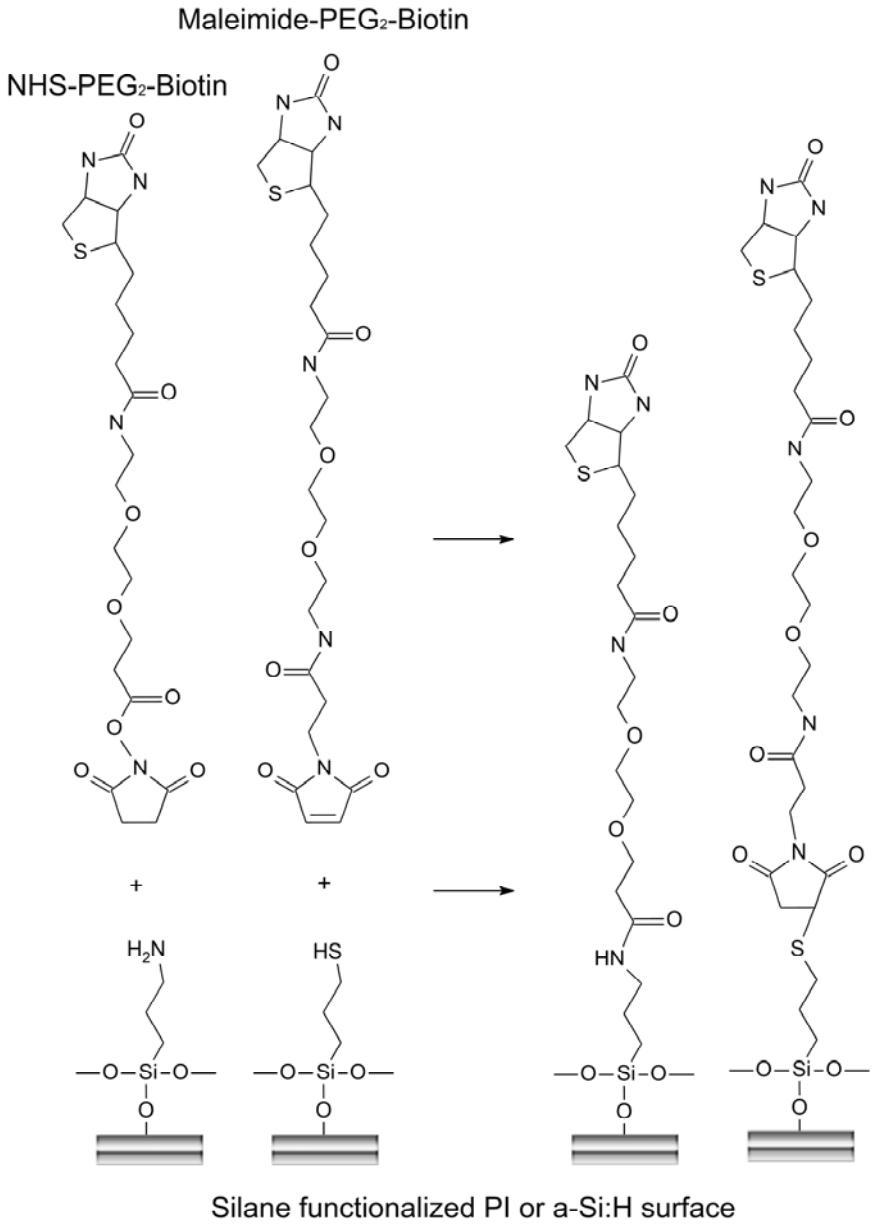


**Figure 8: Biotinylation with N-hydroxysuccinimide (NHS)- or maleimide-$PEG_2$-biotin on amine and sulfhydryl silane functionalized surfaces.**

# 4 Chemical resistance of the MZI layer systems

For the creation of different chemical groups on the surfaces, normally several steps have to be carried out, such as cleaning, activation and functionalization. All these steps require different chemicals and treatments, which affect the MZI layer systems (PI-Ormoclad and a-Si:H-SU-8). Thus, it is validated in this chapter, to ensure that the layers do not get etched or damaged by the employed chemicals.

The cleaning for example can be done with various organic solvents, ultrapure water and in the ultrasonic bath. The most common organic solvents are alcohols (methanol, ethanol, isopropyl alcohol) and also acetone, whereas acetone has to be excluded because it destroys the organic layers. Also a cleaning process in oxygen plasma is possible to remove residuals. Beside this cleaning effect of the oxygen plasma, the different oxygen species in the plasma (*e.g.* oxygen radicals and ozone) can also activate the surface [**53**,**19**], because it may lead to reactive oxygen species on the surface (*e.g.* peroxides groups). The activation and so the creation of active hydrophilic groups (such as hydroxyl groups for a-Si:H or carboxyl groups for PI) on the unreactive a-Si:H and PI surfaces can also be achieved by treating the substrates with different chemicals. The effects of the activation steps on the MZI layer system has to be tested. The progress of the activation can be followed for example by measurement of the surface hydrophilicity by water contact angle at room temperature. By spotting via pipette 5 µL ultrapure water on the untreated and activated surfaces, discrete values of the water contact angle can be analyzed by drop shape for every sample. Every water contact angle measurement was performed twice.

When the activation is achieved, the reactive hydrophilic groups on the surfaces can react in a functionalization step with a specific reactant, such as silanes like described in the last section. This functionalization can be done under various conditions in different organic solvents, under acid aqueous conditions and at different temperatures. To validate the chemical resistance of the MZI-layer system, clad PI and a-Si:H control samples (one halve is covered with Ormoclad or SU-8) are treated according to different methods found in various literatures listed in the last chapter. For the analysis of the effects of each treatment the clad control samples were characterized with the Alfa-Step and the microscope.

The Alfa-Step provides values about the cladding heights (measured on the edge of the cladding). The results of the untreated clad control samples are shown in Table 5 and 6 and give an average cladding height of $1.4 \pm 0.2$ µm for SU-8 and $9.9 \pm 1.1$ µm for Ormoclad.

For characterization by microscope, before and after treatment two pictures of every sample was taken from the imaging boundary between the cladding layer and the a-Si:H surface, on

the edge of the samples. Figure 9 and 10 show the surfaces of the untreated a-Si:H-SU-8 and PI-Ormoclad clad control samples.

**Table 5: Alfa-Step results of the cladding heights for the untreated Si:H-SU-8 clad control samples**

| Sample Signature | edge height [µm] |
|---|---|
| *M10* | 1.3 |
| *M11* | 1.2 |
| *M12* | 1.6 |
| *M13* | 1.4 |
| *M15* | 1.4 |
| *M16* | 1.6 |
| *M17* | 1.6 |
| *M18* | 1.3 |
| *M19* | 1.4 |
| **Average** | 1.4 |
| **Standard Deviation** | 0.2 |

**Table 6: Alfa-Step results of the cladding heights for the untreated PI-Ormoclad clad control samples**

| Sample Signature | edge height [µm] |
|---|---|
| *M42* | 11.6 |
| *M43* | 9.2 |
| *M45* | 9.0 |
| *M46* | 9.2 |
| *M47* | 8.8 |
| *M48* | 10.1 |
| *M49* | 11.2 |
| **Average** | 9.9 |
| **Standard Deviation** | 1.1 |

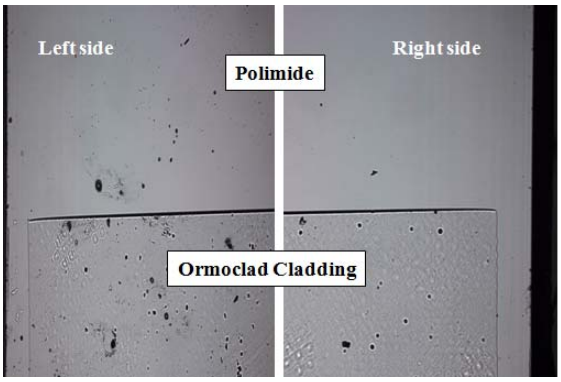


**Figure 9: Microscope pictures of the untreated PI-Ormoclad control sample**

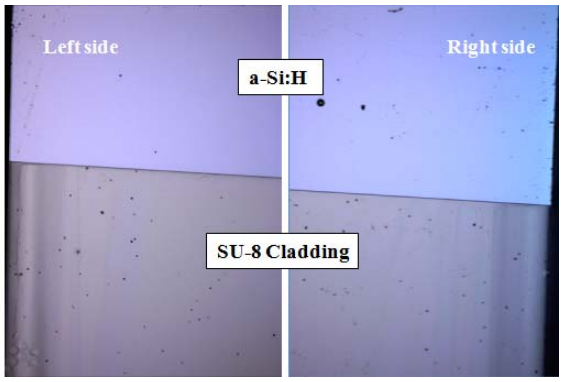


**Figure 10: Microscope pictures of the untreated a-Si:H-SU-8 clad control sample**

In the following subsections chemical resistivity of the layer system of PI and a-Si:H clad control samples is described. The used chemicals have been selected from the literature in the last section and these tests show whether of these protocols are applicable for further functionalization tests, which are more time-consuming.

## 4.1 Chemical resistivity of a-Si:H-SU-8 clad samples

For the activation with base and acids, several procedures with nitric acid (10%), hydrochloric acid, ammonia and sodium hydroxide solution were tested on a-Si:H clad control samples. (See Table 7)

In the test only the hydrochloric acid and the sodium hydroxide solution make the surface hydrophilic (water contact angle gets lowered). The disadvantage is that both, hydrochloric

acid and sodium hydroxide bring unspecific dirt onto the surface, which cannot be washed away with different cleanings. Sodium hydroxide solution treatment also seems to etch or to increase the roughness of the a-Si:H layer, visible by the changes of the surface color. (See Fig. 11)

**Table 7: Activation procedures with base and acids**

| **Description of the procedure** | **Damage to the SU-8 cladding** | **Damages/Changes of the a-Si:H surface** | **If yes: What kind?** | **Hydrophilic a-Si:H surface?** (Change of the water contact angle?) |
|---|---|---|---|---|
| Nitric acid 10 % , 1 h | no | no | - | no |
| Hydrochloric acid 1 M , 1 h | (yes) | (yes) | (More unspecific dirt on the surfaces) | yes |
| Ammonia buffer 0.055 mM (pH 8, 8.5, 9,) for 1 h | (yes) | (yes) | (More unspecific dirt on the surfaces) | no |
| Sodium hydroxide 0.1 M, 10 min | yes | yes | a) More unspecific dirt on the surfaces<br>b) The a-Si:H surface gets etched or roughened, visible by the changes of the surface color | yes |
| Sodium hydroxide 1 M, 10 min | yes | yes | | yes |

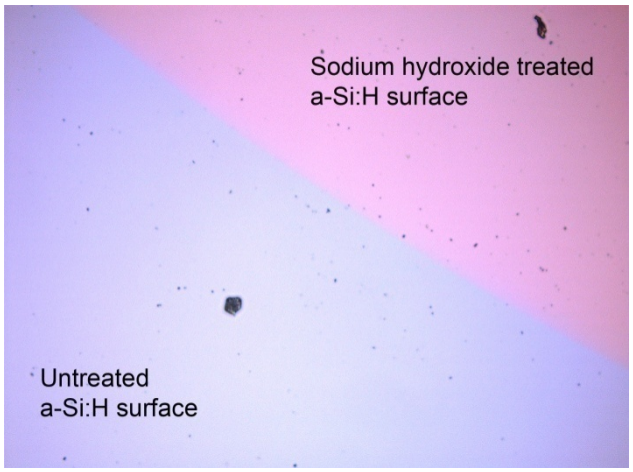


**Figure 11: Microscope picture of the a-Si:H surface: untreated and after sodium hydroxide treatment area. The hydroxide treatment etch or roughens the a-Si:H layer visible by the change of the surface color.**

Besides the base and acid treatment the oxygen plasma could be used to produce a hydrophilic surface on a-Si:H samples. To validate the effect of the oxygen plasma treatment, the samples were be transferred into the plasma system Femto (generator: 2.45 GHz) from the company Diener (Stuttgart, Germany). The sampleswere treated at different temperatures, by 40 W power and 1 mbar oxygen gas pressure and at different times between 1 and 10 min. It could be found that the SU-8 cladding height is stable up to approximately 8 min oxygen plasma treatment, and at longer treatment times (~ 10 min) the SU-8 gets etched on the edge of the sample (see Fig. 12). At higher temperatures of 80°C and 10 min treatment time the SU-8 gets etched significantly, of about 0.6 µm. (See Table 8)

**Table 8: Oxygen plasma treatment and the changes on the surface**

| Oxygen plasma treatment | Damage to the SU-8 cladding | Damages/Changes of the a-Si:H surface | If yes: What kind? | water contact angle (deg.) |
|---|---|---|---|---|
| untreated sample | | | | 50 |
| 1 min, RT | no | no | | 16 |
| 3 min, RT | no | no | | 7 |
| 5 min, RT | no | no | | 15 |
| 8 min, RT | no | no | | 13 |
| 10 min, RT | yes | yes | The SU-8 surface gets etched | 10 |
| 10 min, 80 °C | yes | yes | The SU-8 surface gets etched of about 0.6 µm, detected byAlfa-Step: Before treatment 1.6 µm after treatment 1 µm cladding height. | 12 |

The surface hydrophilic properties in dependence of the oxygen plasma treatment were validated by the water contact angle. The concrete values of the water contact angle are shown in Table 8 and in Fig. 13 the contact angle vs. treatment time is plotted.

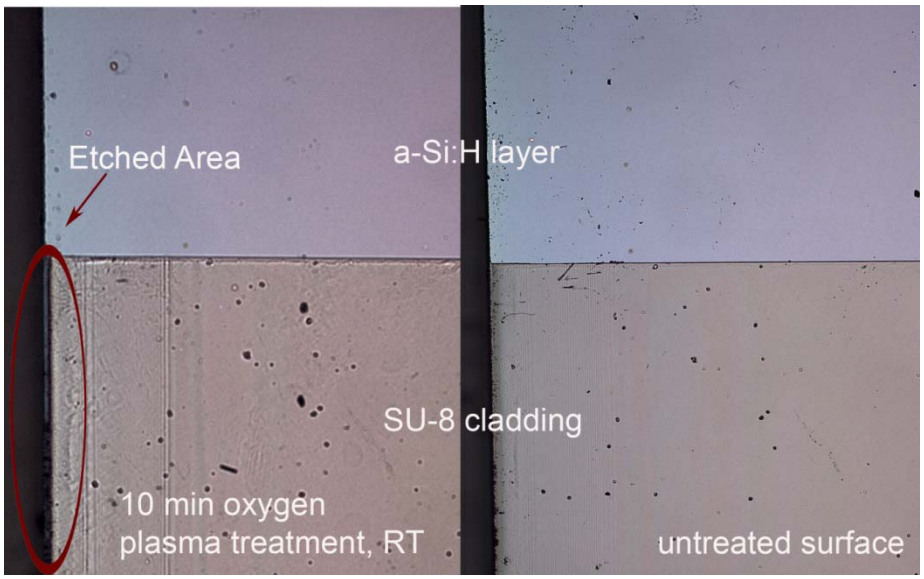


**Figure 12: a-Si:H-SU-8 clad control sample untreated and after 10 min oxygen plasma treatment, RT. After 10 min oxygen plasma treatment at RT the SU-8 cladding gets etched on the edge of the sample.**

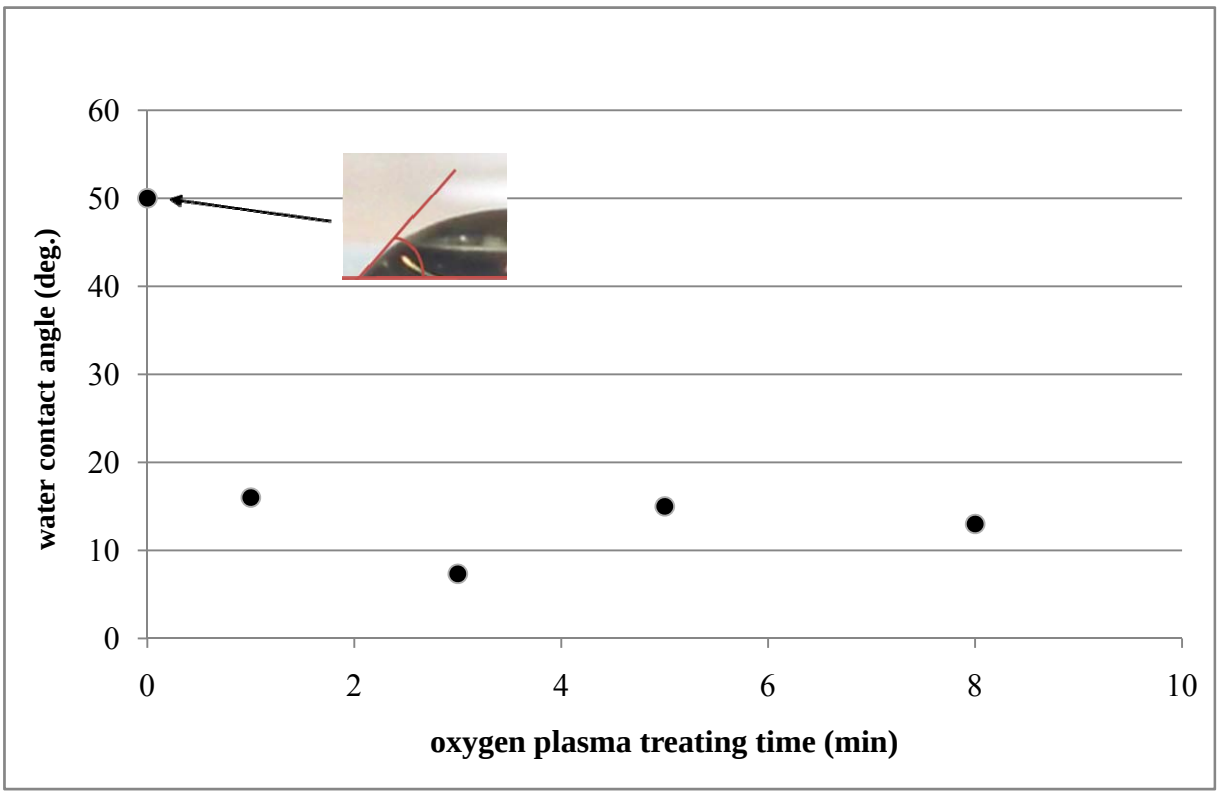


**Figure 13: Plot of the water contact angle (deg.) vs. oxygen plasma treating time (min) at room temperature (RT).**

For the functionalization in different solvents and at different temperature conditions, the chemical resistivity was tested for the a-Si:H-SU-8 clad samples. (See Table 9) It could be found that in hot toluene (60°C) the SU-8 is not stable.

**Table 9: Chemical resistivity of a-Si:H-SU-8 clad samples in different solvents**

| Description of the procedure | See any difference? | If yes: What kind? |
|---|---|---|
| Toluene for 24 h, RT | no | - |
| Toluene 60°C, 3 h | yes | Damage to SU-8 layer |
| Tetrahydrofuran, RT, 6 h | no | - |
| Acetate Buffer pH 5.5 24 h | no | - |
| Methanol, Ethanol, Isopropyl alcohol, RT, 6 h | no | - |
| Chloroform, 10 min | no | no |

## 4.2 Chemical resistivity of PI-Ormoclad samples

For the activation with base and acids, several procedures with nitric acid (10%), hydrochloric acid, ammonia buffer and sodium hydroxide solution were tested. (See Table 10)

Amongst these test only the sodium hydroxide solution makes the surface hydrophilic (water contact angle gets lowered). The disadvantage is that at low treatment times (5 min) the Ormoclad gets damaged and at higher treatment times (30 min) removed from the surface.

Also the polyimide surface gets damaged and partly removed from the surface at higher treatment times.

**Table 10: Activation procedures with base and acids**

| Description of the procedure | Damage to the Ormoclad cladding | Damages/Changes of the PI surface | If yes: What kind? | Hydrophilic PI-surface? |
|---|---|---|---|---|
| Nitric acid 10 % , 1h | no | no | | no |
| Hydrochloric acid 1 M , 1 h | yes | yes | a) More unspecific dirt on the surfaces<br>b) spots/cracks on the Ormoclad cladding | no |
| Ammonia buffer 0.055 mM (pH 8, 8.5, 9) for 1 h | yes | yes | a) More unspecific dirt on the surfaces<br>b) Ormoclad is partly etched | no |
| Sodium hydroxide 1 M, 5 min | yes | yes | a) More unspecific dirt on the surfaces<br>b) Ormoclad is damaged | yes |
| Sodium hydroxide 1 M, 30 min | yes | yes | Ormoclad was removed from the surface, PI got damaged and partly removed from the surface | yes |

Besides the base and acid treatment the oxygen plasma could be used to produce a hydrophilic PI surface. To validate the effect of the oxygen plasma treatment, the samples were be transferred into the plasma system Femto (generator: 2.45 GHz) from the company Diener (Stuttgart, Germany). The samples were treated at room temperature, by 40 W power and 1 mbar oxygen gas pressure at different times between 1 and 10 min and at different temperatures. It could be found that the Ormoclad cladding is stable up to approximately 5 min oxygen plasma treatment, and by longer treatment times the Ormoclad gets damaged. (See Table 11)

**Table 11: Oxygen plasma treatment and the changes on the surface**

| Oxygen plasma treatment | Damage to the SU-8 cladding | Damages/Changes of the a-Si:H surface | If yes: What kind? | water contact angle (deg.) |
|---|---|---|---|---|
| untreated sample | | | | 83 |
| 1 min, RT | no | no | | 12 |
| 3 min, RT | no | no | | 3 |
| 5 min, RT | no | no | | $\leq 3$ |
| 8 min, RT | yes | yes | Ormoclad gets damaged | $\leq 3$ |
| 10 min, 80 °C | yes | yes | Ormoclad and PI gets damaged | $\leq 3$ |

The surface hydrophilic properties in dependence of the oxygen plasma treatment was validated by the water contact angle. At 5 min and higher oxygen plasma treatment times, the contact angle was too low and could not be measured exactly. (See Table 10 and Fig. 13)

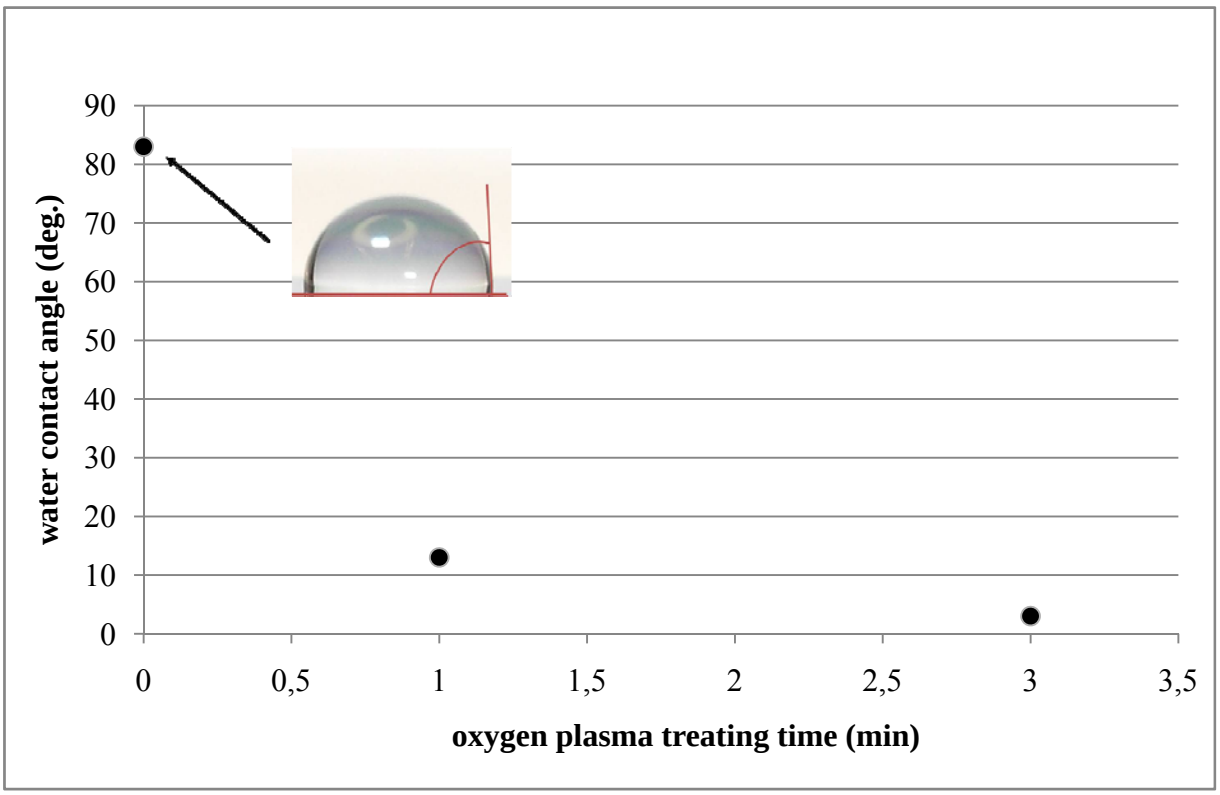


**Figure 14: Plot of the water contact angle (deg.) vs. oxygen plasma treating time (min)**

For the functionalization in different solvents and at different temperature conditions, the chemical resistivity was tested for the PI-Ormoclad clad samples. (See Table 9) It could be found that in hot solvents (toluene 60°C and ethanol 65°C) the PI and Ormoclad layer are not stable.

**Table 12: Chemical resistivity of PI-Ormoclad samples in different solvents**

| Description of the procedure | See any difference? | If yes: What kind? |
|---|---|---|
| Toluene for 24 h, RT | no | - |
| Toluene 60°C, 3 h, stirring; | yes | Damage to PI and Ormoclad layer |
| Methanol, Ethanol, Isopropyl alcohol, RT, 6 h | no | - |
| Ethanol 65 °C, 2 h | yes | unspecific dirt and spots on the PI and Ormoclad layer |
| Acetate Buffer pH 5.5 3 h | no | - |
| Chloroform, 10 min | no | - |

# 5 Functionalization of polyimide and amorphous hydrogenated silicon

In this chapter the functionalization of PI and a-Si:H control samples with amine-, sulfhydryl- and carboxyl groups, as well as the fluorescence labeling and biotinylation are described in detail.

The process of the functionalization was monitored by using several fluorescence labels, such as tertramethyl rhodamine 5-maleimide (TMR5M) and DyLight 649 N-hydroxy succinimide ester (NHS-DyLight). The fluorescence intensities were measured by using the TECAN fluorescence scanner and analyzed with the software ImageJ 1.43u.

The information about the chemicals used in this chapter, such as synthesis can be found in the appendix A.

## 5.1 Photochemical functionalization with carboxyl groups

The functionalization with carboxyl groups has been carried out as described in the literature by Anne Fauchux et. al. [**15**]. In this literature a direct photochemical hydrosilylation with undecylenic acid on hydrogenated silicon to create surface carboxyl groups has been described and proceeded with at short reaction times. For polyimide samples a similar procedure was performed with in the assumption that an oxygen plasma treatment brings reactive oxygen species on the surface that can further react with the alkene in the undecylenic acid. Another reaction possibility on the untreated PI surface is that the benzophenone groups convert under UV-light exposure (~300 nm) into a triplet state intermediate that can further react with the alkenes in the undecylenic acid. The reaction properties of a-Si:H and PI substrate for immobilization of undecylenic acid was tested in this subsection.

**Experimental**

The experiments and their steps for each PI or a-Si:H control sample and the results of the fluorescence scans in pictures are shown in Table 13.

The three, by PECVD, freshly prepared a-Si:H samples (*M120C, M120D, M124*) were treated as follows: One sample was used without pretreatment and two samples were dipped in 40% ammonium fluoride ($NH_4F$) solution for different times (15 sec, 10 min) in assumption to create a fresh Si-H surface and to test if the a-Si:H layer gets damaged by this treatment. It could be found that 10 min dipping of the a-Si:H control sample in 40% $NH_4F$ remove the thin a-Si:H layer completely from the surface. This destroyed a-Si:H control sample (*M120 C*, see Table 13) is not further used in the next steps.

**Table 13: Experiments for direct reactions on the PI and a-Si:H surface**

| | | | Fluorescence scan (λex=633 nm, λem=692 nm) | | |
|---|---|---|---|---|---|
| **Sample Signature** | **Experiments** | **Differences of the sample treatment** | **PMT* 140** | **PMT* 170** | **PMT* 200** |
| ***M97*** | **Protocol for PI samples for direct reaction on the surface: 1)** oxygen plasma treatment, 1 min, 40 W power, 1 mbar, RT **2)** Immediately dipping in functionalization solution of 10% 10-undecylenic acid in MeOH, reaction conditions, UV 302 nm, 3 h **3)** Cleaning: ultrasonic bath 20 min in isopropyl alcohol, RT | 2) without UV supported | 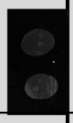 |  | |
| ***M98*** | **4)** Cleaning: 2x ultrapure water, 1x rinsing with glacial acetic acid (98%), 2x ultrapure water, 1x isopropyl alcohol, dried under nitrogen stream **5)** Samples are dipped in EDC-Diamine-solution for 2 h, pH 4.70 | 2) With UV-support 302 nm | 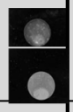 |  | |
| ***M100*** | **6)** Cleaning: 2x ultrapure water, 1x isopropyl alcohol, trying under nitrogen stream **7)** Spotting of the labeling NHS-DyLight solution 50 µM; reaction conditions: 1 h, RT **8)** 2x ultrapure water, 1x isopropyl alcohol, dried under nitrogen stream | Without step 1) and UV supported 302 nm in step 2), |  |  | |
| ***M120 C*** | **Protocol for a-Si:H samples for direct reaction on the surface: 1)** Activation: Dipping in 40% $NH_4F$ solution, time divers **2)** Immediately dipping in functionalization solution of 10% 10-undecylenic acid in MeOH, reaction conditions, UV 302 nm, 3 h **3)** Cleaning: ultrasonic bath 20 min in isopropyl alcohol, RT **4)** Cleaning: 2x ultrapure water, 1x rinsing with glacial acetic acid (98%), 2x ultrapure water, 1x isopropyl alcohol, dried under nitrogen stream **5)** Samples are dipped in EDC-Diamine-solution for 2 h, pH 4.70 **6)** Cleaning: 2x ultrapure water, 1x isopropyl alcohol, trying under nitrogen stream **7)** Spotting of the labeling NHS-DyLight solution 50 µM; reaction conditions: 1 h, RT **8)** 2x ultrapure water, 1x isopropyl alcohol, dried under nitrogen stream | 1) 10 min | | | |
| ***M120 D*** | | 1) 0 min | | 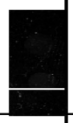 | 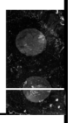 |
| ***M124*** | | 1) 15 sec | |  | 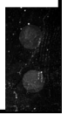 |

* PMT: Photomultiplier tube amplification of the TECAN fluorescence scanner

The three PI control samples (*M97, M98, M100*), used in this test, were different by treated as follows: Two of the PI control samples (*M97*, *M98* see Table 13) were pretreated with oxygen plasma 1 min, to create peroxides on the surface. One of the PI control samples (*M100* see Table 13) was used without any pretreatment.

In the next step (2) the two a-Si:H samples (*M120 D* - untreated, *M124* - 15 sec dipped in the 40% $NH_4F$, see Table 13) and the three PI control samples were transferred into a functionalization solution of 10% 10-undecylenic acid in MeOH in a petri dish. Then an UV lamp[3] with 302 nm light emission was taken to irradiate the a-Si:H samples for 3 h and the two (*M98, M100,* see Table 13 ) PI control samples for 1 h. One of the PI control sample (*M97,* see Table 13), which was before treated with oxygen plasma, was not irradiated with UV light. This PI control sample (*M97*) should give information about the reaction properties

[3] UV Lamp: Modell UVM-57, MID UV 302 nm, 230 V, from the company UVP, Upland, California, USA.

of the peroxide groups that may react with the alkene in the undecylenic acid without further UV support.

After this step (2), the samples were cleaned in isopropyl alcohol with the ultrasonic bath for 20 min, washed with water (2x), than rinsed with glacial acetic acid, washed again with ultrapure water (2x) and isopropyl alcohol (1x), and at last dried under nitrogen stream. Now all PI and a-Si:H control samples were functionalized with carboxyl groups. These functionalized surfaces were in step 5 transferred into the EDC-Diamine solution (EDC and the ethylenediamine solved in MES[4] buffer pH 4.7). In the occurring reaction the carboxylic group via a two step reaction an amide with an amine containing reagent [**54**]. (See Fig. 16) In this experiment, the ethylenediamine was used instead of an amine tagged reactant for biomolecular interactions *e.g.* amine tagged DNA-strands.

This reaction with ethylenediamine leads to surface amines, which were labeled in the following step (7) by spotting with a pipette 5 µl of the 50 µM NHS-DyLight soluion (NHS-DyLight solved in 0.2 M carbonate buffer pH 9.0) on the surfaces. After a reaction time of 1 h, the sample was washed with ultrapure water, isopropyl alcohol and dried under nitrogen stream. The fluorescence intensity of surface bound NHS-DyLight was measured with TECAN fluorescence scanner at 633 nm excitation and 692 nm emission wavelength and analysed with the software ImageJ 1.42u.

**Reference samples**

To verify possible background fluorescence intensities untreated PI and a-Si:H, as well as an oxygen plasma pretreated PI control sample were as reference also labeled with NHS-DyLight and measured over the fluorescence scanner, but no fluorescence intensity could be detected with the highest used PMT amplification of 200. This means that no significant background fluorescence intensity and/or surface amine group concentration exists on the untreated PI and a-Si:H as well as on the oxygen plasma pretreated PI control samples.

To verify the carboxylic group concentration results of the imide moiety of the PI substrate, the untreated and the oxygen plasma activated PI control samples were dipped in EDC-Diamine solution for 2 h and cleaned as mentioned before. After this reaction the resulting amine groups were labeled again with the NHS-DyLight.

It was be found that on the untreated PI sample no and on the oxygen plasma pretreated PI sample a low fluorescence intensity (at PTM 200) occurs. This means that on the untreated PI surface no significant carboxylic group concentration exists. On the other hand, via oxygen

[4] 2-(N-Morpholino)ethanesulfonic acid

plasma some of the surface imide rings got opened and formed a low concentration of carboxylic groups. (See Fig. 15)

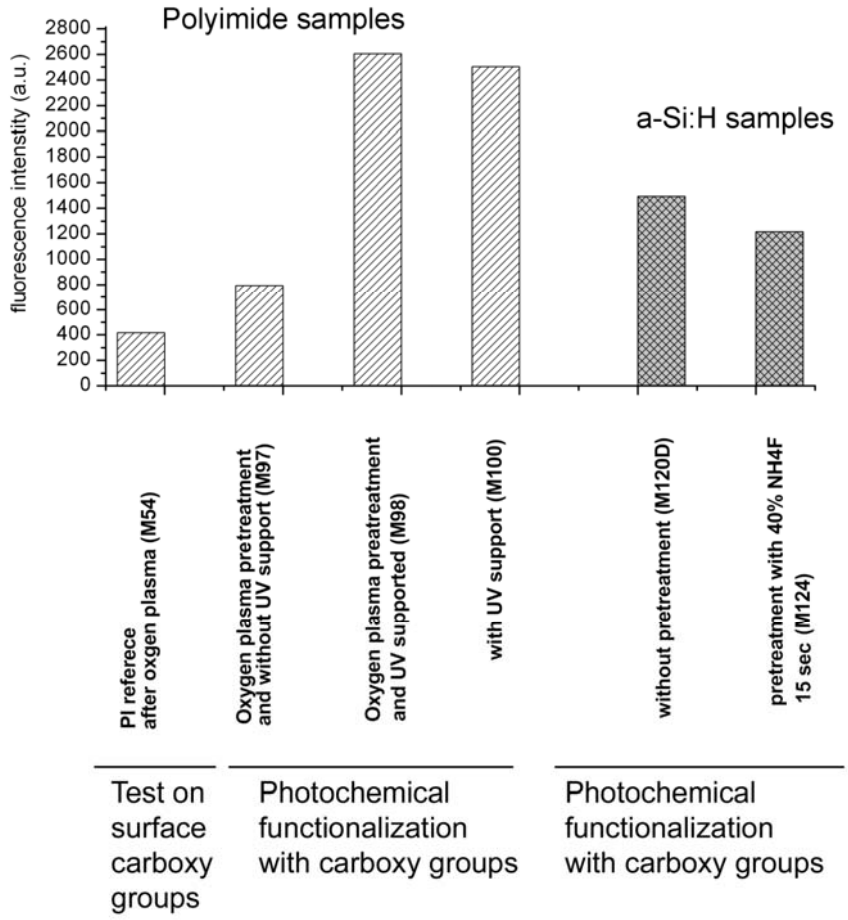


**Figure 15: Measurements of the fluorescence intensity of the labeled amino groups with NHS-DyLight on different samples.**

## Results

The results of the functionalization with carboxylic groups of a-Si:H and PI samples can be concluded as follows: The a-Si:H sample without pretreatment with 40% $NH_4F$ (*M120 D*) showed the highest fluorescence intensity. This means that enough Si-H bonds were available at a freshly prepared sample. Background fluorescence could not be detected.

The PI samples with (*M98*) and without (*M100*) the oxygen plasma pretreatment and with UV support showed almost equal results for fluorescence intensity. These results may indicate that the reaction of the undecylenic acid with the substrate proceeds via triplet state intermediate of the benzophenone group (see Fig. 16) under the described conditions, and is almost independent of the oxygen plasma treatment.

The reference samples show that on the untreated PI surfaces no background fluorescence exists, what means that no free amine and no carboxylic groups are available on the surface.

Only the oxygen plasma treatment leads to a low background fluorescence intensity, which may result from imide ring opening and its conversion into carboxylic groups on the surface. In comparison of the a-Si:H to the PI with undecylenic acid functionalized control samples the PI samples showed a higher fluorescence intensity (see Table 13, PMT 170), which indicate a higher surface concentration of the bound amino groups on the surface.

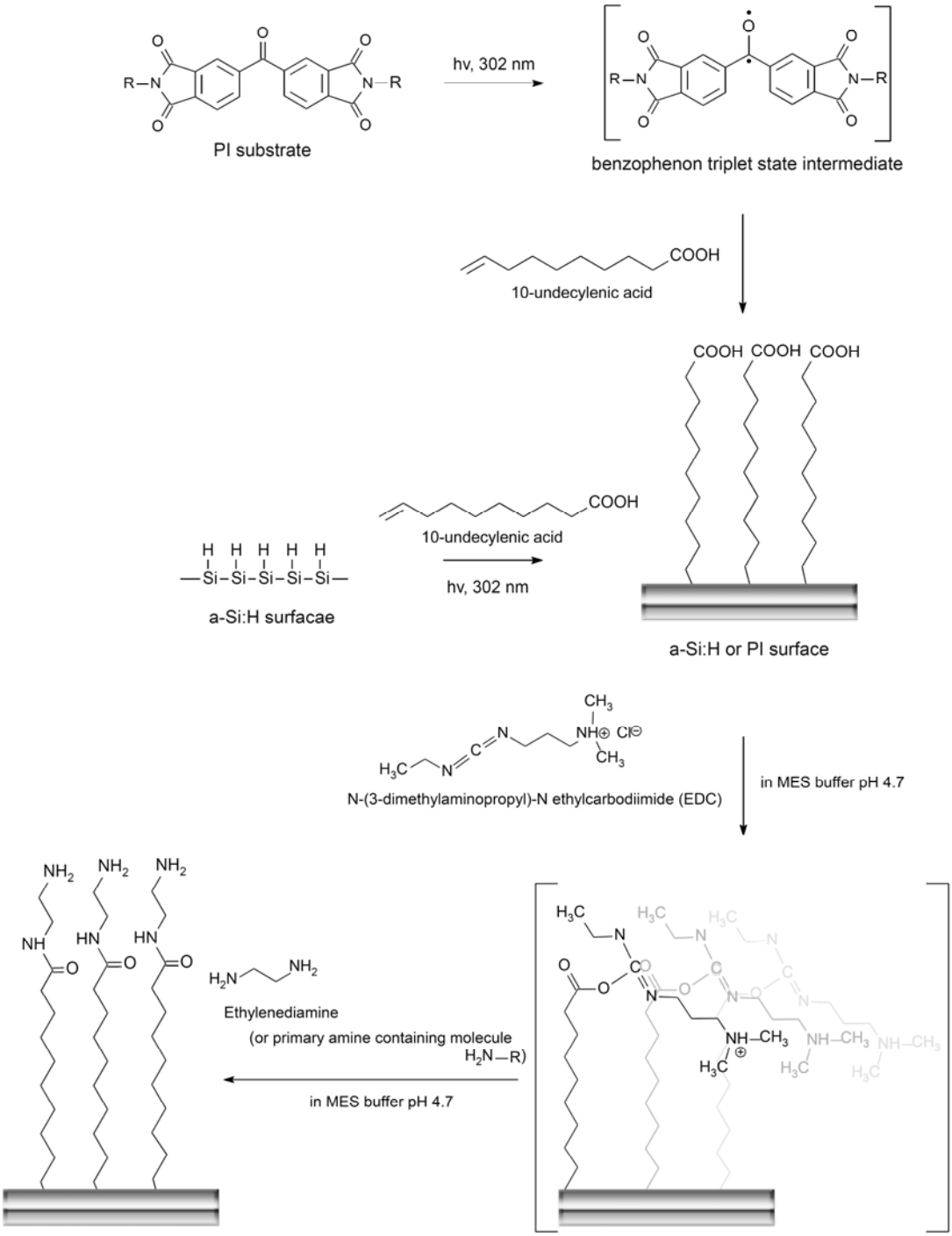


**Figure 16: Reaction path for the polyimide and a-Si:H surfaces for the photoreaction with undecylenic acid, followed by the EDC and ethylenediamie reaction. The amino groups resulting from this reaction were labeled with NHS-DyLight to optimize the reaction conditions.**

## 5.2 Silanization

The functionalization with the silanes MPTMS or APTMS is done in multiple steps consisting of activation, silanization and labeling with TMR5M or NHS-DyLight. The optimization of these steps is outlined below in more detail.

**Activation**

The polyimide and a-Si:H surfaces are relatively chemically inert and hydrophobic. For silanization hydrophilic surfaces with appropriate chemical groups for the reaction with the silanes are needed to guarantee an efficient chemical derivatization. Therefore the activation was employed with the oxygen plasma exposure that did not damage the MZI-layer system. For this purpose the controls samples (2x2 cm) with PI or a-Si:H layer were transferred into the Femto plasma system for different times. (Polyimide: 0, 10, 30 sec and 1, 3, 5 min; a-Si:H: 1, 3, 5, 8 min). For monitoring and optimizing the effect of the different activation times in terms of silanization degree, the oxygen plasma activated samples were dipped in acidic aqueous MPTMS solution for 1 h for polyimide and for 6 h for a-Si:H control samples at room temperature. Afterwards the samples were cleaned in isopropyl alcohol with the ultrasonic bath for 20 min, washed with ultrapure water and isopropyl alcohol and at last dried under nitrogen stream. Then the silanized surface was labelled with 10 µM TMR5M (in ultrapure water with 10% (v/v) isopropanol and 10% (v/v) phosphate buffer 0.05 M pH 7.0) for 1 h. After labeling the control samples were again cleaned, two times with ultrapure water, 1 h shaking in ultrapure water, and again washing one time in ultra pure water and at last one time with isopropyl alcohol and dried under nitrogen stream. The fluorescence intensities of the different samples were then measured at 532 nm excitation wavelength and 575 nm emission filter of the fluorescence scanner. (Results are shown in Fig. 17)

With increase of the oxygen plasma treatment time, the fluorescence intensity can be enhanced, which was attributed to the introduction of a higher density of reactive oxygen species on the surface. These reactive oxygen species can be derivatized with MPTMS and enable the formation of the more dense silane layer, which is accompanied by higher surface coverage with thiols. The highest fluorescence intensity was obtained for PI control samples at 1 min and for a-Si:H samples 3 min oxygen plasma treatment time. At higher treatment times (PI $\geq$ 3 min, a-Si:H $\geq$ 5 min) the fluorescence intensity decreased. This effect may indicate the onset of etching processes of the polyimide leading to erosion of the layer [**37**]. In the case of a-Si:H the reactive oxygen species may be converted at higher oxygen plasma treatment times into an inert silicon oxide layer.

To validate the influence of different acid and basic treatments the 3 min oxygen plasma activated a-Si:H surfaces were treated with sodium hydroxide (NaOH 1 M, 30 sec) and hydrochloric acid (HCl 1 M, 30 sec and 1 h) to create hydroxyl groups. The fluorescence intensity after silanization with MPTMS and labeling with TMR5M were compared with the oxygen plasma only activated a-Si:H surface.

It can be found that an activation only with oxygen plasma exposure for 3 min of a-Si:H layer gives the highest fluorescence intensity.

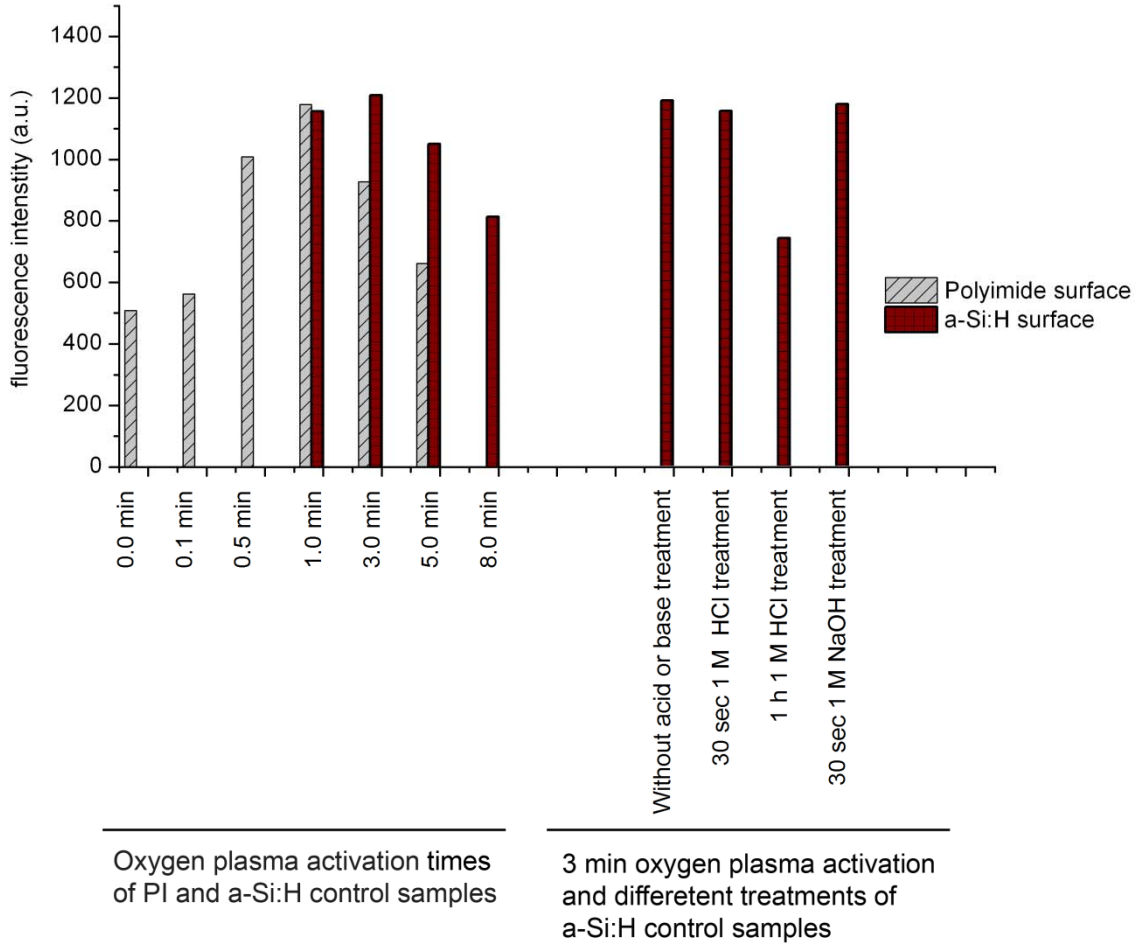


**Figure 17: Optimization of the oxygen plasma activation times and the different additional basic and acid treatments on the activated a-Si:H surface.**

### Silanization with different silanes

The activation with the oxygen plasma formed a hydrophilic surface with increased oxygen concentrations. Some of the oxygen species on the surface may react with alkoxy silanes by condensation forming stable C-O-Si (PI) or Si-O-Si (a-Si:H) bonds between substrate and the silanes 3-Mercaptopropyl trimethoxysilane (MPTMS) and 3-Aminopropyl trimethoxysilane (APTMS). In any case, the hydrophilic surface favors the adhesion of the silane layer. The

silanization yield on the activated PI or a-Si:H surfaces was tested with different MPTMS or APTMS solutions in organic or aqueous solvents. The results are described below.

Silanization with APTMS

The used APTMS solutions are the acidic aqueous APTMS with and without TritonX-100 and the toluene APTMS solution and the acidic aqueous APTMS solution with 50 % (v/v) isopropyl alcohol (ISO).

For the APTMS silanization the 1 min oxygen plasma activated PI and the 3 min oxygen plasma activated a-Si:H samples were dipped in the different 3% (v/v) APTMS solutions for 1 h. Then the samples were cleaned in ultra pure water with the ultrasonic bath for 20 min, afterwards flushed with ultra pure water and isopropyl alcohol and dried under nitrogen stream. The clean and dry samples were then labeled by spotting with an pipette 5 µl of 50 µM NHS-DyLight solution (50 µg NHS-DyLight is dissolved in 1 ml in 0.2 M carbonate buffer pH 9.0) on the surface and let react for 1 h. The labeled samples were cleaned again in ultrapure water (2x), were then shaken for 1 h in ultrapure water, washed one time more in ultrapure water and isopropyl alcohol (1x) and at least dried under nitrogen stream, before measured in the TECAN fluorescence scanner. In Fig. 18 the optimization of the APTMS silanization for a-Si:H and PI samples is illustrated.

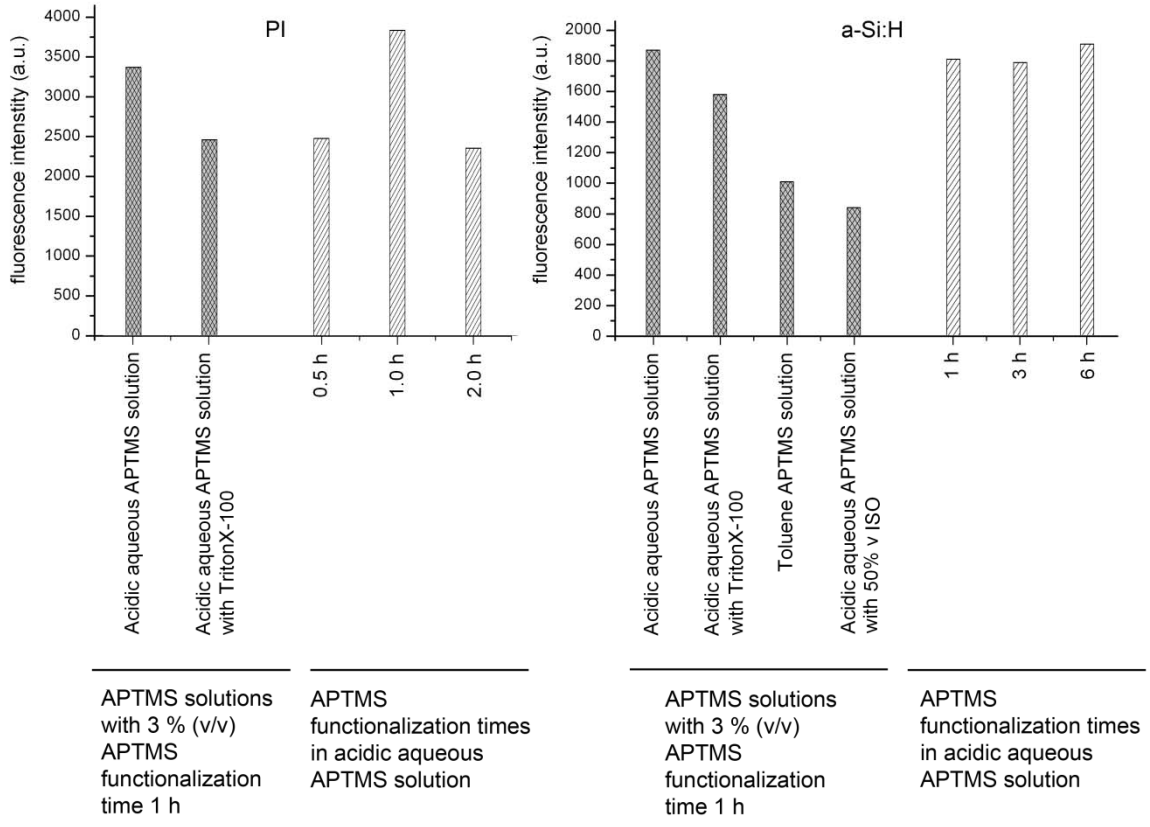


**Figure 18: Optimization of APTMS functionalization for PI and a-Si:H control samples**

The highest fluorescence intensity for PI and a-Si:H silanization was reached with the acidic aqueous APTMS solution, which was therefore adopted as preferable silanization reagent. Next, the optimal reaction time for the APTMS silanization step was examined. For this purpose the a-Si:H control samples where dipped in the acidic aqueous solution for 1, 3 and 6 h and the PI control samples for 0.5, 1 and 2 h. For both substrates the fluorescence intensity does not further increase after 1 h, which indicates that the reaction is complete after that time.

Silanization with MPTMS

The used MPTMS solutions were the acidic aqueous MPTMS (with TritonX-100), the toluene MPTMS solution with and without DMAP (basic catalyst), as well as the THF (Tetrahydrofuran) MPTMS solution.

For the MPTMS silanization the 1 min oxygen plasma activated PI and 3 min oxygen plasma activated a-Si:H samples were dipped in the different MPTMS solutions.

The PI samples were dipped for 1 h in the different 3% (v/v) MPTMS solutions. After silanization the samples were labeled by spotting with a pipette 5 µl of 10 µM TMR5M solution (dissolved in 10% (v/v) isopropanol and 10% (v/v) phosphate buffer 0.05 M pH 7.0) on the surface and then let react for 1 h. The labeled samples were cleaned again in ultrapure water (2x), were then shaken for 1 h in ultrapure water, washed one time more in ultrapure water and isopropyl alcohol (1x) and at least dried under nitrogen stream, before measured in the TECAN fluorescence scanner.

The highes fluorescence intensity for PI silanization was reached for the acidic aqueous MPTMS solution, which was therefore adopted as preferable silanization reagent for the PI substrate. The optimal reaction time for the MPTMS silanization of PI substrates was evaluated by dipping the PI control samples for 30 min, 1 and 2 h in the acidic aqueous MPTMS solution. The fluorescence intensity does not further increase after 1 h, which indicates that the reaction is complete after that time. (See Fig. 19)

The MPTMS functionalization of the a-Si:H samples showed the best results with the THF MPTMS solution for 1 h treatment. This solution contained 15% (v/v) MPTMS in contrast to the other solutions that contain 3% (v/v) MPTMS. The reason for the concentration difference is that in the THF solvent the MPTMS has a good solubility and can be added at higher quantities while the solubility of MPTMS in the other solvents is limited and cannot be increased. The fluorescence intensity behavior for the THF MPTMS solution at higher treatment times show a decrease, what may indicate that the thiol groups concentration on the surface is decreased at higher treatment times.

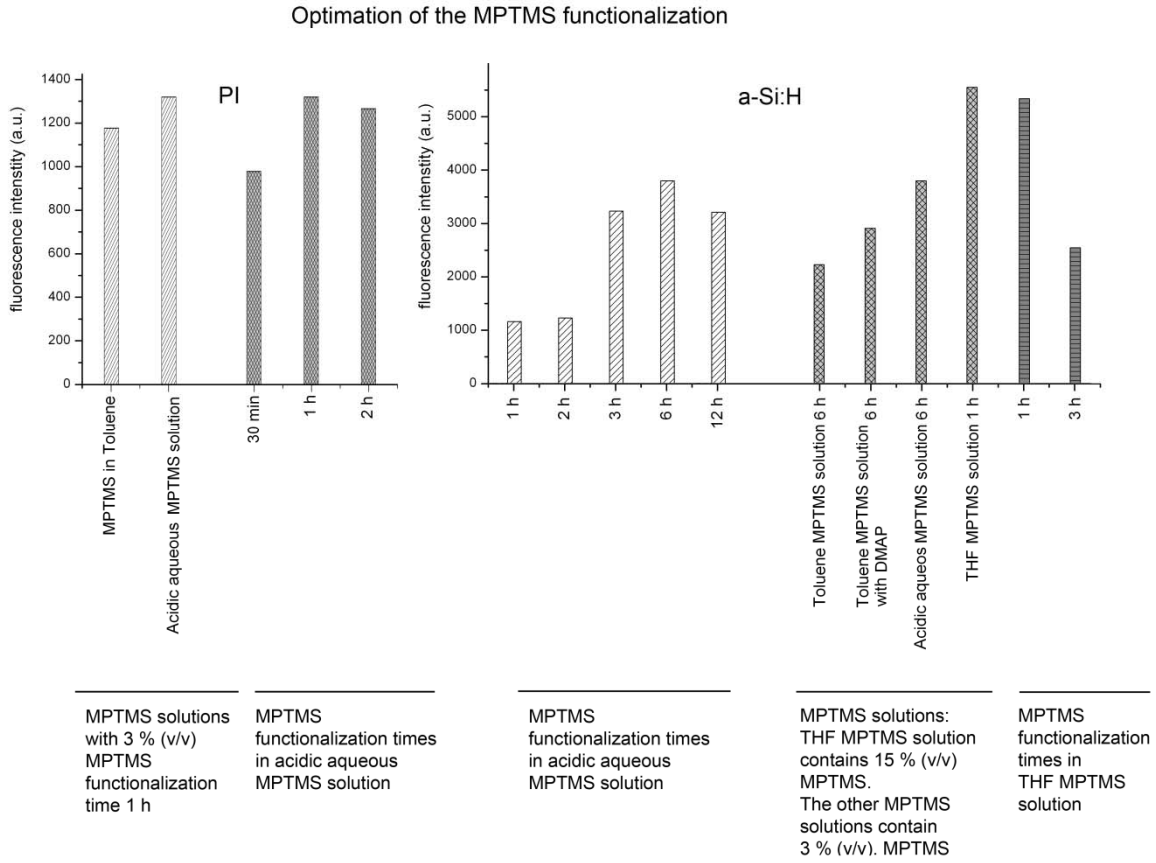


**Figure 19: Optimization of the MPTMS functionalization of PI and a-Si:H control samples. The reason for the concentration difference of the THF MPTMS solution is that the MPTMS has a good solubility in THF and can be added at higher quantities, meanwhile the solubility of MPTMS in the other solvents is lower and cannot be increased.**

By the MPTMS functionalization of the a-Si:H control samples with the acidic aqueous solution not only the fluorescence intensity was lower (than in the THF MPTMS solution), also the surface showed a higher roughness at higher functionalization times (12 h) resulting from some residues of the polymeric condensation of the MPTMS. The polymerization of the MPTMS and the accumulation on the surface may avoid a further increase of the fluorescence intensity, because not all thiol groups in the polymeric layer are available for the binding to the maleimide in the TMR5M fluorescence label. In Fig. 20 the AFM pictures of the a-Si:H samples functionalized with acidic aqueous and with THF MPTMS solution, with the mean roughness ($R_a$) of 3.6 and 0.55 respectively, are shown.

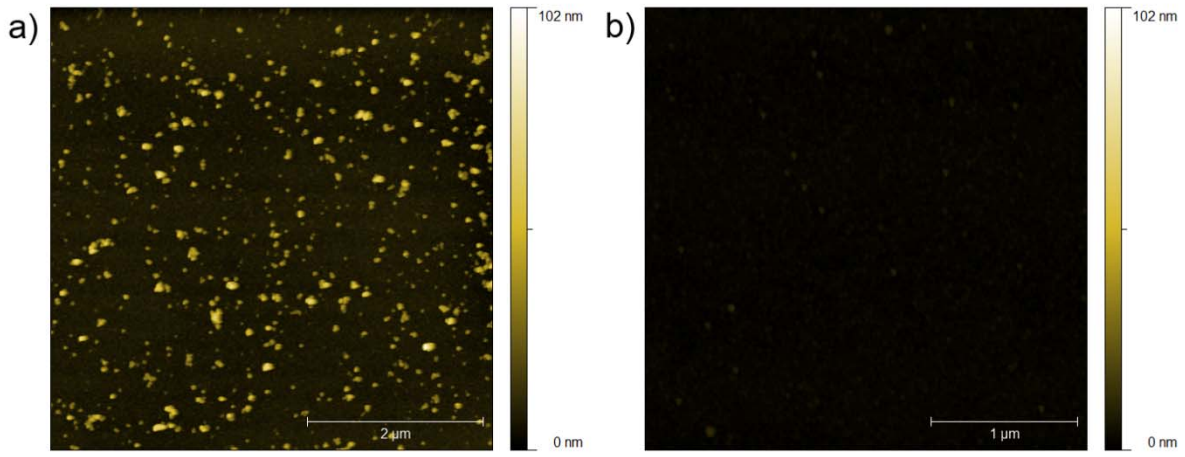


**Figure 20: AFM pictures of the a-Si:H control samples and functionalization with different MPTMS solutions: a) Acidic acid MPTMS solution, 12 h, RT. $R_a$ 3.6 b) THF MPTMS solution 1 h, RT. $R_a$ 0.55**

## 5.3 Fluorescence labeling and Biotinylation

After MPTMS (or APTMS) silanization, the surface carries reactive sulfhydryl (or amine) functional groups which can readily react with the maleimide (or the N-hydroxy succinimide) moiety of the fluorescence label TMR5M (or NHS-DyLight) used for monitoring of the extent of surface modification or of the M-$PEG_2$-biotin (or NHS-$PEG_2$-biotin) used as biorecognition ligand for streptavidin. (See Fig. 8)

The MPTMS functionalization and so the surface covering with sulfhydryl groups lead to considerations and to optimization procedures, that are described at this point. Due to exposure to oxygen *e.g.* air dissolved in reaction solutions, a certain fraction of thiols might be inactivated by oxidation to disulfides. To re-activate such inert disulfides, phosphine reagents such as triphenyl phosphine or tris(2-carboxyethyl)phosphine can be used for reduction [**55**]. The effect of a triphenyl phosphine pre-treatment on the surface concentration of reactive thiols was tested by monitoring the fluorescence intensity after labelling with TMR5M. It was found that this additional reduction step does not improve the resultant surface coverage with reactive thiols.

The reaction time for the maleimide coupling step was optimized with TMR5M and monitoring by UV spectrophotometry in MPTMS solution at 300 nm as described in detail in the literature [**56**]. The optimal reaction time was found by measurement of the transmission at 300 nm at different times (0, 15 min, 30 min, 1 h, 2 h). At 1 h reaction time the transmission does not change anymore and the reaction was complete.

Furthermore, the optimal concentration of the maleimide reagent was determined by spotting with a pipette different concentrations of the label TMR5M (dissolved in ultrapure water with

10% (v/v) isopropanol and 10% (v/v) phosphate buffer 0.05 M pH 7.0.) on the surface and analyzing their fluorescence intensity after 1 h reaction time and washing like it is described before. Thereby, it was found that the fluorescence intensity increases up to a concentration of 5 µM TMR5M, while it stays constant at higher concentrations (see Fig. 21). With this information the concentration of M-$PEG_2$-biotin for functionalization was also fixed at 5 µM under the same conditions as the labeling with TMR5M.

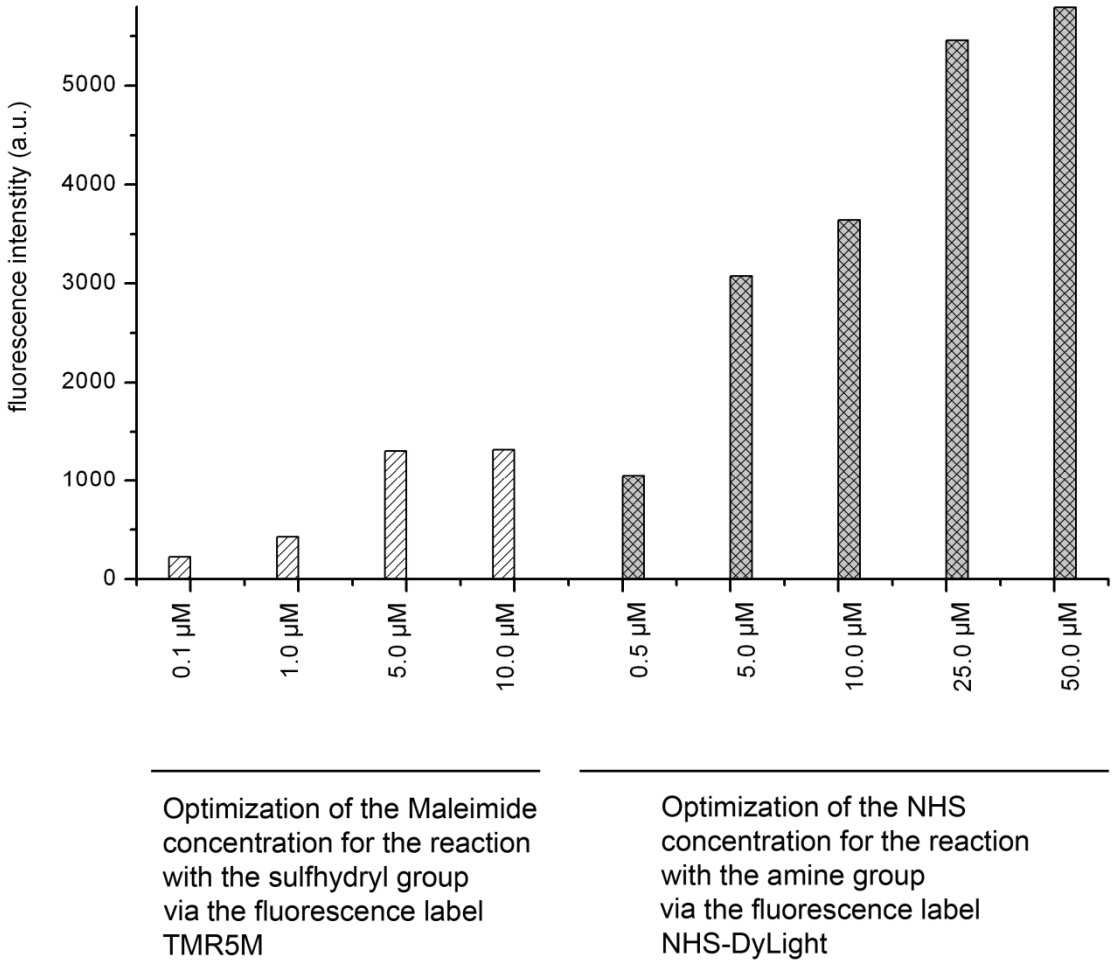


**Figure 21: Optimization of the Maleimide concentration for the reaction with the sulfhydryl group over the fluorescence label TMR5M and the NHS concentration for the reaction with the amine group via the fluorescence label NHS-DyLight**

The APTMS functionalization leads to surface amino groups that can react with the NHS moiety in the NHS-DyLight label or in the NHS-$PEG_2$-biotin. Less efforts were put into optimization of this reaction, as compared to the before described reaction of the thiol with the maleimide group. Only the optimal concentration of the NHS reagent was determined by spotting with a pipette different concentrations of the label NHS-DyLight (dissolved in 0.2 M carbonate buffer pH 9.0) on the amine functionalized surface and analyzing their fluorescence

intensity after 1 h reaction time and washing like it is described before. It was found that the fluorescence intensity increases up to a concentration of 25 µM TMR5M, while it stays almost constant at higher concentrations (see Fig. 21). With this information the concentration of NHS-$PEG_2$-biotin for functionalization was also fixed at 25 µM under the same conditions as the labeling with NHS-DyLight.

## 6 Immobilization of Chromeon 642-streptavidin

For the streptavidin immobilization the MPTMS functionalization way was chosen in the assumption that the sulfhydryl group leads to lower unspecific interactions of the analyte molecules with the functionalized sensor surface. This assumption was based on the fact that the sulfhydryl groups are neutral under physiological conditions avoiding unspecific adsorption by electrostatic interactions which can prevail with amino modified surfaces.

To realize the streptavidin binding to the MPTMS silanized PI and a-Si:H substrates, the maleimide-$PEG_2$-biotin (M-$PEG_2$-biotin) was bound to the surface. The optimized protocol of the functionalization step from activation until the immobilization of streptavidin, for the a-Si:H and PI control samples, is shown in Table 14.

**Table 14: Optimized functionalization protocol for PI and a-Si:H surfaces for streptavidin immobilization**

| Step | Type | Procedure |
|---|---|---|
| **1** | Activation | Oxygen plasma activation, 1 mbar, 40% Power (≈40 W), RT **PI: 1 min; a-Si:H: 3 min** |
| **2 a-Si:H surface** | Functionalization with MPTMS | Samples are dipped in the THF MPTMS solution for 1 h |
| **2 PI surface** | Functionalization with MPTMS | Samples are dipped in acidic aqueous MPTMS solution for 1 h |
| **3** | Cleaning | 5 min[5] ultrasonic bath in isopropyl alcohol |
| **4** | Cleaning | washing with ultrapure water (2x) and in isopropyl alcohol (1x), dried under nitrogen stream |
| **5** | Biotinylation | The samples are dipped in M-$PEG_2$-Biotin solution for 2 h, RT |
| **6** | Cleaning | washing with ultrapure water (2x), shaking in ultrapure water 1 h, washing in ultrapure water (1x) and in isopropyl alcohol (1x) and dried under nitrogen stream |
| **7** | Storage | The samples are stored in vacuum in the exsiccator |
| **(8)** | (Blocking) | The samples are dipped in BSA (0.1 mg BSA/ml 150 mM PBS buffer) and shaken for 30 min in this solution |
| **9** | Cleaning | 30 sec 2x ultrapure water and 30 min shaking in ultrapure water, dried under nitrogen stream |
| **10** | Immobilization of Chromeon 642-Streptavidin | 1 µM Chromeon 642-Streptavidin is spotted with a pipette on the a-Si:H and PI surfaces |
| **11** | Cleaning | The samples are cleaned with ultrapure water 2 x and then dried under the nitrogen stream |

[5] The influence of the ultrasonic bath on the fluorescence intensity was verified, and it was found that the intensity does not change also by 20 min treatment. The surfaces are already clean after 5 min treatment in the ultrasonic bath and so this time is chosen.

For the immobilization of the streptavidin the fluorescence labeled Chromeon 642-streptavidin was chosen to analyse the surface binding and surface concentration of streptavidin on the PI and a-Si:H surfaces. Chromeon 642-streptavidin is streptavidin labeled with an NHS-Ester fluorescence marker [**57**] by reaction with the amino groups in the protein. The binding capacity of biotin to the labeled streptavidin is not influenced by this modification.

To ensure that the thin waveguide layers do not get etched and damaged during the functionalization procedure atomic force microscopy (AFM) is used to provide additional information about the surface roughness at each level of modification. This is important to guarantee a efficient light guiding without additive insertion losses caused by *e.g.* an increased surface roughness.

Valuable information about the success of the respective chemical reactions was obtained by surface analyses with the X-ray photoelectron spectroscopy (XPS), which was carried out after each step of functionalization and after immobilization of streptavidin.

## 6.1 Streptavidin immobilization on the unblocked surfaces

The a-Si:H and PI samples were prepared according to the protocol in Table 14, except step 8, the blocking with BSA. The streptavidin binding to the surface was conveniently monitored and optimized by use of fluorescence-labelled streptavidin. Thus, 1 µM Chromeon 642-streptavidin in 150 mM PBS buffer was spotted four times via pipette on ten biotinylated PI and two a-Si:H samples. After a reaction time of 1 h and cleaning, the samples were analyzed by fluorescence scan. The fluorescence intensity was measured at 633 nm excitation wavelength and 692 nm emission filter with a fluorescence scanner.

For the quantification of the surface concentrations of streptavidin a calibration set was prepared on untreated PI and a-Si:H control samples. To do so, different concentrations (10-200 fmol/mm$^2$) of Chromeon 642-streptavidin were spotted on untreated PI and a-Si:H control samples and the spots were dried at room temperature in the dark to create a solid standard array. With the resulting calibration curves (see Fig. 22) a concentration of 144 ± 20 fmol/mm$^2$ was determined for ten PI biotinylated and a concentration of 27 ± 2 fmol/mm$^2$ for the two a-Si:H samples (Values are listed in Table 15 and 16). The result for the surface coverage with streptavidin on the PI surface is better than what can be expected in theory on a perfectly planar surface. The streptavidin ligand has a size of 4.5×4.5×5.8 nm$^3$ [**58**] and occupies a binding area of 26 nm$^2$. By optimal (100%) packing density the concentration of the streptavidin on the planar surface would be estimated as 64 fmol/mm$^2$. The published

closest coverages of streptavidin on planar surfaces are about 66% (42 fmol/mm$^2$) for two dimensional crystals [**58**,**59**] and 40% (26 fmol/mm$^2$) [**19**] on a silicon surface with a streptavidin monolayer. Higher concentrations of streptavidin, e.g. 37,000 fmol/mm$^2$ have been achieved employing a three-dimensional binding matrix [**10**]. The result of 144 ± 20 fmol/mm$^2$ on the PI substrate evidences a more than two-dimensional binding behavior of streptavidin on the polyimide surface. The results on the a-Si:H surface is like expected for a planar silicon surface with 27 ± 2 fmol/mm$^2$ a moderate concentration value.

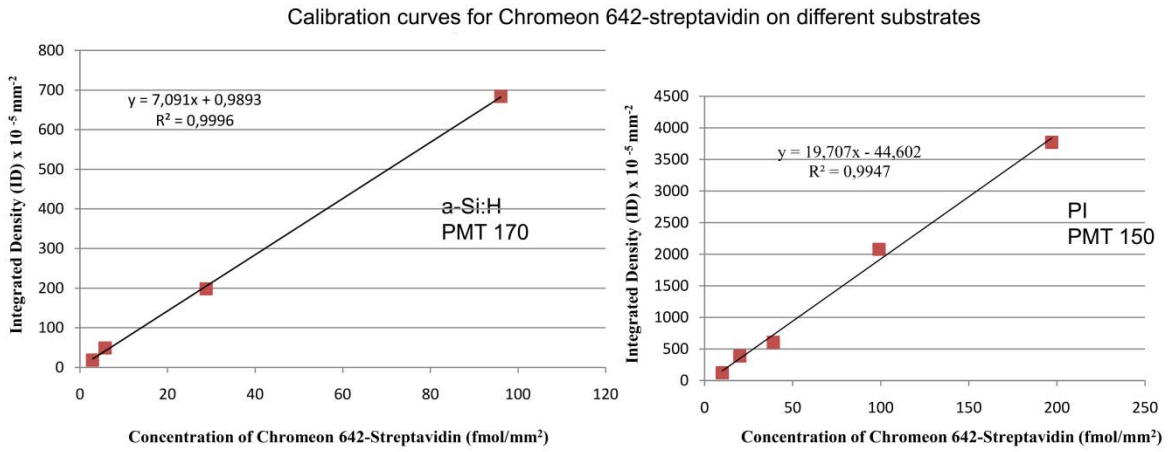


**Figure 22: Calibration curves of Chromeon 642-streptavidin on different substrates**

**Table 15: Concentration of the Chromeon 642-streptavidin on the ten polyimide control samples**

| Slide | Integrated Density (ID) x 10 $^{-5}$ mm$^{-2}$ | Mean concentration of the surface (fmol/mm$^2$) | standard deviation[6] |
|---|---|---|---|
| M205 | 2615 | 135 | 15 |
| M207 | 2583 | 133 | 33 |
| M208 | 2976 | 153 | 24 |
| M209 | 2521 | 130 | 22 |
| M210 | 3210 | 165 | 9 |
| M211 | 3091 | 159 | 47 |
| M212 | 3499 | 180 | 17 |
| M213 | 2809 | 145 | 10 |
| M177 | 2175 | 113 | 15 |
| M176 | 2539 | 131 | 8 |
| Mean Value | 2802 | 144 | 20 |

**Table 16: Concentration of the Chromeon 642-streptavidin on the two a-Si:H control samples**

| Slide | Integrated Density (ID) x 10 $^{-5}$ mm$^{-2}$ | Mean concentration of the surface (fmol/mm$^2$) | standard deviation[6] |
|---|---|---|---|
| M138 | 198.26 | 27.82 | 2.40 |
| M137 | 191.02 | 26.80 | 2.25 |
| Mean Value | 194.64 | 27.31 | 2.32 |

[6] On every sample, four spots of immobilized Chromeon 642-streptavidin were measured. Then the standard deviation over this four spots was performed for every sample.

## 6.2 BSA blocking to verify the specific and unspecific binding behavior

Both specific and unspecific binding can contribute to the concentration of 144 fmol/mm$^2$ streptavidin on the PI and with 27 ± 2 fmol/mm$^2$ streptavidin on the a-Si:H surface in above binding experiments on the biotinylated control samples. To deconvolute specific and unspecific binding contributions, streptavidin binding was determined on reference samples with silanized surface and biotinylated surface before and after blocking unspecific binding sites with BSA. No fluorescence of Chromeon 642-streptavidin could be detected on the prepared silanized reference samples after BSA blockade. In contrast, the unblocked untreated PI samples showed an unspecific binding of 63 ± 25 fmol/mm$^2$ of Chromeon 642-streptavidin to the polyimide surface. The BSA blocked biotinylated PI surface on the other hand showed after Chromeon 642-streptavidin immobilization an fluorescence intensity corresponding to approximately 80 fmol/mm$^2$ streptavidin on the biotinylated BSA blocked PI surface. This proves that there is indeed a specific binding of streptavidin to the biotinylated PI surface.
On the a-Si:H surface a similar behavior can be found, and after BSA blocking a fluorescence intensity corresponding to approximately 20 ± 2 fmol/mm$^2$ streptavidin on the biotinylated BAS blocked a-Si:H surface can be detected.
However, the non-negligible unspecific binding suggests that there is still some room for improvement of the surface chemistry in order to reduce non-specific binding contributions.
The use of BSA may lead to an unspecific blocking of loaded groups on the sample surfaces, and because of the big size of the albumin protein, also biotin binding sites may be blocked for a binding to the Chromeon 642-streptavidin. The blocking strategy with iodoacetamide and *N*-ethylmaleimide can be used to block specifically the free thiol groups of the silanized or biotinylated PI or a-Si:H sample surfaces. To prove if this more specific blocking strategy does lead to a reduction of the unspecific binding sites, the possibilities of iodoacetamide and *N*-ethylmaleimide were tested as described before for the BSA. It could be found that neither iodacetamide, nor N-ethylmaleimide do suppress the unspecific interactions, because the blocked and unblocked silanized reference samples shows almost similar fluorescence intensities, which proves that the unspecific interactions could not be reduced.
So the BSA blocking is here the best strategy to suppress unspecific interactions of the a-Si:H and PI surfaces with the Chromeon 642-streptavidin.

## 6.3 AFM analysis of the optimized modified surfaces

While a roughened surface might yield higher surface areas and consequently more ligands on the sensing layer, the thickness and surface roughness of the waveguide layer are critical factors, which have to be kept under careful control. For this reason the surface roughness were monitored by atomic force microscopy (AFM). PI and a-Si:H samples were analyzed by AFM in tapping mode before treatment, after MPTMS modification and biotin functionalization, as well as after streptavidin immobilization (see Fig. 23, 24).

**AFM analysis of a-Si:H control samples**

The untreated a-Si:H thin film, processed by the PECVD, showed a smooth surface with a mean roughness, $R_a$, of 0.54 nm. After the MPTMS functionalization the surface roughness stayed almost constant at a $R_a$ of 0.51 nm. The surface behavior of the biotin functionalized sample was similar, with a $R_a$ of 0.60 nm, and also did not change much after Chromeon 642-strepavidin immobilization, with a $R_a$ of 0.53. These results prove that the proposed a-Si:H film functionalization method does not cause a significant change of the surface roughness.

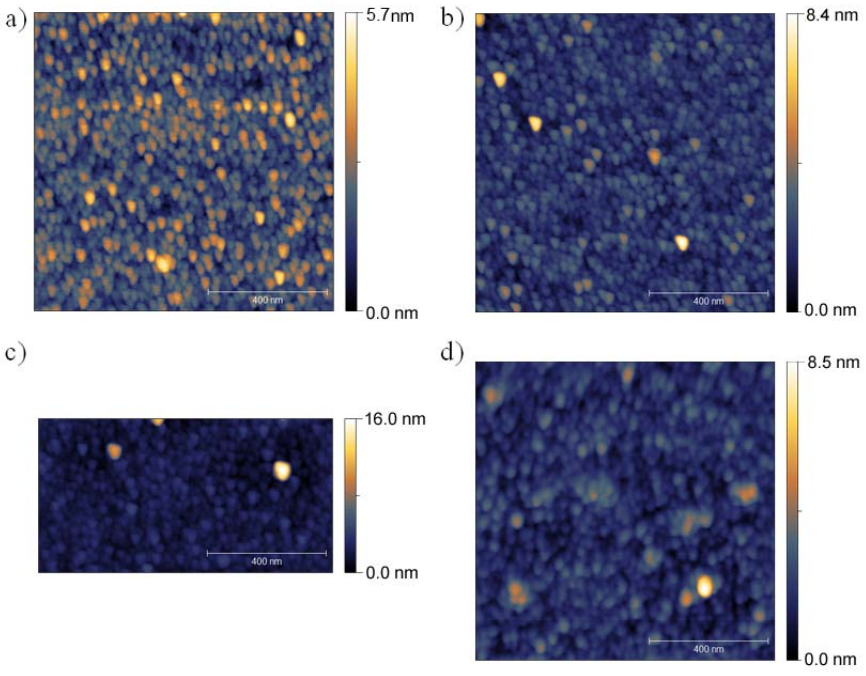


**Figure 23: AFM measurements of the a-Si:H surface for a) the untreated surface, b) the MPTMS functionalized surface, c) the biotin functionalized surface and d) the surface after immobilization of Chromeon 642-streptavidin**

### AFM analysis of PI control samples

The untreated polyimide film showed a smooth surface with a mean roughness, $R_a$, of 0.379 nm. After the MPTMS functionalization the surface roughness increased to a $R_a$ of 0.56 nm and some nanoporous structures with a maximal depth of 10 nm with a diameter of up to 50 nm has been found. The surface behavior of the biotin functionalized sample was similar, with a $R_a$ of 0.57 nm. After the immobilization of Chromeon 642-streptavidin the surface shows in comparison less nanoporous structures and the maximal depth was about 3 nm.

These results prove that the proposed polyimide film functionalization method does not cause a significant change of the surface roughness. The variations in the sub-nanometer range do not induce an appreciable propagation loss of the guided light, when the polyimide is used as waveguide layer in evanescent wave photonic biosensors.

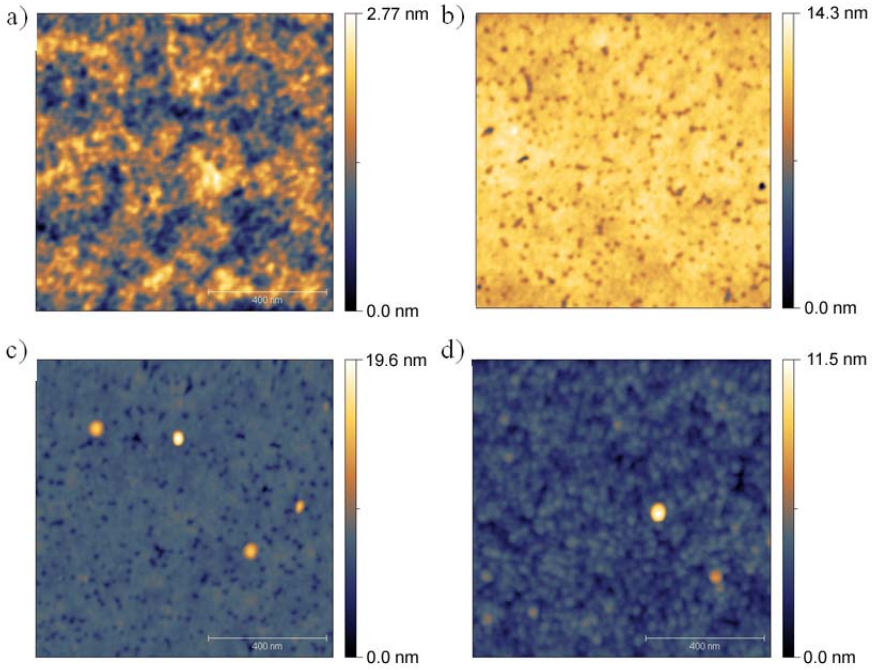


**Figure 24: AFM measurements of the polyimide surface for a) the untreated surface, b) the MPTMS functionalized surface, c) the biotin functionalized surface and d) the surface after immobilization of Chromeon 642-streptavidin**

## 6.4 XPS analysis of each step of the optimized functionalization procedure

Surface chemical compositions as investigated by XPS with a takeoff angle of 30 ° can give valuable information on the progress and success of surface reactions. Thus, XPS spectra have been acquired for the untreated PI and a-Si:H surface, after the oxygen plasma treatment, the MPTMS and biotin functionalization steps, as well as after the streptavidin immobilization, after each individual step has been optimized. For a better comparison of the PI and a-Si:H samples, each substrate is fabricated on the same day and stored under the same conditions before they are functionalized according to the protocols, and at finaly measured with the XPS.

**XPS analysis of a-Si:H control samples**

The untreated a-Si:H surface show the expected peaks of oxygen (531.54 eV), nitrogen (396.29 eV) and carbon (283.79), as well as the peaks of silicon (149.75 and 99.86 eV) according to the composition of the amorphous hydrogenated silicon surface (see Fig. 1, section 1.1). In section 1.1 the variation of the oxygen content on the surfaces in dependence of the storage in air was described. For the used protocol, it is assumed that due to the oxygen plasma treatment, the oxygen content on the surface is no critical factor, and so the samples are stored in air and still contain silicon oxide on the surface.

By deconvolution of the different atom peaks of the XPS spectra with the software CasaXPS Version 2.3.15 and peak identifyication supported by different literatures [**60**,**61**,**62**,**63**], information on the relative surface concentration of the different bonding states of the atomic species and how they vary during the surface modification process can be derived. Figure 25 shows the deconvoluted peaks before and after the optimized functionalization steps and after the streptavidin immobilization. In Fig. 26 and Table 17 the relative atom composition of the surface at the distinct levels of modification as determined by integration from the atom peaks of the XPS spectra are summarized.

The oxygen plasma treatment, as the first step of the functionalization protocol, oxygenizes the silicon surface, which can be seen from the increaseof the oxygen content (see Fig. 26). Furthermore, the plasma treatment cleans the surface, which can be recognized by the decrease of the carbon and the nitrogen concentration on the surface.

The analysis of the deconvoluted oxygen peak shows that some ether like oxygen species (Si-O or Si-O-Si) and peroxides (534.2 eV) occur on the surface after plasma treatment, meanwhile the nitrogen peak and as result the binding status of the nitrogen atoms stays constant. Generally the nitrogen peaks on the a-Si:H surface are shifted, which shows that the

nitrogen is bound as the silicon nitride ($Si_xN_y$, 396.4 eV), with only a small content of nitrogen oxide (N-O, 397.0 eV) bonding.

The biggest influence of oxygen plasma can be recognized by the carbon and silicon peak. The carbon gets oxygenized and partly removed from the surface, so that only a small rest concentration remains, which may belong to the carbon that is covalently bound to the silicon (Si-C, 282.8 eV). The silicon peak shows before treatment already a peak splitting in silicon (99.5 eV) and silicon oxides ($Si_xO_y$, 102.6 eV), because the sample is stored in air before use. With the oxygen plasma treatment the silicon oxides get more than doubled.

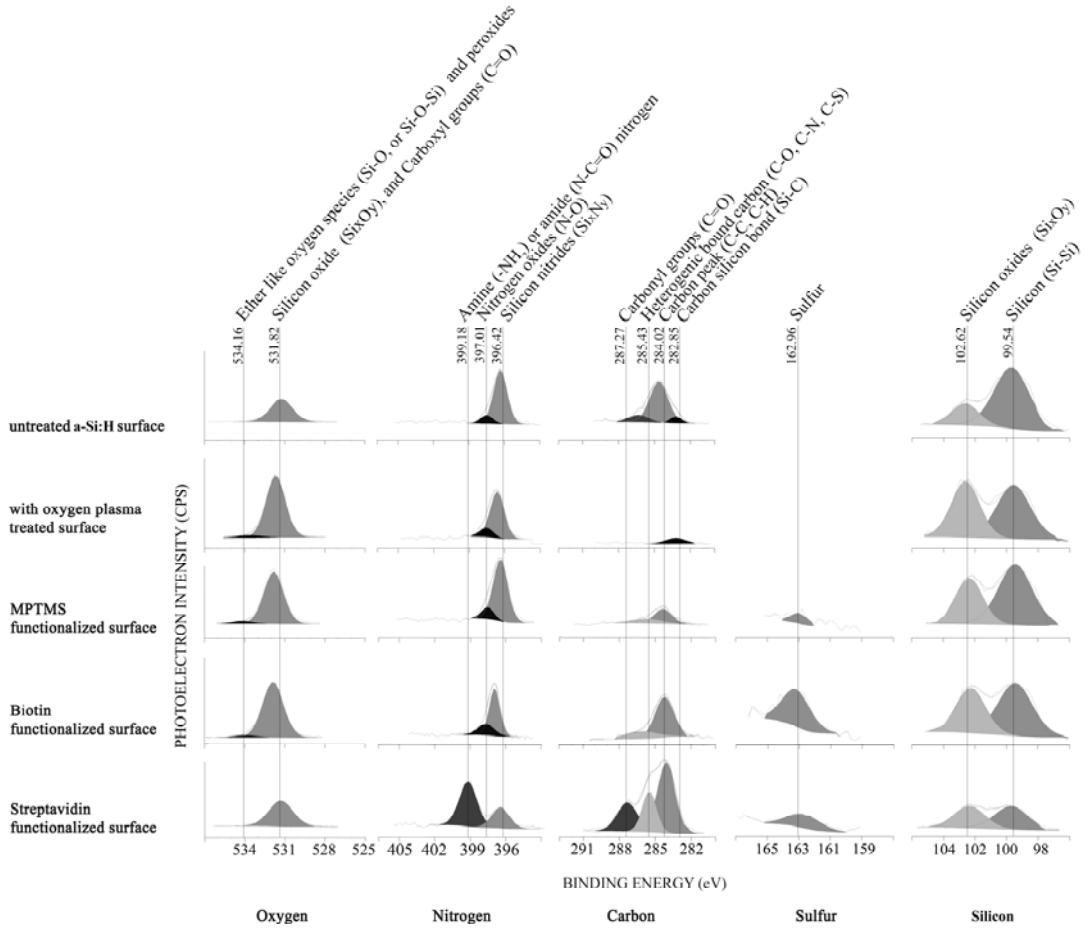


**Figure 25: Deconvoluted XPS-spectra of the relevant peaks before and after the different functionalization steps and after streptavidin immobilization.**

The next functionalization step, the dipping of the activated a-Si:H control samples into the MPTMS solution in THF for 1 h, shows no significant changes in the XPS spectra for the oxygen and nitrogen peaks. A significant change can be recognized for the carbon concentration and the introduction of a sulfur peak to the XPS spectra (see Fig. 26 and Table 17), which was not present before. The detected sulfur concentration of the surface result

from the sulfur atom per unit MPTMS and is directly proportional to the bound MPTMS concentration on the surface. The carbon peak can be deconvoluted into subpeaks of the carbon bond (C-C, C-H, 284.0 eV) and the carbon bond to heteroatoms such as nitrogen, oxygen or sulfure (285.4 eV). This heterogenic bound carbon subpeak could contain ethers (C-O-C), carbon oxygen (C-O, C-OH), carbon nitrogen (C-N) or carbon sulfur (C-S) compounds, but these structures cannot be further resolved from the XPS spectra. In the case of the MPTMS functionalization step, the heterogenic bound carbon subpeaks may contain only the terminal carbon of the propyl chain with the sulfur, which is supported by the atom ratio of 1:3.3 for heterogenic bound carbon to other carbon species. The split silicon peak shows only a low change of the silicon oxide to silicon ratio, whereas the relative silicon percentage of all increased. (See Fig. 25) This results are in course of the surface functionalization.

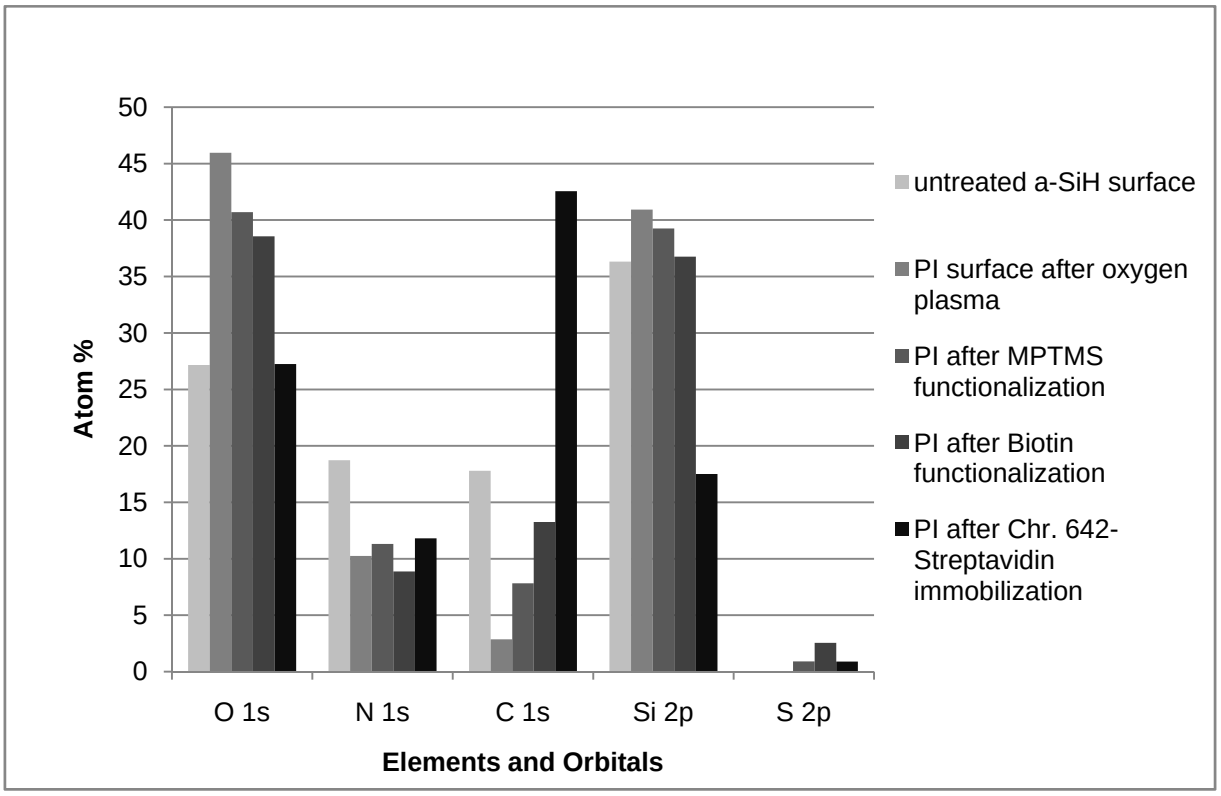


**Figure 26: Atom composition of the polyimide surfaces before and after the functionalization steps and the immobilization of streptavidin.**

**Table 17: Surface composition of the elements before and after each step of functionalization and immobilization of Chromeon 642-streptavidin**

| | untreated a-SiH surface | | PI surface after oxygen plasma | | PI after MPTMS functionalization | | PI after Biotin functionalization | | PI after Chr. 642-Streptavidin immobilization | |
|---|---|---|---|---|---|---|---|---|---|---|
| **Elements and Orbitals** | **Atom %** | **Standard deviation** | **Atom %** | **Standard deviation** | **Atom %** | **Standard deviation** | **Atom %** | **Standard deviation** | **Atom %** | **Standard deviation** |
| O 1s | 27.16 | 0.62 | 45.95 | 0.65 | 40.71 | 0.70 | 38.56 | 0.62 | 27.25 | 0.63 |
| N 1s | 18.73 | 0.62 | 10.25 | 0.54 | 11.31 | 0.38 | 8.88 | 0.36 | 11.81 | 0.61 |
| C 1s | 17.79 | 0.93 | 2.86 | 0.54 | 7.82 | 0.95 | 13.25 | 0.86 | 42.56 | 0.98 |
| Si 2p | 36.32 | 0.72 | 40.93 | 0.63 | 39.26 | 0.70 | 36.76 | 0.65 | 17.50 | 0.59 |
| S 2p | | | | | 0.90 | 0.26 | 2.55 | 0.30 | 0.89 | 0.25 |

The following surface modification step, the binding of M-PEG$_2$-biotin to the silanized surface, increases the carbon concentration and the sulfur concentration on the surface, because the biotin contain one sulfur atom per molecular unit M-PEG$_2$-biotin. (See Fig. 26 and Table 17) The silicon, oxygen and nitrogen concentration on the surface goes down and the peak deconvolution do not show any significant changes (see Fig. 25).

The streptavidin binding to the biotinylated a-Si:H surface gave the most significant change in the XPS spectrum. The carbon and nitrogen concentration increased, while the concentrations of oxygen, silicon and also sulfur degreased. (See Fig. 26 and Table 17) The peak deconvolution of the nitrogen peak shows now a high concentration on amines and amides (amine/amide peak at 399.2 eV). Also the carbon peak splits in several subpeaks of carbonyl (C=O, 287.2 eV), heterogenic carbon (C-O, C-N, C-S, 285.4 eV) and the carbon peak (284.0 eV). This behavior indicates that the binding of streptavidin to the surface was successful and support the results from the fluorescence measurement.

### XPS analysis of PI control samples

The untreated PI surface shows the expected peaks of oxygen (531.21 eV), nitrogen (399.71 eV) and carbon (283.96 eV), as well as the peaks of silicon (152.24 and 101.21 eV) according to the composition of the polyimide Pyralin® PI-2771. (See Fig. 2, section 2.1) By deconvolution of the different atom peaks of the XPS spectra, information on the relative surface concentrations of the different bonding states of the atomic species and how they vary in the course of the surface modification process can be derived. In Fig. 27, a detailed overview of the main peaks of such deconvoluted spectra before and after the functionalization steps are given. The relative atom compositions of the surface at the distinct

levels of modification as determined by integration from the atom peaks of the XPS spectra are summarized in Fig. 28 and Table 18.

The first step of the polyimide surface modification protocol, the oxygen plasma activation, increases the oxygen content on the surface, while the carbon peak decreases (Fig. 28 and Table 18). The analysis of the oxygen peaks in the XPS spectra shows that especially the concentration of carbonyl oxygen (C=O) and the peak of C-O species is increased. The carboxyl groups (O=C-OH) are still present after the treatment, but low concentrated, and shows that the oxygen plasma is not useful to generate a reasonable number of carboxyl groups on the surface, which is an important difference to alkaline hydrolysis [**64**,**65**,**66**].

In the literature it is suggested that the oxygen plasma causes a formation of ether and other C-O species, such as peroxides, on the surface that lead to an etching process of the polyimide via the formation of carbon dioxide and monoxide gas [**37**]. From the results it might be concluded that the oxygen plasma first forms a critical level of highly reactive oxygen species on the surface before a significant etching process starts. Via increase of these reactive oxygen groups one should be able to regulate the MPTMS binding capacity. At a critical level of the oxygen concentration on the surface a significant etching process occurs. This leads to a decrease of adhesion and lower binding of MPTMS, and thus of subsequent biotin ligand and streptavidin as well. In the XPS spectra also a change of the nitrogen peak can be noticed upon plasma oxygen treatment. Close to the original amine ($-NH_2$) and amide (O=C-N) peak an additional peak of nitrogen oxides (N-O) can be found (Fig. 27). Further, the carbon C-C/C-H peak is decreased while C=O and C-O are both increased. This is supposed to be favorable for the bonding and adhesion of the subsequent silane layer.

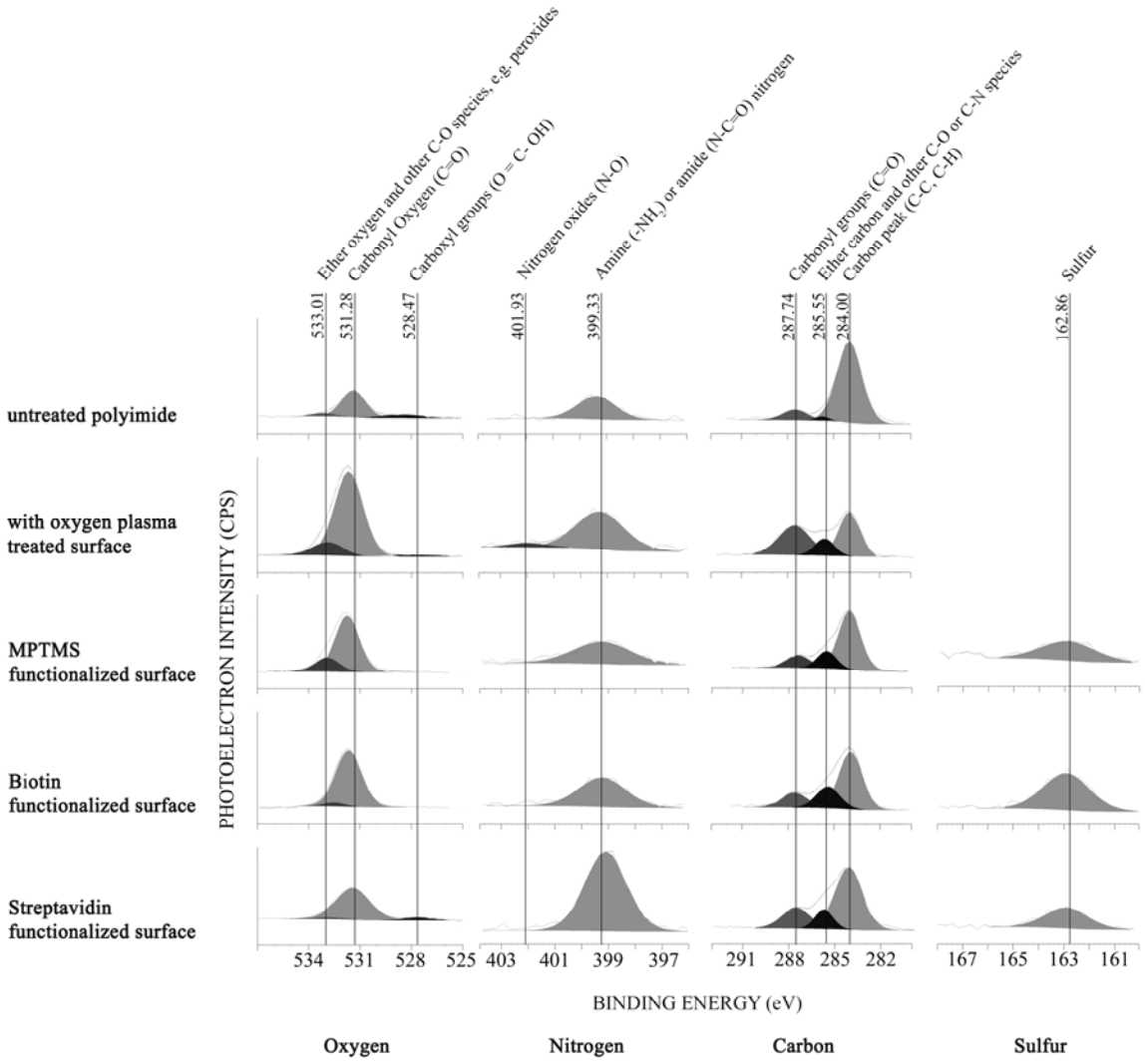


**Figure 27: Deconvoluted XPS-spectra of the relevant peaks before and after the different functionalization steps and after streptavidin immobilization on PI samples**

The next functionalization step is the dipping of the oxygen plasma activated polyimide films into the acidic aqueous MPTMS solution. As can be seen from Fig. 27, the relative intensity of the O1s peak decreases while that of the C1s peak slightly increases as expected. The resulting changes in the atom bonding states of the XPS spectra indicate a decrease of the carbonyl groups (e.g. peak at 287.7 eV), while the C-O species increase (peak at 285.6 eV). This behavior may stem from the reaction of MPTMS with surface bound oxygens. In this reaction reactive oxygen groups (e.g. C-O-H) react with alkoxysilanes of MPTMS by a condensation reaction forming a stable C-O-Si bond leading to covalent attachment to the surface. The change in the oxygen peaks, especially the fact that the carboxyl group peak vanishes after MPTMS functionalization, reveal that the carboxyl groups completely react with the MPTMS. MPTMS carries one sulfur atom, its binding to the surface introduces a sulfur peak in the XPS spectrum which was not present before (see Fig. 27). From the

integral, a sulfur concentration on the surface of 1.15% can be calculated (see Fig. 28 and Table 18).

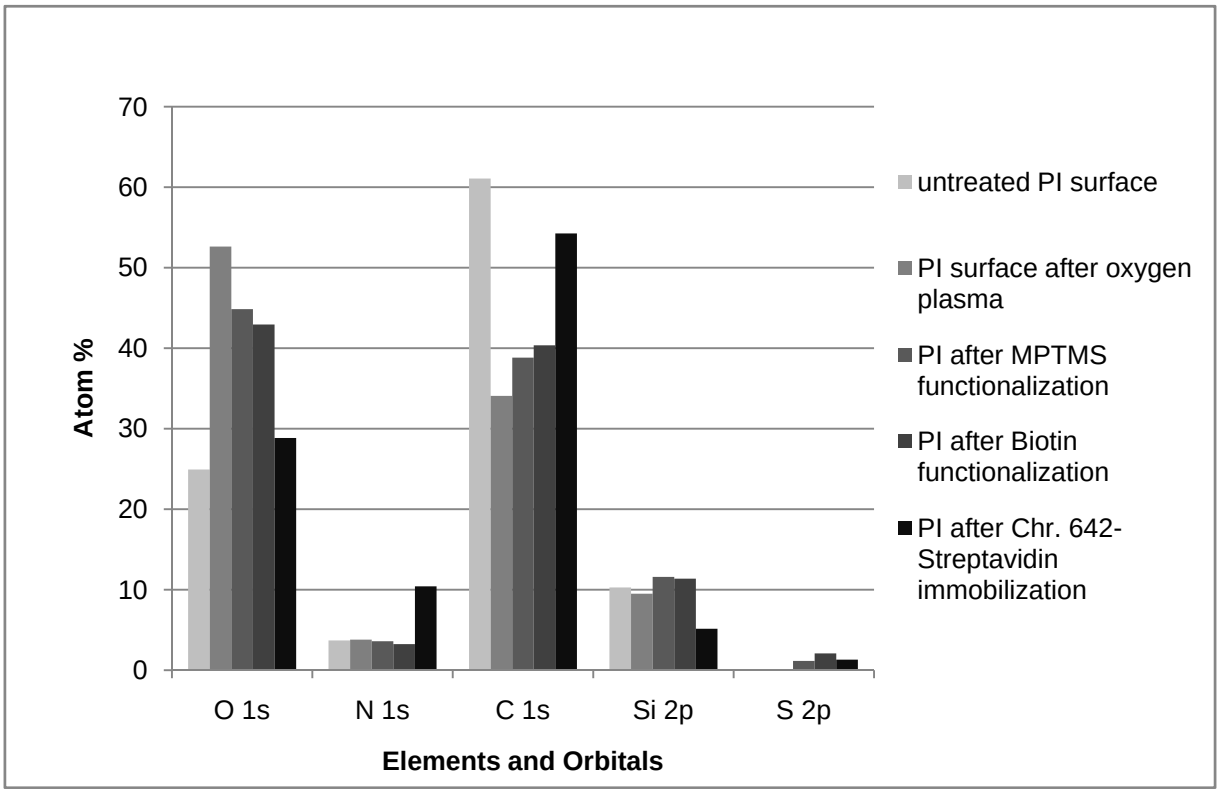


**Figure 28: Atom composition of the polyimide surfaces before and after the functionalization steps and the immobilization of streptavidin.**

**Table 18: Surface composition of the elements before and after each step of functionalization and immobilization of Chromeon 642-streptavidin**

| | untreated PI surface | | PI surface after oxygen plasma | | PI after MPTMS functionalization | | PI after Biotin functionalization | | PI after Chr. 642-Streptavidin immobilization | |
|---|---|---|---|---|---|---|---|---|---|---|
| **Elements and Orbitals** | **Atom %** | **Standard deviation** | **Atom %** | **Standard deviation** | **Atom %** | **Standard deviation** | **Atom %** | **Standard deviation** | **Atom %** | **Standard deviation** |
| O 1s | 24.94 | 0.66 | 52.62 | 0.58 | 44.85 | 0.56 | 42.93 | 0.55 | 28.84 | 0.63 |
| N 1s | 3.69 | 0.48 | 3.79 | 0.38 | 3.60 | 0.51 | 3.23 | 0.37 | 10.42 | 0.57 |
| C 1s | 61.08 | 0.83 | 34.08 | 0.59 | 38.82 | 0.60 | 40.36 | 0.62 | 54.26 | 0.74 |
| Si 2p | 10.28 | 0.39 | 9.50 | 0.33 | 11.59 | 0.37 | 11.38 | 0.34 | 5.16 | 0.33 |
| S 2p | – | – | – | – | 1.15 | 0.16 | 2.10 | 0.16 | 1.32 | 0.20 |

Like MPTMS, also M-$PEG_2$-biotin has incorporated one sulfur atom per molecule. Therefore, the concentration of sulfur on the surface should again increase with the biotinylation. In the case of a 100% reaction between the maleimide groups of M-$PEG_2$-Biotin with the thiol functional groups of the thiol-modified surface the sulfur concentration is expected to be

twice as high as on the MPTMS functionalized sample. In the measurements the sulfur concentration was 1.8 times higher than by the MPTMS functionalized sample (Fig. 27), indicating a reaction rate of approximately 80%.

The XPS spectrum after the immobilization of Chromeon 642-streptavidin is mainly characterized by significant increases of nitrogen (amine/amide peak at 399.3 eV) and carbon on the surface (see Fig. 27 and Fig. 28). The deconvoluted spectra indicate that the introduced nitrogen is coming from the amide backbone and the amino groups of the protein. Moreover, the relative intensity of the carbonyl band (at 287.7 eV) is increased compared to C-O and C-C/C-H species due to the peptide bonds in the immobilized protein (Fig. 27). It is also striking that the peak for carboxyl groups (528.5 eV), as may be expected for a protein, can be found in the spectra again. This indicates that the binding of streptavidin to the surface was successful and supported the results from the fluorescence measurements.

# 7 Summary

In this section the PI and a-Si:H waveguide layer were characterized with the XPS and literature supported. According to the knowledge about the substrate chemistry, specific functionalization literature has been found and summarized.

The chemical resistivity tests excluded some of the found ways to functionalize the waveguide layers. So is, for example, the alkaline hydrolysis no possible method to functionalize the PI-Ormoclad MZI´s because the layer system is not resistant against the sodium hydroxide treatment.

Initially, functionalization of the PI and a-Si:H system was considered to the chemical resistivity tests with either on of tree different chemical groups, namely carboxyl-, amine- or sulfhydryl groups. From this state, different chemical methods could be used for further bimolecular interactions experiments.

The sulfhydryl functionalization was then chosen for the streptavidin immobilization. Therefore the silanized surface was biotinylated and then the fluorescence labeled Chromeon 642-streptavidin was bound to the surface to validate the binding behavior to the surfaces.

It was found, that on the unblocked PI control sample 144 ± 20 fmol/mm$^2$ and on the unblocked a-Si:H control sample 27 ± 2 fmol/mm$^2$ Chromeon 642-streptavidin bind to the surface. The blocking with BSA hinders the binding of the Chromeon 642-streptavidin to the unspecific binding sites and allows a specific binding of 80 ± 20 fmol/mm$^2$ and 20 ± 2 fmol/mm$^2$ streptavidin on the biotinylated BSA blocked PI and a-Si:H surface.

AFM measurements indicate that the thin layer PI and a-Si:H gets neither damaged nor thinned and that the surface roughness stays below a mean roughness, $R_a$, of 0.60 nm. XPS measurements provide further information, how the functionalization with MPTMS on the oxygen plasma activated PI and a-Si:H surfaces take place and shows the atom composition of the surfaces before and after the functionalization steps. The developed protocols create a modified PI and a-Si:H surface with good binding capacity for streptavidin while keeping the surfaces intact. This opens up the way for the use of PI and a-Si:H-MZI´s as photonic biosensors for streptavidin detection.

**1** Dahmen C, Janotta A, Dimova-Malinovska D (2003) Surface functionalization of amorphous silicon and silicon suboxides for biological applications. Thin Solid Films 427:201–207

**2** Ponpon JP, Bourdon B (1982) Oxidation of glow discharge a-Si:H. Solid-State Electronics., 25(9):875-876

**3** MicroChem information to SU-8 proparties: http://www.microchem.com/products/pdf/SU-8-table-of-properties.pdf, 16.02.2010

**4** Sarah LT, Popat K, Desai TA (2006) Off-wafer fabrication and surface modification of asymmetric 3D SU-8 microparticles. NATURE PROTOCOLS 1(6):3153-3158

**5** Hong G, Holmes AS, Heaton ME (2004) SU8 resist plasma etching and its optimization. Microsystem Technologies, 10:357–359

**6** Cheong FC, Varghese B, Sindhu S (2007) Direct removal of SU-8 using focused laser writing. Applied Physics A 87:71–76

**7** Myllymaa S, Myllymaa K, Korhonen H (2010) Surface characterization and in vitro biocompatibility assessment of photosensitive polyimide films. Colloids and Surfaces B: Biointerfaces 76:505–511

**8** Technical Informations: PI2771 Photosensitive polyimide. *Processing Guidelines*. HD Microsystems, Neu-Isenburg, Germany

**9** McGrath JE, Dunson DL, Mecham SJ, Hedrick JL (1999) Synthesis and Characterisation of Segment Polyimide-Polyorganosiloxane Copolymers. Progress in Polyimide Chemistry I 140:61-105

**10** Pippig F, Holländer A (2010) Hydrogel nanofilms for biomedical applications: synthesis via polycondensation reactions. Supported Information. Macromol. Biosci. 10:1093–1105

**11** Micro resist technology GmBH information to Ormoclad: http://www.microresist.de/produkte/ormocer/pdf/pi_ormocore_clad_de_07083001_ls_neuDesign.pdf, 20.11.2010

**12** Information from Micro resist technology GmBH: Processing guidelines. Ormocer® - Ormoclad, Removal. p .4

**13** Buriak JM (1999) Organometallic chemistry on silicon surfaces: formation of functional monolayers bound through Si–C bonds. Chem. Commun. 1999(12):1051-1060

**14** De Stefano L, Rendina I, Rossi AM, Rossi M (2007) Biochips at work: porous silicon microbiosensor for proteomic diagnostic. Journal of Physics: Condense Matter 19:935007

**15** Faucheux A, Gouget-Laemmel AC, de Villeneuve C H (2006) Well-Defined Carboxyl-Terminated Alkyl Monolayers Grafted onto H-Si(111): Packing Density from a Combined AFM and Quantitative IR Study. *Langmuir 22:*153-162

**16** Hermanson GT (2008) Bioconjugate Techniques. Elsevier, London, p. 565ff

**17** Zhuravlev LT (2000) The surface chemistry of amorphous silica. Colloids and Surfaces A: Physicochemical and Engineering Aspects 173:1–38

**18** Ishizuka N, Kobayashi H, Minakuchi H, Nakanishi K (2002) Monolithic silica columns for high-efficiency separations by high-performance liquid chromatography. Journal of Chromatography A 960: 85–96

**19** Xu X, Densmore A, Delâge A (2008) Folded cavity SOI microring sensors for high, Optical Society of sensitivity and real time measurement of biomolecular binding. Optical Express 16(19):1517-15148

**20** Hermanson GT (2008) Bioconjugate Techniques. Elsevier, London, p. 562ff

**21** Hermanson GT (2008) Bioconjugate Techniques. Elsevier, London, p. 567f

**22** Howarter JA, Youngblood JP (2006) Optimization of Silica Silanization by 3-Aminopropyltriethoxysilane. Langmuir 22:11142-11147

**23** Kallury KMR, Macdonald PM, Thompson M (1994) Effect of Surface Water and Base Catalysis on the Silanization of Silica by (Aminopropyl) alkoxysilanes Studied by X-ray Photoelectron Spectroscopy and 13C Cross-Polarization/Magic Angle Spinning Nuclear Magnetic Resonance. Langmuir 10:492-499

**24** B. Sepulveda, J. Sanchez del Rio, M. Moreno, "Optical biosensor microsystems based on the integration of highly sensitive Mach–Zehnder interferometer devices", *JOURNAL OF OPTICS A: PURE AND APPLIED OPTICS*, Vol. 8, p. 561, 2006

**25** Bertin A, Schlaad H (2009) Mild and Versatile (Bio-)Functionalization of Glass Surfaces via Thiol-Ene Photochemistry. Chem. Mater. 21:5698–5700

**26** Gan S, Yang P, Yang W (2009) Photoactivation of Alkyl C-H and Silanization: A Simple and General Route to Prepare High-Density Primary Amines on Inert
Polymer Surfaces for Protein Immobilization. Biomacromolecules 10:1238–1243

**27** Verdianz T, Simbürger H, Liska R (2005) Surface modification of imide containing polymers I: Catalytic groups. European polymer Journal 42(2006): 638-654

**28** Ying Jiang L, Shung Chung T, (2010) Homogeneous polyimide/cyclodextrin composite membranes for pervaporation dehydration of isopropanol. Journal of Membrane Science 346(2010):45-58

**29** Hermanson GT (2008) Bioconjugate Techniques. Elsevier, London, p. 205

**30** Wilde LM, Farace G, Roberts CJ, Davies MC (2001) Molecular patterning on carbon based surfaces through photobiotin activation. Analyst 126:195–198

**31** Thomas RR, Buchwalter LS, Buchwalter LP, Chao TH (1995) Organic chemistry on a polyimide surface. Macromolecules 25:4559

**32** Huang XD, Bhangale SM, Moran PM, Yakovlev NL, Pan J (2003) Surface modification studies of Kapton®HN polyimide films. Polymer International 52:1064-1069

**33** Kim HJ, Park YJ, Choi J, Han HS, Hong YT (2009) Surface modification of polyimide film by coupling reaction for copper metallization Journal of Industrial and Engineering Chemistry 15(2009):23–30

**34** Leary Jr HJ, Campbell DS (1984) Aminosilane and metal modifications of polyimide surfaces. Polym Sci Technol 29:517–23

**35** Ali M, Schiedt B, Healy K, Neumann R, Ensinger W (2008) Modifying the surface charge of single track-etched conical nanoporesin polyimide. Nanotechnology 19 (2008): 085713 (6pp)

**36** Hermanson GT (2008) Bioconjugate Techniques. Elsevier, London, p. 216ff

**37** Wei Z, Weiping L, Huicong L, Liqun Z (2010) Erosion of a Polyimide Material Exposed to Simulated Atomic Oxygen Environment. Chinese Journal of Aeronautics 23:268-273

**38** Zhu B, Iwata H, Hirata I, Ikada Y, (2000) Hydrophilic modification of a polyimide film surface. J. Adhesion Sci. Technol 14(3):351–361

**39** Flitsch R, Shih Y (1990) A study of modified polyimide surfaces as related to adhesion. J. Vac. Sci. Technol. A 8(3):2379-2381

**40** Nakamura Y, Suzuki Y, Watanabe Y (1996) Effect of oxygen plasma etching on adhesion between polyimide films and metal. Thin Solid Films 290-291:367-369

**41** Sambrook J, Russell DW (2001) Molecular cloning: a laboratory manual. Cold Spring Harbor, New York, USA, Volume 3, 2001[3], p.101

**42** Betancor L, L´opez-Gallego F, Hidalgo A (2006) Different mechanisms of protein immobilization on glutaraldehyde activated supports: Effect of support activation and immobilization conditions. Enzyme and Microbial Technology 39:877–882

**43** Hermanson GT (2008) Bioconjugate Techniques. Elsevier, London, p. 919ff

**44** N.M. Green, (1975) Avidin. Adv. Protein Chem. 29:85-133

**45** Busse S, Scheumann V, Menges B, Mittler S (2002) Sensitivity studies for specific binding reactions using the biotin/streptavidin system by evanescent optical methods. Biosensors and Bioelectronics 17(2002):704-710

**46** Trong L, Aubert DG, Thomas NR, Stenkamp RE (2006) The high-resolution structure of (+)-epi-biotin bound to streptavidin. Acta Crystallogr. Sect. D 62: 576-581; PDB Protein data base: http://www.rcsb.org/pdb/explore/explore.do?structureId=2GH7, 22.11.2010

**47** Su X, Wu Y-J, Robelek R, Wolfgang (2005) Surface Plasmon Resonance Spectroscopy and Quartz Crystal Microbalance Study of Streptavidin Film Structure Effects on Biotinylated DNA Assembly and Target DNA Hybridization. *Langmuir 21:* 348-353

**48** Hermanson GT (2008) Bioconjugate Techniques. Elsevier, London, p. 726ff

**49** Piehler J, Brecht A, Valiokas R, Liedberg B, Gauglitz G (2000) A high-density poly(ethylene glycol) polymer brush for immobilization on glass-type surfaces. Biosensors & Bioelectronics 15(9-10) :473–481

**50** Zalipsky S (1995) Functionalized Poly(ethy1ene glycol) for Preparation of Biologically Relevant Conjugates *Bioconjugafe Chem.* 6(2)150-1 65

**51** Mehne J, Markovic G, Pröll F (2008) Characterisation of morphology of self-assembled PEG monolayers: a comparison of mixed and pure coatings optimised for biosensor applications. Anal Bioanal Chem 391:1783–1791

**52** Wilde LM, Farace G, Roberts CJ, Davies MC (2001) Molecular patterning on carbon based surfaces through photobiotin activation. Analyst 126:195–198

**53** B. Dorvel, B. Reddy, I. Block Vapor-Phase Deposition of Monofunctional Alkoxysilanes for Sub-Nanometer-Level Biointerfacing on Silicon Oxide Surfaces, *Advanced Functional Matererials*, Vol. 20 p. 87–95, 2010*

**54** Hermanson GT (2008) Bioconjugate Techniques. Elsevier, London, p. 216ff

**55** Preinerstorfer B, Lubda D, Lindner W, Lämmerhofer M (2006) Monolithic silica-based capillary column with strong chiral cation-exchange type surface modification for enantioselective non-aqueous capillary electrochromatography. Jornal of Chromatography A 1106:94-105

**56** Hermanson GT (2008) Bioconjugate Techniques. Elsevier, London

**57** Gruber M, Wetzl B, Oswald B (2005) A New Fluorescence Resonance Energy Transfer Pair and Its Application to Oligonucleotide Labeling and Fluorescence Resonance Energy Transfer Hybridization Studies. Journal of Fluorescence 15(3):207-214

**58** Spinke J, Liley M, Schmitt FJ (1993) Molecular recognition at self-assembled monolayers: Optimization of surface functionalization. J. Chem. Phys. 99(9):7012-7019

**59** Darst SA, Ahlers M, Meller PH (1991) Two-dimensional crystals of streptavidin on biotinylated lipid layers and their interactions with biotinylated macromolecules. Biophys. J. Biophysical Society 59:387-396

**60** Wallart X, Villeneuve CH, Allongue P (2005)Truly Quantitative XPS Characterization of Organic Monolayers on Silicon: Study of Alkyl and Alkoxy Monolayers
on H-Si(111). J. AM. CHEM. SOC. 127: 7871-7878

**61** Wittenber NT; Hoenigman JR, Mddenman WE (1978) AES and XPS of silicon nitride films of varying refractive indices. J.Vac. Sci. Technol. 15(2):348-352

**62** Liu H, Hamers RJ (1998) An X-ray photoelectron spectroscopy study of the bonding of unsaturated organic molecules to the Si(001) surface. Surface Science 416(1998):354–362

**63** Ahn D, Kim C, Lee J, Park B (2008) The effect of nitrogen on the cycling performance in thin-film Si1_xNx anode. Journal of Solid State Chemistry 181(2008):2139– 2142

**64** Thomas RR, Buchwalter LS, Buchwalter LP, Chao TH (1995) Organic chemistry on a polyimide surface. Macromolecules 25:4559

**65** Huang XD, Bhangale SM, Moran PM, Yakovlev NL, Pan J (2003) Surface modification studies of Kapton®HN polyimide films. Polymer International 52:1064-1069

**66** Kim HJ, Park YJ, Choi J, Han HS, Hong YT (2009) Surface modification of polyimide film by coupling reaction for copper metallization Journal of Industrial and Engineering Chemistry 15(2009):23–30

# Part IV: Surface sensing real-time measurements of streptavidin and DNA with MZI sensors

## Content

## Surface sensing real-time measurements of streptavidin and DNA with MZI sensors

In the previous chapter, the functionalization protocols for a-Si:H- and PI-MZI sensors for streptavidin immobilization were established. Now, these protocols are modified for surface sensing real-time measurements of streptavidin and to create a platform for DNA hybridization experiments on MZI sensors. These protocols are given in Table 1 and 2.

For the measurements and experiments, the main parameters such as flow rates (20 µl/min) of the liquids through the fluidic system and measurement temperature (22°C) are kept constant.

For the PI-MZI sensors the following adjustment was made by all measurements:

At the beginning of a measurement (see Table 1, step 11) of high concentration ranges, the wavelength of the tunable laser light source was adjusted to a point where the MZI showed maximum transmission. Although this point does not show maximum sensitivity for small changes of the effective index of the propagating mode, it simplifies the calculation of the phase shift out of the sensor transmission by the measurement of high concentrations. In order to facilitate measurements of low concentrations with small resulting phase shifts it is beneficial to start close to a point of minimum transmission by adjusting the wavelength of the laser source. If the transmitted power is measured on a linear scale, the most sensitive point of the MZI transmits half of the maximum power. When measuring on a logarithmic scale the points of maximum sensitivity are shifted towards the transmission minimum. The higher the extinction ratio, the higher is the maximum sensitivity, and the closer are the points of maximum sensitivity to the transmission minimum.

The same is true for the a-Si:H-MZI sensors, but the adjusting of the wavelength to a maximum or minimum transmitted power is not as easy as by the PI-MZI sensors, because of the a-Si:H-MZI do not show this kind of wavelength behavior.

The first measurements in this chapter for a-Si:H- and PI-MZI sensors were performed to gain information about the sensor stability after the functionalization steps, as well as the selectivity and reproducibility of the streptavidin real-time measurements. In this work these measurements are defined as reference measurements.

To monitor the streptavidin binding to the surface during the real-time measurement, the fluorescence marked streptavidin named Chromeon 642-streptavidin is used to enable an extern control fluorescence scan and to facilitate the analysis of the real-time measurement results. Every Chromeon 642-streptavidin measurement is done on a separate MZI sensor, because the reuse of sensor elements is prevented by the strong biotin-streptavidin binding on

the surface, which could not be fully dissociated by treatment of the MZI sensors with highly concentrated biotin or 2-mercaptoethanol solutions.

**Table 1: Protocol for a-Si:H and PI-MZI sensor functionalization and real-time measurement of Chromeon 642-streptavidin**

| Step | Type | Procedure |
|---|---|---|
| **1** | Activation | Oxygen plasma activation, 1 mbar, 40% Power (≈40 W), RT<br>PI-MZI sensors: 1 min; a-Si:H-MZI sensors: 3 min |
| **2 a-Si:H-MZI** | Functionalization with MPTMS | a-Si:H-MZI sensors are dipped in the THF MPTMS solution for 1 h |
| **2 PI-MZI** | Functionalization with MPTMS | PI-MZI sensors are dipped in acidic aqueous MPTMS solution for 1 h |
| **3** | Cleaning | 5 min ultrasonic bath in isopropyl alcohol |
| **4** | Cleaning | Washing with ultrapure water (2x) and in isopropyl alcohol (1x), dried under nitrogen stream |
| **5** | Biotinylation | The samples are dipped in M-$PEG_2$-biotin solution for 2 h, RT |
| **6** | Cleaning | Washing with ultrapure water (2x), shaking in ultrapure water 1 h, washing in ultrapure water (1x) and in isopropyl alcohol (1x) and dried under nitrogen stream |
| **(7)** | Storage | The samples are stored in vacuum in the exsiccator |
| **8** | Blocking | The samples are dipped in BSA (0.1 mg BSA/ml 150 mM PBS buffer) and shake for 30 min in this solution |
| **9** | Cleaning | 2x ultrapure water and 30 min shaking in ultrapure water, dried under nitrogen stream |
| **10** | MZI sensor mounting for real-time measurement | MZI sensor gets mounted to the MZI setup with the fluidic system for measurements in fluidic environments. |
| **11** | Homogenous measurements | The fluidic system is first filled with ultra pure water. Then a homogenous measurement on the MZI sensor while exchanging ultra pure water against 150 mM PBS buffer is done. |
| **10** | Real- time measurement of the immobilization of Chromeon 642-Streptavidin | 150 mM PBS buffer is exchanged against Chromeon 642-streptavidin dissolved in 150 mM PBS buffer. Thereby, the Chromeon 642-streptavidin concentration varies between 0.1 µg – 50 µg/ml (≙ 1.67 nM – 833.3 nM). The surface sensing measurement is done during the rinsing of Chromeon 642-streptavidin over the MZI sensor in the fluidic system. After this surface sensing measurement the Chromeon 642-streptavidin dissolved in 150 mM PBS buffer is exchanged again to 150 mM PBS buffer. |
| **11** | Reference homogenous measurement | A homogenous measurement on the MZI senor during the exchanging ultra pure water against 150 mM PBS buffer is done. |
| **12** | Cleaning | Ultra pure water is rinsed over the sensor surface for 10 min. |

For surface sensing DNA experiments, the blocking of the sensor surface is omitted and unlabelled streptavidin is used instead of the fluorescence labeled Chromeon 642-streptavidin. To guarantee a maximum streptavidin concentration bound on the sensor surface, high concentrations (3.3 µM ≙ 200 µg/ml) of streptavidin are used. (See Table 2). The following surface sensing DNA experiments are performed one after the other on freshly prepared MZI sensors, to verify the functionalization reproducibility and to avoid possible carry-over effects. The used DNA is a single strands DNA (ssDNA).

**Table 2: Protocol for a-Si:H and PI-MZI surface sensing DNA experiments**

| Step | Type | Procedure | |
|---|---|---|---|
| **1-6** | | As described in Table 1 | |
| **(7)** | Storage | The samples are stored in vacuum in the exsiccator | |
| **8** | MZI sensor mounting for real-time measurement | MZI sensor gets mounted to the MZI setup with the fluidic system for measurements in fluidic environments.. | |
| **9** | Homogenous measurements | The fluidic system is first filled with ultra pure water. Then a homogenous measurement on the MZI senor during the exchanging ultra pure water against 150 mM PBS buffer is done. | |
| **10** | Functionalization of the sensor surface with streptavidin (unlabelled) | 150 mM PBS buffer gets exchanged against streptavidin (200 µg/ml ≙ 3.3µM) dissolved in 150 mM PBS buffer. | |
| **11** | Cleaning | 150 mM PBS is rinsed over the sensor surface for 10 min. | |
| **12** | DNA experiments | **12A:** Reference measurement with complementary and non complementary DNA to verify unspecific interactions | Complementary ssDNA and non complementary ssDNA:<br>These ssDNA strands are subsequently rinsed after step 11 over the MZI sensor surface to test for unspecific interactions. |
| | | **Or** | (on a new MZI sensor) |
| | | **12B**: Online functionalization with biotin tagged DNA strands | Binding of biotin tagged ssDNA strands to the streptavidin layer on the MZI sensor:<br>Directly after step 11 the biotin tagged ssDNA strands (1µM) disolved in 150 mM PBS buffer are rinsed over the surface. Thereby, the binding of the biotin tagged ssDNA to the streptavidin layer is monitored. |
| **13** | Cleaning | 150 mM PBS is rinsed over the sensor surface for 10 min. | |
| **14** | DNA hybridization experiments | **14A**: Selectivity test with non complementary DNA | Non complementary ssDNA:<br>Selectivity is tested after the functionalization with biotin tagged ssDNA strands to prove if unselective hybridization occurs. |
| | | **Or** | (on a new MZI sensor) |
| | | **14B**: Hybridization experiment with complementary DNA | Complementary ssDNA<br>Directly after functionalization with biotin tagged ssDNA strands, the complementary ssDNA disolved in PBS buffer is rinsed over the surface. This is done to monitor the hybridization of the immobilized biotin tagged ssDNA with the complementary ssDNA. |
| **15** | Cleaning | 150 mM PBS is rinsed over the sensor surface for 10 min. | |
| **16** | Reference homogenous measurement | A homogenous measurement on the MZI sensor during the exchanging ultra pure water against 150 mM PBS buffer is done. | |
| **17** | Cleaning | Ultra pure water is rinsed over the sensor surface for 10 min. | |

The DNA experiments (see Table 2, step 12 A,B) were carried out after the cleaning of the streptavidin functionalized surface and the measurements A, B one after the other on a new MZI sensor.

These experiments should give information about the unspecific interactions of the complementary and non complementary DNA, as well as the binding behavior of biotin tagged DNA strands to the streptavidin functionalized a-Si:H-MZI and PI-MZI sensor surface. After these previous measurements, the surface sensing DNA hybridization experiments (see Table 2, step 14 A,B) were performed on different sensor surfaces, which were functionalized with biotin tagged DNA strands. For these tests, non complementary DNA strands were rinsed over the functionalized sensor surfaces, to test the selectivity of the hybridization process. The hybridization itself was analyzed by rinsing complementary DNA strands over the, with biotin tagged DNA strands functionalized, sensor surfaces.
The used DNA strands are listed in Table 3 and purchased from VBC Biotech GmbH. The concentration of the DNA strands disolved in 150 mM PBS buffer was kept constant at 1 µM. The complementary and non complementary DNA strands were labeled on the 5´-end with the Cy3 and Cy5, which opens up the possibility to externally verify the measurement results with fluorescence scans.

**Table 3: Used DNA-ssDNA strands purchased from VBC Biotech GmbH**

| Name | Modification | Sequence | Use | Chemicals | Protocol |
|---|---|---|---|---|---|
| **Biotin-tagged DNA** | 3´-Biotin | 5´-TCG CCA TTC GTT GAC TAC TTC TTA T -3´ | Functionalization with biotin tagged DNA strands | The 25-mer ssDNA purchased from the VBC Biotech GmbH, Campus Vienna | Stock solution is prepared by dissolving in 150 mM PBS buffer, stored at -20°C |
| **Complementary DNA** | 5´-Cy3 | 3´-AGC GGT AAG CAA CTG ATG AAG AAT A-5´ | Hybridization/ unspecific interaction to the streptavidin functionalzed sensor surface | The 25-mer ssDNA purchased from the VBC Biotech GmbH, Campus Vienna | Stock solution is prepared by dissolving in 150 mM PBS buffer, stored at -20°C |
| **Non complementary DNA** | 5´-Cy5 | 3´-TTGCTC TGA GGC AGA GTT T- 5` | Selectivity tests | The 19-mer ssDNA purchased from the VBC Biotech GmbH, Campus Vienna | Stock solution is prepared by dissolving in 150 mM PBS buffer, stored at -20°C |

The results of performed surface sensing real-time measurements of streptavidin and DNA performed on PI- and a-Si:H-MZI sensors are given in detail in the following chapters for a-Si:H and PI-MZI sensors.

# 1 Real-time measurements of streptavidin on a-Si:H-MZI sensors

## 1.1 Reference measurements

### Sensor stability

The a-Si:H-MZI sensor, consisting of a a-Si:H waveguide and a SU-8 cladding layer, was first tested with respect to stability of the sensor surface after each step of the functionalization protocol. Therefore, before functionalization and after oxygen plasma treatment, biotinylation, BSA blocking and streptavidin immobilization, wavelength scans on a-Si:H-MZI sensors were carried out in air.

These wavelength scans were performed for MZIs with a waveguide width in the range from 1950 nm to 2300 nm, for wavelength from 1280 up to 1380 nm, with a scan rate of 5 nm/min. The number of oscillations of the sensor signal in this wavelength range before treatment was 21 and equal for all measured MZI´s. The average extinction ratio is about 15 dB and the transmission was greater than -32 dBm at low and greater than -28 dBm at high wavelengths. In Fig. 1, the wavelength scan for the MZI2200 is depicted.

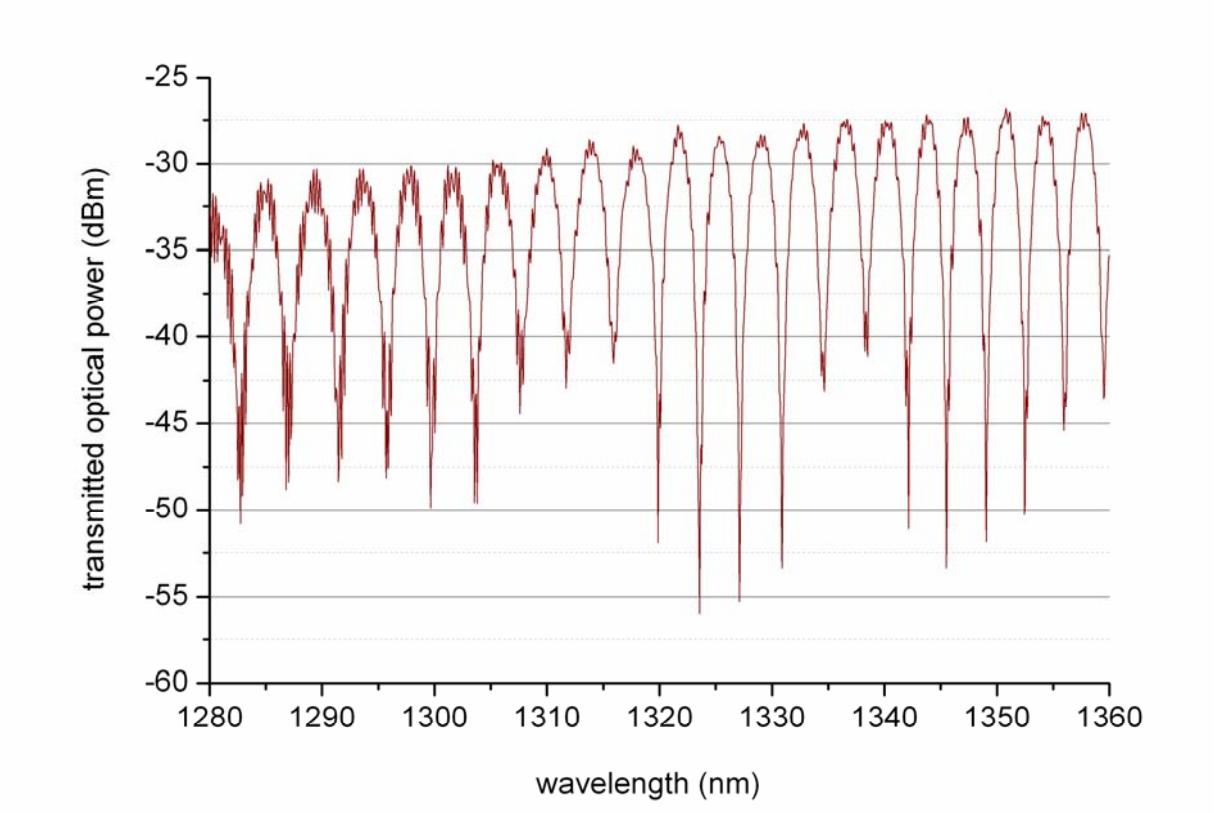


**Figure 1: Wavelength scan of MZI2200 in the wavelength range of 1280 nm to 1380 nm, with a scan rate of 5 nm/min.**

The MZI sensor was treated according to the protocol in Table 1 and after each functionalization step wavelength scans were performed.

It could be found that the transmission and the extinction ratio after these treatments stayed constant, but the numbers of oscillations changed.

This shows that, at least in the measurement arm of the MZI, changes in the waveguide or sensing layer height and/or refractive index appear during the functionalization. In Table 4 the numbers of oscillations in the wavelength scan before and after the several functionalization steps of the protocol are listed.

**Table 4: Numbers of the oscillations in the wavelength scan before and after the sample treatments**

| Sample treatment (step) | Numbers of the oscillations in the wavelength scan |
|---|---|
| **untreated** | 21 |
| **after activation (step 1)** | 25 |
| **after functionalization with MPTMS(step 2 a-Si:H-MZI)** | 26 |
| **after biotinylation (step 5)** | 26 |
| **after blocking (step 8)** | 24 |
| **after immobilization of Chromeon 642-Streptavidin (step 10)** | 21 |

The behavior of the samples indicates that the oxygen plasma activation has a great influence on the surface characteristic, because the oscillation number increased up to 25. This result shows the cleaning effect of the oxygen plasma, which removes carbon and nitrogen residues and oxygenates the silicon surface. (Detailed Information are given in Part III, section 6.4)

The MPTMS functionalization has a smaller influence on the surface parameters as the oxygen plasma, but induces an increase of the oscillation number to 26. The biotinylation did not change the number of oscillations, but the blocking with BSA and the immobilization of Chromeon 642-streptavidin, decreased the number of oscillations which again indicates a change in the sensing layer thickness and/or of the refractive index.

In summary, these results show that the a-Si:H-MZI sensor is not negatively affected by the functionalization, because the important parameters of transmission and extinction ratio stay constant. The changes of the oscillation numbers verify that the a-Si:H-MZI sensor surface gets modified during the process of functionalization. This modification is going to be analyzed in the following subsections.

**Binding of the maleimide moiety to the a-Si:H-MZI sensor surface**

The binding of the maleimide moiety to the a-Si:H surface should only take place on the MPTMS functionalized MZI sensor on the sulfhydryl functional group, to prevent unspecific binding of the Maleimide-$PEG_2$-biotin (M-$PEG_2$-biotin) to the sensor surface. This unspecific binding of the maleimide moiety would lead to less homogenous packing of the sensing layer molecules, and would further influence the immobilization of streptavidin negatively.

To test the maleimide binding to the a-Si:H-MZI sensor surface, the TMR5M (tetrametyl rhodamine 5-maleimide) fluorescence label was used to have the possibility of a control via fluorescence scan.

First one a-Si:H-MZI sensor was exposed to oxygen plasma (step 1, Table 1), and then dipped in a THF solution without MPTMS (THF with 0.4 % HCl conc.). After 1 h and cleaning of the MZI sensor, it was mounted in the measurement setup with the fluidic system on the top, to measure in liquid environments.

The fluidic system was first filled with ultra pure water, which was in the next measurement step exchanged against binding buffer (ultra pure water with 10 % phosphate buffer 0.05 M and 10% isopropyl alcohol, pH 7.3). After the MZI response became stable, the binding buffer was exchanged against 5 µM TMR5M dissolved in binding buffer and when the signal stabilizes, the liquids were exchanged vice versa (see Fig. 2). It was found that no significant amount of TMR5M binds to the a-Si:H-MZI surface without MPTMS, because no persistent phase shift, caused by a binding of TMR5M to the surface, occured. The control fluorecence scan of the MZI showed no fluorescence intensity in the MZI measurement window, which confirms that no unspecific and no irreversible binding of the maleimide moiety takes place on the sensor surface.

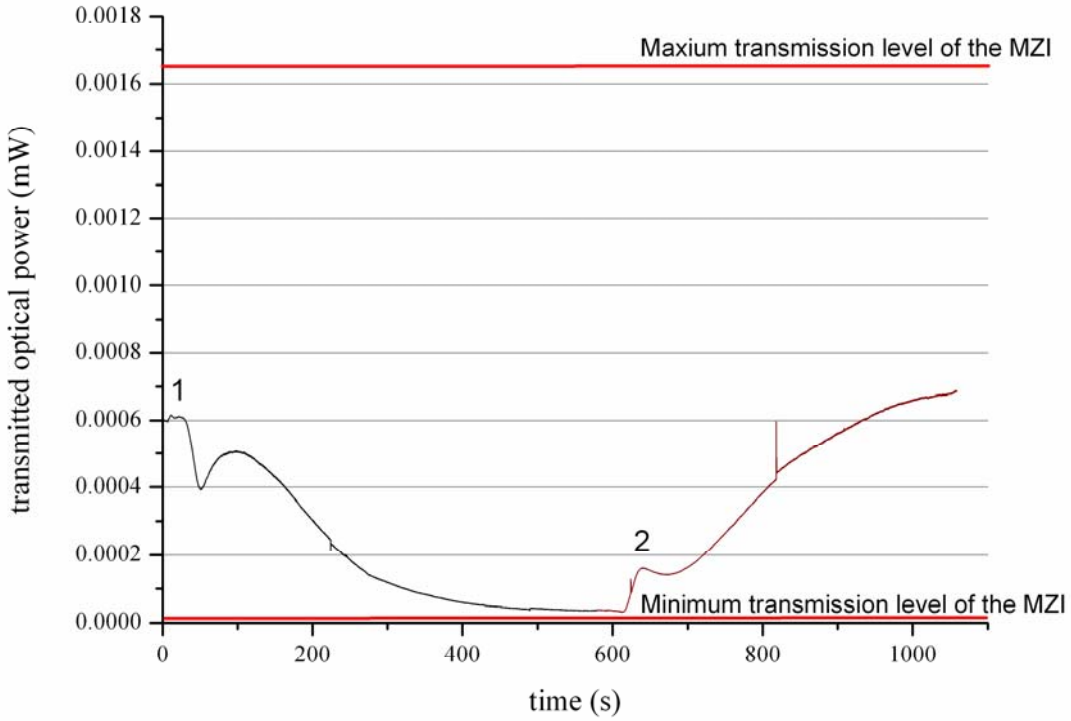


**Figure 2: The red lines show the maximum and minimum transmission level of the MZI sensor. The monitored signals 1 and 2 of the MZI show the transmitted optical power during the reference measurement of the binding behavior of the maleimide moiety to the a-Si:H-MZI surface without MPTMS functionalization: 1. Binding buffer is exchanged against 5 µM TMR5M dissolved in binding buffer ($n_{TMR5M}$=1.3385); 2. 5 µM TMR5M dissolved in binding buffer gets exchanged against binding buffer; No persistent phase shift occurs, because the phase shifts resulting from step 1 and 2 in this measurement are equal. This proves that no binding of TMR5M on the surface takes place.**

The next test was done to prove the binding of the maleimide to the sulfhydryl group in the MPTMS layer. Therefore, a MZI sensor was functionalized with MPTMS (see Table 1, step 2) and cleaned as described (step 4, see Table 1). Then, the MZI sensor was mounted again into the setup, and the fluidic system was fixed on the top and filled with ultra pure water. A similar measurement was performed like mentioned before and the signal versus time was monitored and is depicted in Fig. 3.

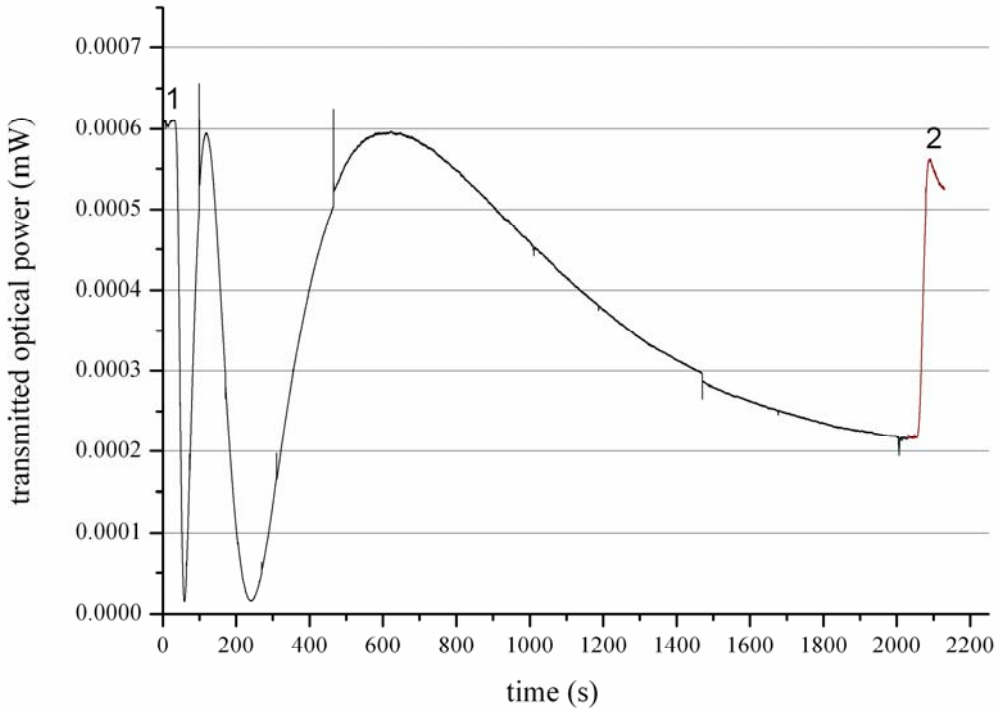


**Figure 3: Transmitted optical power during the surface sensing of the binding behavior of the maleimide moiety to sulfhydryl group in the MPTMS layer on the sensor surface: 1. Binding buffer is exchanged against 5 µM TMR5M dissolved in binding buffer ($n_{TMR5M}$=1.3385) and an interference signal occurs, which belongs to the binding of TMR5M to MPTMS layer on the sensor surface; 2. 5 µM TMR5M disolved in binding buffer gets exchanged against binding buffer; In the surface sensing measurement an persistent phase shift occurs. In step 1 in this measurement the induced phase shift is about 4.5π, while the reverse phase shift in step 2 amounts to only 0.5π. From this data it can be concluded that the phase shift difference of 4π belongs to the binding of the TMR5M to the MPTMS layer on the surface.**

From this measurement, it can be concluded that the maleimide binds specifically to the sulfhydryl group in the MPTMS layer, because the rinsing of the TMR5M dissolved in binding buffer over the surface gives a phase shift of about 4.5π (see Fig. 4), while the exchange against pure binding buffer only induces a phase shift of about 0.5π. Therefore, the phase shift resulting from the binding process is about 4π.

In addition, a fluorescence scan of this MZI-sensor after the measurement verified binding of TMR5M, and therefore, supports the measurement result.

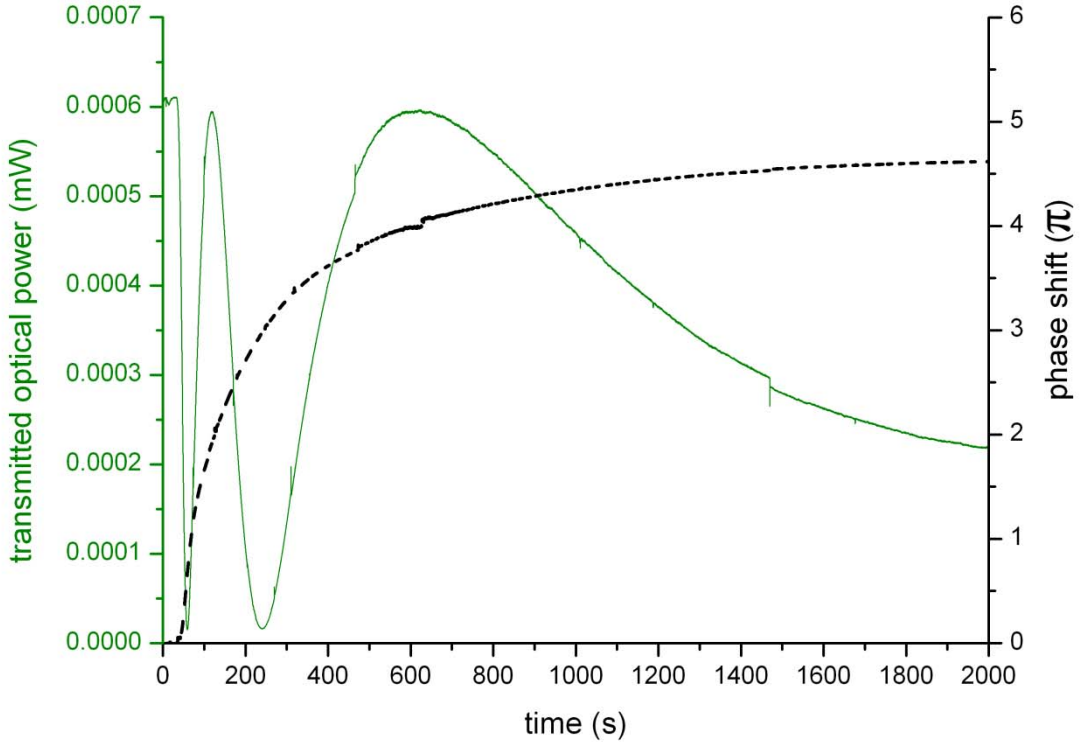


**Figure 4: Green line: Transmitted optical power during the binding of TMR5M to the MPTMS layer on the a-Si:H-MZI sensor; black dash line: Calculated phase shift as function of time**

### Binding of the Chromeon 642-streptavidin to the a-Si:H-MZI sensor surface

To analyze the binding behavior of Chromeon 642-streptavidin several a-Si:H-MZI sensors were prepared.

First, reference measurements were done on untreated and MPTMS functionalized a-Si:H-MZI sensors (see Table 1) with 10 µg/ml Chromeon 642-streptavidin, to gain information on the sensor response for unspecific interactions with the surface. Therefore, the samples got mounted into the measurement setup, with the fluidic system on top, which was filled with ultra pure water after mounting. Then, the water was exchanged against 150 mM PBS buffer and as soon as the MZI response was stable, the 150 mM PBS buffer was exchanged against 10 µg/ml (166 nM) Chromeon 642-streptavidin dissolved in 150 mM PBS buffer.

Herein an phase shift of 10π for the untreated and of 12π for the MPTMS functionalized unblocked surface, as well as a fluorescence intensity belonging to the unspecifically bound Chromeon 642-streptavidin was observed.

Then, the same measurement was performed with the MPTMS functionalized MZI sensor blocked with BSA (fabricated like described in Table 1, without steps 5-7). On this sensor surface the BSA blocking should suppress non-specific interactions, so that no phase shift in

the surface sensing measurement of a Chromeon 642-streptavidin should remain after rinsing with pure PBS buffer. In Figure 5, the measurement of 10 µg/ml (166 nM) Chreomeon 642-streptavidin on this a-Si:H-MZI sensor is depicted. As mentioned before, no remaining phase shift could be found in this measurement after end of step 2, which indicated that no non-specific binding on the surface take place after blocking with BSA. This result was also supported by an external fluorescence scan, where no fluorescence intensity could be measured on this a-Si:H-MZI sensor surface.

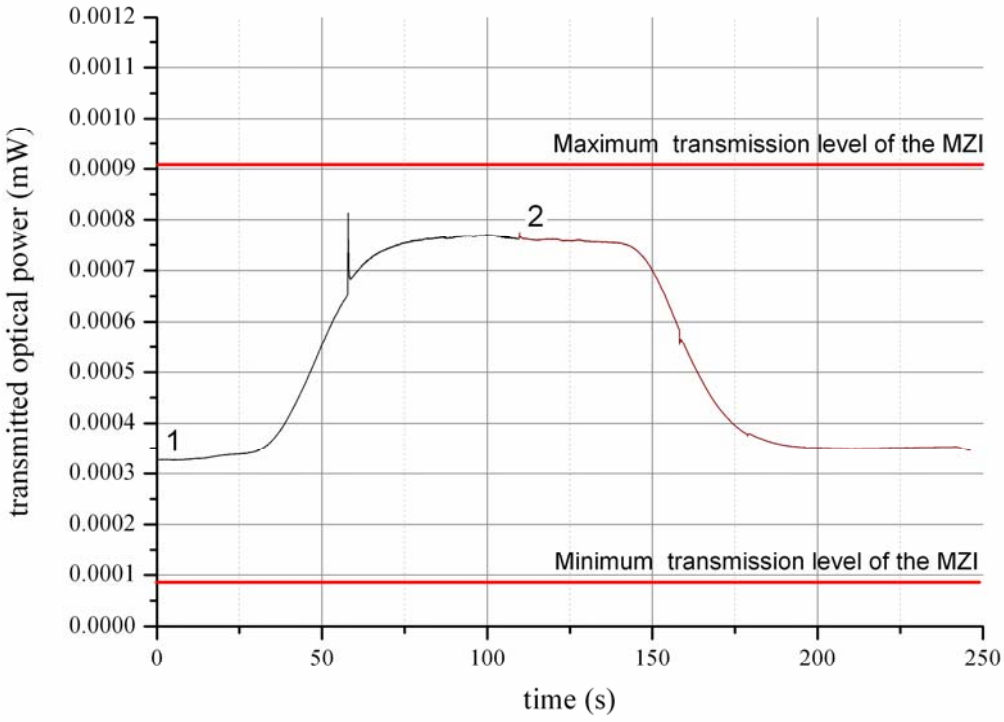


**Figure 5: The red lines show the maximum and minimum transmission level of the MZI sensor. The monitored signals 1 and 2 of the MZI show the transmitted optical power during the reference measurement of the binding behavior of Chromeon 642-streptavidin to the BSA blocked MPTMS functionalized a-Si:H-MZI sensor: 1. PBS buffer ($n_{PBS}$=1.3381) is exchanged against 10 µg/ml (166 nM) Chromeon 642-streptavidin dissolved in PBS buffer ($n_{Strep}$=1.3381); 2. 10 µg/ml (166 nM) Chromeon 642-streptavidin dissolved in PBS buffer is exchanged against PBS buffer; There is no phase shift resulting from a binding of Chromeon 642-streptavidin to the sensor surface, because the phase shifts of step 1 and 2 in this measurement are of equal size and in contrary direction.**

To verify the specific and unspecific binding of Chromeon 642-streptavidin to the biotinylated MZI sensors, the following tests were performed: Four biotinylated and four biotinylated BSA blocked a-Si:H-MZI sensors were, one after the other, mounted on the setup and measurements of 10 µg/ml (166 nM) Chromeon 642-streptavidin were performed. In Fig.

6, the calculated phase shifts from these surface sensing measurements on unblocked and BSA blocked MZI samples are plotted.

In Table 5, the values of the phase shifts at different times are given. The unblocked sensors have a lower standard deviation and, as expected, higher phase shifts at all times. At 2500 s, the phase shifts obtained from the blocked and non-blocked samples differed by about 26 %. This indicates that about 26 % of the binding of Chromeon 642-streptavidin on the a-Si:H-MZI sensor surfaces is non-specific, which can be successfully blocked by BSA treatment.

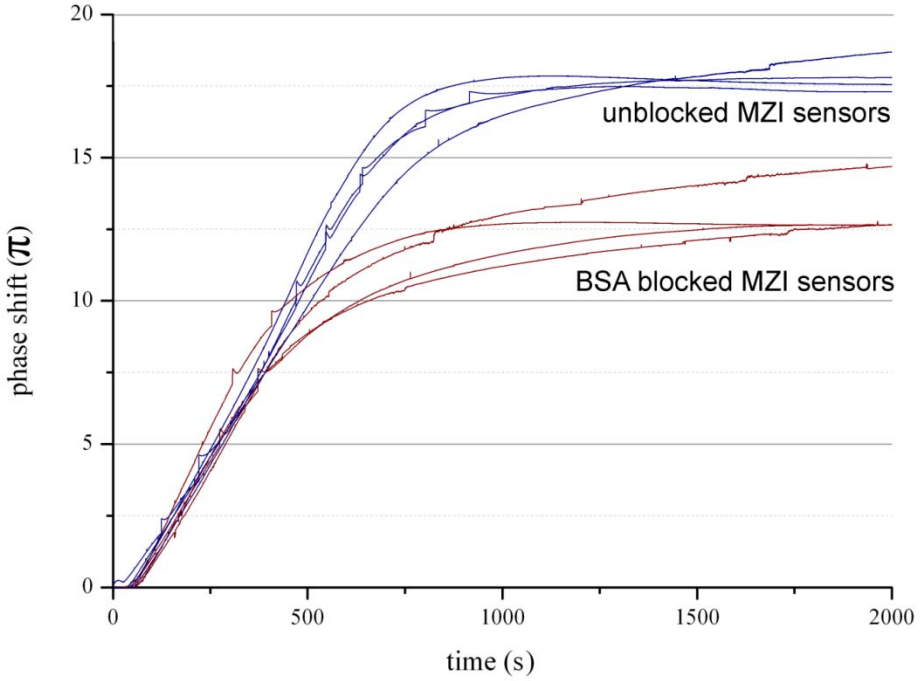


**Figure 6: Calculated phase shifts from surface sensing measurements of Chromeon 642-streptavidin binding on unblocked and BSA blocked MZI sensors**

**Table 5: Phase shifts at different measurement times for unblocked and BSA blocked MZI sensors**

| | Phase shift (π) at different times for unblocked MZI sensors | | |
|---|---|---|---|
| **time (s)** | **500** | **1000** | **2500** |
| ***P217*** | 11.60 | 17.75 | 17.80 |
| ***P218*** | 10.60 | 17.25 | 17.40 |
| ***P219*** | 10.80 | 17.10 | 17.80 |
| ***P206*** | 9.80 | 16.50 | 19.25 |
| **Average** | **10.40** | **16.95** | **18.15** |
| **standard deviation** | **0.53** | **0.40** | **0.97** |

| | Phase shift (π) at different times for unblocked MZI sensors | | |
|---|---|---|---|
| **time (s)** | **500** | **1000** | **2500** |
| ***P209*** | 8.75 | 11.60 | 12.60 |
| ***P204*** | 10.50 | 12.40 | 15.20 |
| ***P190*** | 9.55 | 13.00 | 12.70 |
| ***P191*** | 8.80 | 11.20 | 13.05 |
| **Average** | **9.40** | **12.05** | **13.39** |
| **standard deviation** | **0.82** | **0.81** | **1.22** |

## 1.2 Measurement of different concentrations of streptavidin on a-Si:H-MZI sensors

In the previous subsection it was proved, that the BSA blocking suppresses unspecific binding to the surface and the remaining signal on the blocked MZI sensor surface is about 26 % smaller than on the unblocked MZI sensor surface at the measurement of 10 µg/ml Chromeon 642-streptavidin.

With this knowledge the a-Si:H-MZI sensors were fabricated as it is described in Table 1, and then, different concentrations (0.1-50 µg/ml) of Chromeon 642-streptavidin were measured as mentioned before.

In Fig. 7, the phase shifts calculated from the transmitted optical power was plotted versus time, gained from the real-time measurements on the a-Si:H-MZI sensors for different Chromeon 642-streptavidin concentrations.

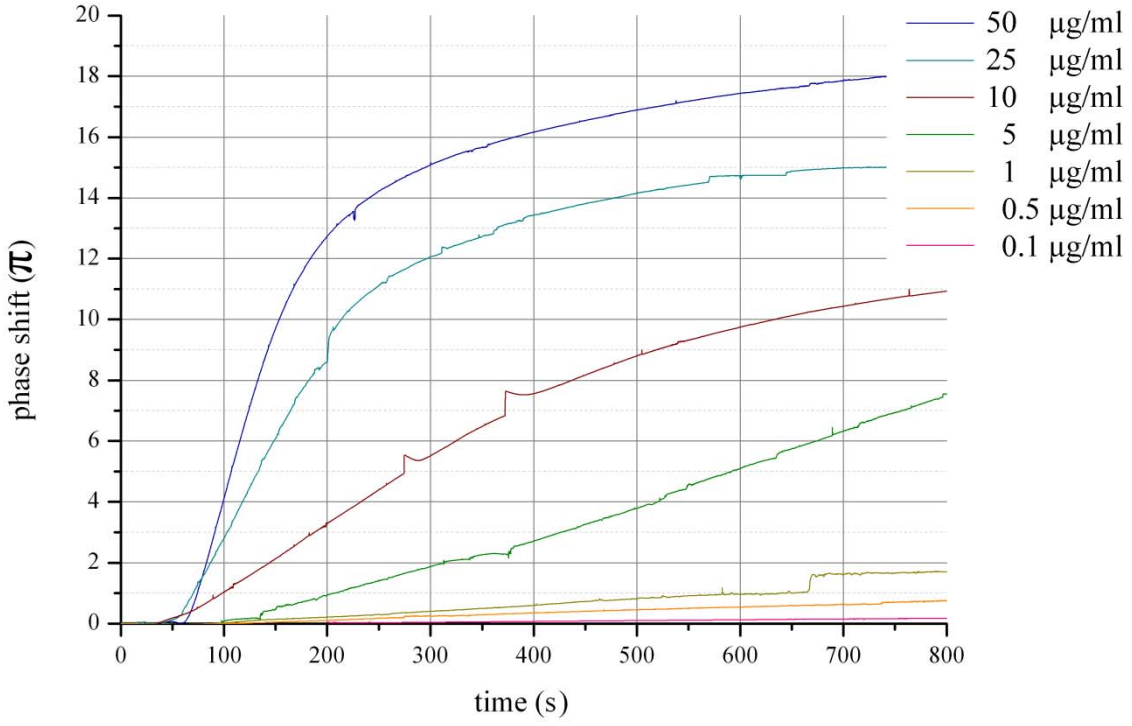


**Figure 7: Phase shifts calculated from the transmitted optical power during the real-time measurements of Chromeon 642-streptavidin on a-Si:H-MZI sensors; The steps in the measurement curves (e.g. for 1 µg/ml at a time of ~660 s) are caused by the correction of a misalignment of the input or output fiber. The setup suffers from a slow mechanical drift, which is intentionally corrected by activation of the fiber autoalignment system. The automatic switching of the optical power meter between different measurement ranges can also result in peaks in the measurement curves, e.g. in the curve of 10 µg/ml at a time of ~270 s and ~370 s.**

For small concentrations, the phase shifts show an almost linear behavior as function of time, which indicates that the binding of Chromeon 642-streptavidin appeared continuously. For concentrations of 10 µg/ml or higher, the phase shifts show this linear behavior at the beginning of the measurement only and the curves start to flatten out after this linear increase indicating a saturation effect. This saturation effect make the further binding of Chromeon 642-streptavidin to the biotinylated surface slower, caused by sterical hindrance and depletion of free biotin on the surface.

When the phase shift is plotted against the Chromeon 642-streptavidin concentrations (see Fig. 8 and Table 6) for different times, this saturation effect can be shown more clearly.

For a time of 300 s the plotted curve of phase shift versus concentration showed a linear behavior from 0.1 to 25 µg/ml that equals to 1.6 to 416 nM. By analyzing the slope of the linear range a chemical sensitivity of 0.48π per µg/ml or 0.028π per nM could be found. At 2500 s, the curve shows a more logarithmic behavior over the whole measurement range (0.1-50 µg/ml), which indicates that a saturation appeared and that the binding of Chromeon 642-streptavidin to the surface was limited by a reduced free biotin molecule concentration on the surface.

The smallest measured concentration of Chromeon 642-streptavidin was 0.1 µg/ml (1.6 nM), showing phase shift of 0.5π at 2500 s.

**Table 6: Phase shift obtained from the surface sensing measurement of Chromeon 642-streptavidin at 300 s and 2500 s**

| Concentration of Chromeon 642-Streptavidin (µg/ml) | Concentration of Chromeon 642-Streptavidin (nM) | phase shift (π) after 300 s | phase shift (π) after 2500 s |
|---|---|---|---|
| 0.10 | 1.6 | 0.04 | 0.50 |
| 0.50 | 8.3 | 0.25 | 2.20 |
| 1.00 | 16.6 | 0.40 | 4.30 |
| 5.00 | 83.3 | 3.2 | |
| 10.00 | 166.6 | 5.50 | 15.20 |
| 25.00 | 416.6 | 12.00 | 17.90 |
| 50.00 | 833.3 | 15 | 21.25 |

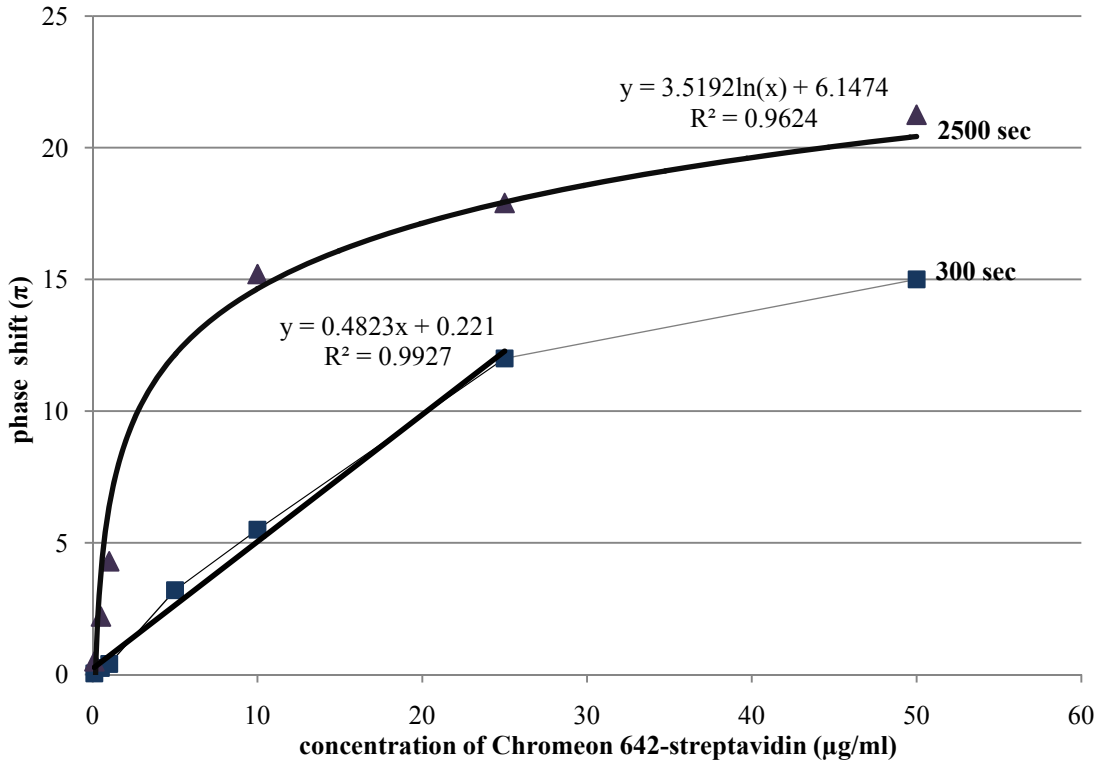


**Figure 8: Phase shifts at t=300 s and t=2500 s obtained from surface sensing measurements, plotted against the concentration of Chromeon 642-streptavidin. For 300 s, a linear behavior between 0.1-25 µg/ml can be found, while the curve for 2500 s shows a logarithmic behavior in the whole measurement range from 0.1-50 µg/ml**

A Langmuir curve fitting (detail information is given in appendix B) with the StatGraph software gives a value of the dissociation constant ($K_d$) of biotin-Chromeon 642-streptavidin interaction of 79.1 ± (33.9118) x $10^{-9}$ M on the blocked a-Si:H-MZI sensors.

## 2 DNA experiments on a-Si:H-MZI sensors

The biotinylated a-Si:H-MZI sensor got mounted in the measurement setup, with the fluidic system on top, which was filled with ultrapure water.

Then, water was exchanged against 150 mM PBS buffer and once the sensor response is stable, unlabelled streptavidin (200 µg/ml) dissolved in 150 mM PBS buffer was rinsed over the sensor surface.

After approximately 10 min, the MZI sensor response became stable, which indicates that the maximum streptavidin density on the surface was reached. Then, the streptavidin containing PBS buffer was exchanged against pure PBS buffer again. The PBS buffer was rinsed over the surface for about 2 min to clean the streptavidin functionalized surface.

This described procedure was done on every new MZI sensor before performing surface sensing DNA experiments. Thereby, the DNA concentrations dissolved in 150 mM PBS buffer were held constant at 1 μM.

## 2.1 Reference measurements for DNA experiments

As reference measurements for the surface sensing DNA experiments, two types were chosen. On is the exclusion of the unspecific binding of the complementary and non complementary DNA strands to the streptavidin functionalized a-Si:H-MZI surface and the other one is the binding of the biotin tagged DNA strands to the named surface for the purpose of testing the binding capacity.

The reference measurements with complementary and non complementary DNA showed no phase shift for the complementary and a low phase shift (0.25π) for the non complementary DNA strands, which proves that no significant unspecific interactions of these DNA stands with the streptavidin functionalized surface exists. (See Fig. 9)

In contrast, the rinsing of biotin tagged single stranded DNA (1μM) over the MZI streptavidin functionalized surface leads to a phase shift of approximately 2.4π (repeated two times, with similar results: see Fig. 9), according to the binding of the biotin tag to the streptavidin layer.

## 2.2 DNA Hybridization

First, biotin tagged DNA was rinsed for approximately 2 min over the streptavidin functionalized surface . Then, the fluidic system was cleaned by rinsing with 150 mM PBS buffer for approximately 10 min. Afterwards, the PBS buffer was exchanged against complementary DNA strands (1μM) dissolved in PBS buffer and the signal was monitored. The hybridization between the immobilized biotin tagged single stranded DNA (ssDNA) and its complementary ssDNA was measured two times and gave a phase shift of 2.3 ± 0.2π. (See Fig. 9)

## 2.3 Selectivity

To ensure selectivity of the hybridization the same experiment as described before, was performed with the non complementary DNA strand. In this experiment, no phase shift

occured during the rinsing of the non complementary DNA strands over the a-Si:H-MZI sensor surface functionalized with the biotin tagged DNA strands. (See Fig 9)

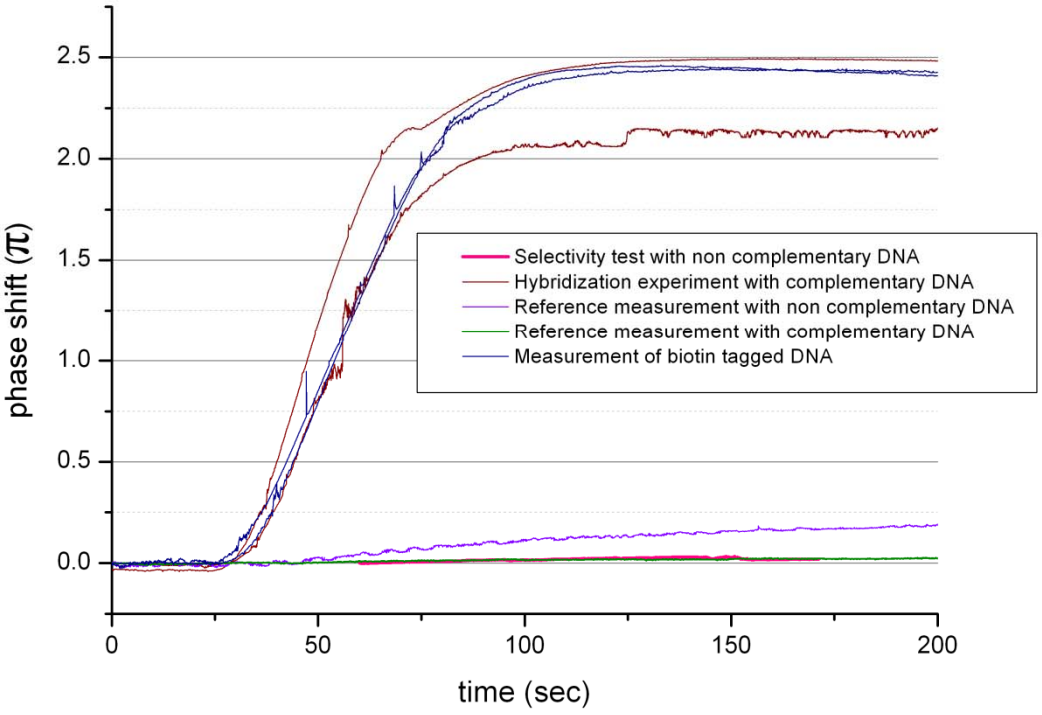


**Figure 9: DNA Hybridization experiments on the streptavidin functionalized a-Si:H-MZI sensor surface**

The results given in Fig. 9 are supported by the results of the fluorescence intensity on the a-Si:H sensor surface.

# 3 Real-time measurement of streptavidin on PI-MZI sensors

## 3.1 Reference measurements

### Sensor stability

Before and after several steps of the functionalization protocol (see Table 1) wavelength scans between 1280 and 1360 nm, with a scan rate of 5 nm/min in 0.01 nm steps, were performed for the PI-MZI sensors. Thereby, it was found that neither the transmission nor the extinction ratio in the wavelength scan changed during the functionalization procedure. A detailed analysis as it was done on the a-Si:H-MZI sensors was not performed for the PI-MZI sensors.

### Binding of the maleimide moiety to the PI-MZI sensor surface

In this section, the binding of the maleimide moiety to the PI-MZI surface was analyzed in order to validate that the maleimide binding occurs specifically on the MPTMS functionalized PI-MZI sensor only. The interaction between the maleimide group and the sensor surface should only take place on the sulfhydryl functional group, therefore preventing unspecific binding of the Maleimide-$PEG_2$-biotin (M-$PEG_2$-biotin) to the surface, which may lead to less homogenous packing of the sensing layer molecules.

To enable the possibility of an external fluorescence control scan, the maleimide binding to the PI-MZI sensor surface was tested using the TMR5M (tetrametyl rhodamine 5-maleimide) fluorescence label. First, a PI-MZI sensor was transferred into the oxygen plasma (step 1, Table 1), and then dipped in an acidic aqueous solution without MPTMS (Acetate buffer with Triton X-100). After 1 h dipping and the cleaning procedure (see Table 1, step 4), the PI-MZI sensor was mounted on the measurement setup with the fluidic system on top.

The fluidic system was first filled with ultra pure water, which was in the next measurement step exchanged against binding buffer (ultra pure water with 10 % phosphate buffer 0.05 M and 10% isopropyl alcohol, pH 7.3). Once the PI-MZI sensor response was stable, the binding buffer was exchanged against 5 µM TMR5M solved in binding buffer and as soon as the signal was stable again, the liquids were exchanged vice versa (see Fig. 10). It was found that the TMR5M did not bind to the PI-MZI surface without MPTMS, because no persistent phase shift, belonging to an irreversible binding of TMR5M to the surface, occured. With the fluorecence contol scan of the PI-MZI sensor, no fluorescence intensity was detected in the

measurement window of the sensor. This confirms that no significant amount of unspecific binding of the maleimide moiety takes place on the polyimide waveguide layer.

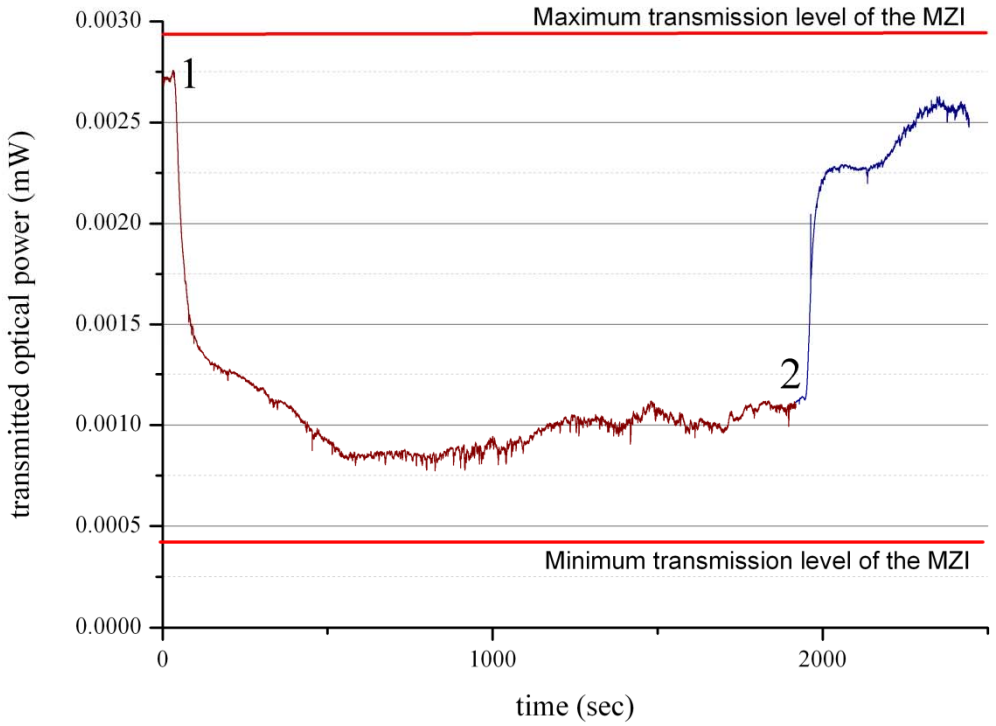


**Figure 10: The red lines show the maximum and minimum transmission level of the MZI sensor. The monitored signals 1 and 2 of the MZI show the transmitted optical power during the reference measurement of the binding behavior of the maleimide moiety to the PI surface without MPTMS: 1. Ultra pure water ($n_w$= 1.3329) was exchanged against binding buffer ($n_{buffer}$=1.3387) and an interference signal caused by the refractive index change was monitored ($\Delta n$=[$n_{buffer}$-$n_w$]=0.0058); 2. Binding buffer was exchanged against 5 µM TMR5M dissolved in binding buffer ($n_{TMR5M}$=1.3385); 3. 5 µM TMR5M dissolved in binding buffer was exchanged against binding buffer; No persistent phase shift, resulting from an irreversible binding of the TMR5M to the PI-MZI sensor surface was found.**

In the next test the binding of the maleimide to the MPTMS functionalized MZI sensor was evaluated. Therefore, a MZI sensor with MPTMS layer was prepared and then mounted on the setup, with the fluidic system on top, which was filled with ultra pure water after mounting.

The results from the surface sensing measurement of the TMR5M showed no good reproducibility after four repetitions and also no significant phase shift (0.3-0.5 additive phase shift) was obtained. To prove a specific binding of the TMR5M to the MPTMS functionalized PI-MZI sensor surface, the results of the fluorescence scans were compared with the previous results of the reference measurements. It was found that on the MPTMS functionalized MZI measurement window fluorescence intensity occurs, in contrast to the PI-

MZI surface without MPTMS where no flourecence intensity was measured. This indicates specific binding of TMR5M on the MPTMS functionalized MZI sensor surface. It seems that the sensitivity of the PI-MZI sensor and/or the reproducibility of the experiment is insufficient to validate the binding behaviour of TMR5M employing a MZI real-time measurement.

**Binding of the Chromeon 642-Streptavidin to the PI-MZI sensor surface**

In course of first experiments, it was found that the PI-waveguide was not stable against the 150 mM PBS buffer. During rinsing of the PBS buffer the sensor signal is drifting. After a couple of hours of rinsing, the extinction ratio, as well as the transmission of the MZI was reduced (extinction ration ≤ 5dB). This indicates that 150 mM PBS buffer attacks the thin PI waveguide layer in the measurement window and subsequently leads to an inoperability of the PI-MZI sensor after a certain time frame.

In contrast to the untreated PI-MZI sensor surface, the MPTMS functionalized sensor is stable if PBS buffer is rinsed over the sensor. For this purpose a MPTMS functionalized PI-MZI sensor was mounted on the measurement setup with the fluidic system on top. Then, 150 mM PBS buffer was rinsed for 40 min over the sensor surface, while monitoring the transmitted optical power (see Fig. 11).

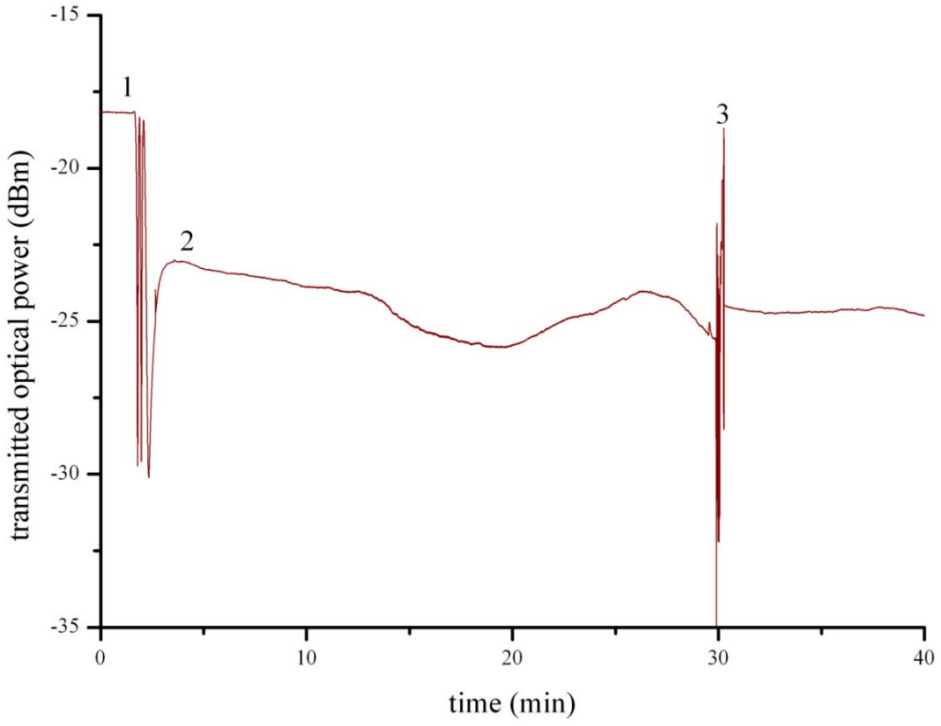


**Figure 11: Stability of the PI-MZI sensor functionalized with MPTMS in PBS buffer: 1 Ultra pure water was exchanged against PBS buffer; 2 PBS buffer was rinsed over the MPTMS functionalized PI-MZI surface and a small shift of approximately 3 dBm occurs, 3 Correction of the misalignment of the input or output fiber. After the correction, the signal remained stable again.**

After this stability test, a surface sensing measurement of 10 µg/ml Chromeon 642-streptavidin was performed on MPTMS functionalized PI-MZI sensors. In this experiment a phase shift of 2π was observed belonging to the unspecifically bound Chromeon 642-streptavidin. The non-specific binding of streptavidin was, in addition, verified by a fluorescence scan. This indicates that also on the PI-MZI sensor a blocking with BSA is necessary to prevent unspecific interactions.

To verify the successful blocking of the surface employing BSA, 10 µg/ml Chromeon 642-streptavidin in PBS buffer was rinsed over a BSA blocked MPTMS functionalized PI-MZI sensor, in the same way as above. In Fig. 12, this measurement is given. In this experiment, no persisting phase shift could be monitored, indicating that no unspecific binding on the surface take place after blocking with BSA. This result was also supported by an external fluorescence scan, where no fluorescence intensity could be measured on the BSA blocked MPTMS functionalized PI-MZI sensor.

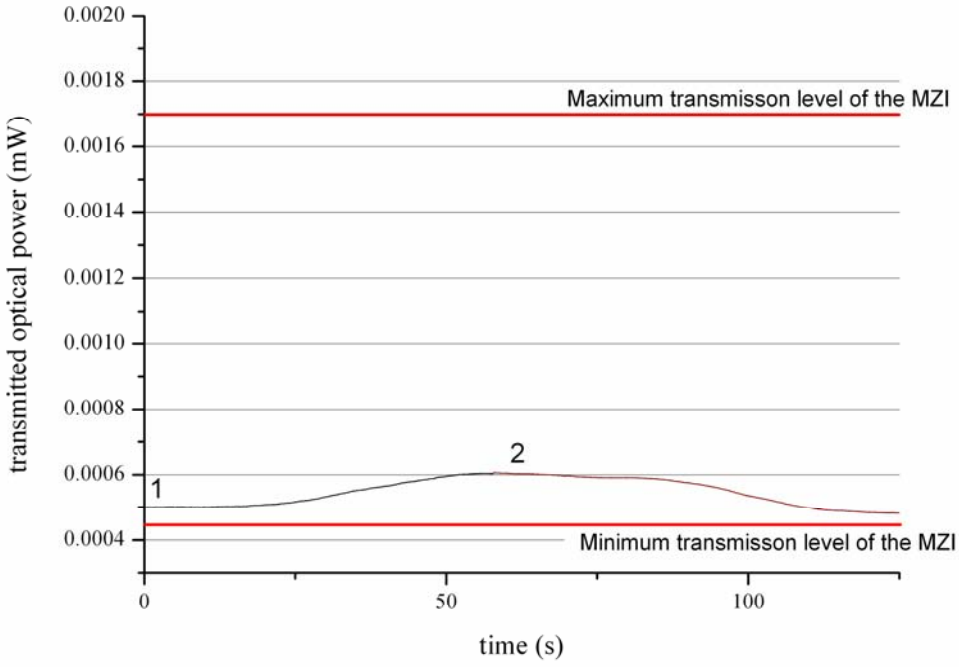


**Figure 12: The red lines show the maximum and minimum transmission level of the MZI sensor. The monitored signals 1 and 2 of the MZI show the transmitted optical power during the reference measurement of the binding behavior of Chromeon 642-streptavidin to the BSA blocked MPTMS functionalized PI-MZI sensor: 1. PBS buffer was ($n_{PBS}$=1.3381) exchanged against 10 µg/ml (166 nM) Chromeon 642-streptavidin dissolved in PBS buffer ($n_{Strep}$=1.3381); 2. 10 µg/ml (166 nM) Chromeon 642-streptavidin dissolved in PBS buffer was exchanged against pure PBS buffer; 2. PBS buffer was exchanged against ultra pure water ($n_w$=1.3329) and an interference signal occurs according to the refractive index change ($\Delta n=[n_{PBS}-n_w]$=0.005); There is no persisting phase shift resulting from an irreversible binding of Chromeon 642-streptavidin to the sensor surface.**

To analyze the specific and unspecific binding of Chromeon 642-streptavidin to the biotinylated MZI sensors, four biotinylated and four biotinylated BSA blocked PI-MZI sensors, were subsequently mounted on the setup and 10 µg/ml (166 nM) Chromeon 642-streptavidin in PBS were measured. In contrast to BSA blocked samples, where rinsing with PBS buffer after the streptavidin binding process, does not result in a significant reduction of the phase shift, the rinsing with PBS buffer after the measurement on non blocked samples reduces the phase shift by about 10 % because unspecific bound streptavidin is washed away. In Fig. 13, the calculated phase shifts from the surface sensing measurements on unblocked and BSA blocked PI-MZI sensors are plotted. In Table 7 compares the values of the phase shifts at different times for unblocked and BSA blocked PI-MZI sensors. The unblocked sensors have lower standard deviation and a higher phase shift at 1000 s. At 2500 s, when the MZI responses are mostly stable, the unspecific to the specific phase shift differs by about 40 %. This indicates that about 40 % unspecific binding of Chromeon 642-streptavidin on the PI-MZI sensor surfaces occurs, which can be completely blocked employing the BSA treatment.

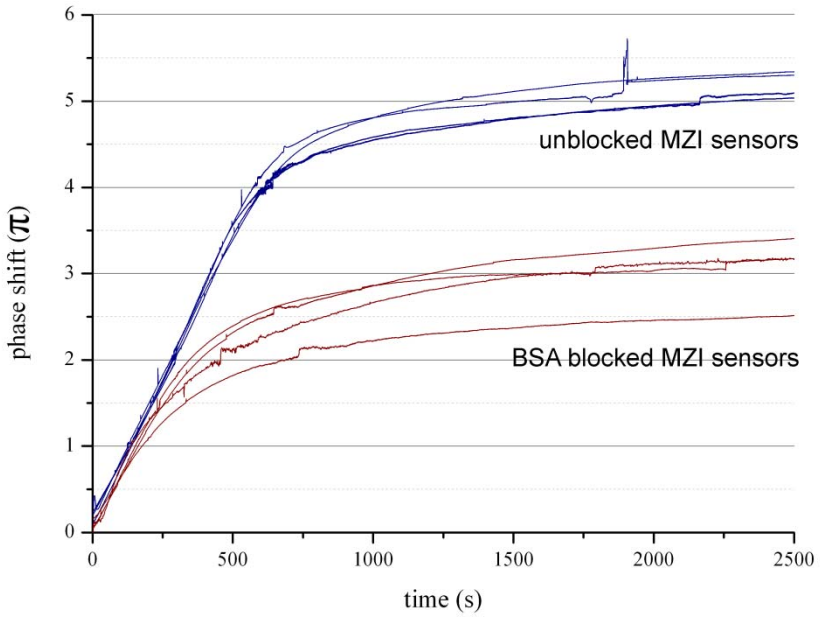


**Figure 13: Calculated phase shifts of the surface sensing measurements of Chromeon 642-streptavidin on unblocked and BSA blocked PI-MZI sensors; The automatic switching of the optical power meter between different measurement ranges can also result in peaks in the measurement curves, e.g. in BSA blocked MZI sensor curves at a time of ~500 s.**

**Table 7: Phase shifts at different times for unblocked and BSA blocked PI-MZI sensors**

| | Phase shift (π) at different times for unblocked MZI sensors | | |
|---|---|---|---|
| **time (s)** | **500** | **1000** | **2500** |
| ***R349*** | 2.16 | 4.57 | 5.31 |
| ***R355*** | 2.12 | 4.40 | 5.07 |
| ***R356*** | 2.23 | 4.40 | 5.01 |
| ***R358*** | 2.21 | 4.65 | 5.28 |
| **Average** | 2.18 | 4.50 | 5.17 |
| **standard deviation** | 0.05 | 0.13 | 0.15 |

| | Phase shift (π) at different times for blocked MZI sensors | | |
|---|---|---|---|
| **time (s)** | **500** | **1000** | **2500** |
| ***R404*** | 2.33 | 2.80 | 3.42 |
| ***R363*** | 1.82 | 2.20 | 2.50 |
| ***R366*** | 2.40 | 2.80 | 3.16 |
| ***R429*** | 2.12 | 2.60 | 3.15 |
| **Average** | 2.11 | 2.60 | 3.06 |
| **standard deviation** | 0.29 | 0.28 | 0.39 |

## 3.2 Measurement of different concentration of streptavidin on PI-MZI sensors

The BSA blocking eliminates unspecific binding of Chromeon 642-streptavidin to the PI-MZI sensor surface. In this chapter, Chromeon 642-streptavidin measurements at concentrations between 0.1 and 50 µg/ml on BSA blocked PI-MZI sensors are shown. The results of these real-time measurements are depicted as phase shift vs. time in Fig. 14.

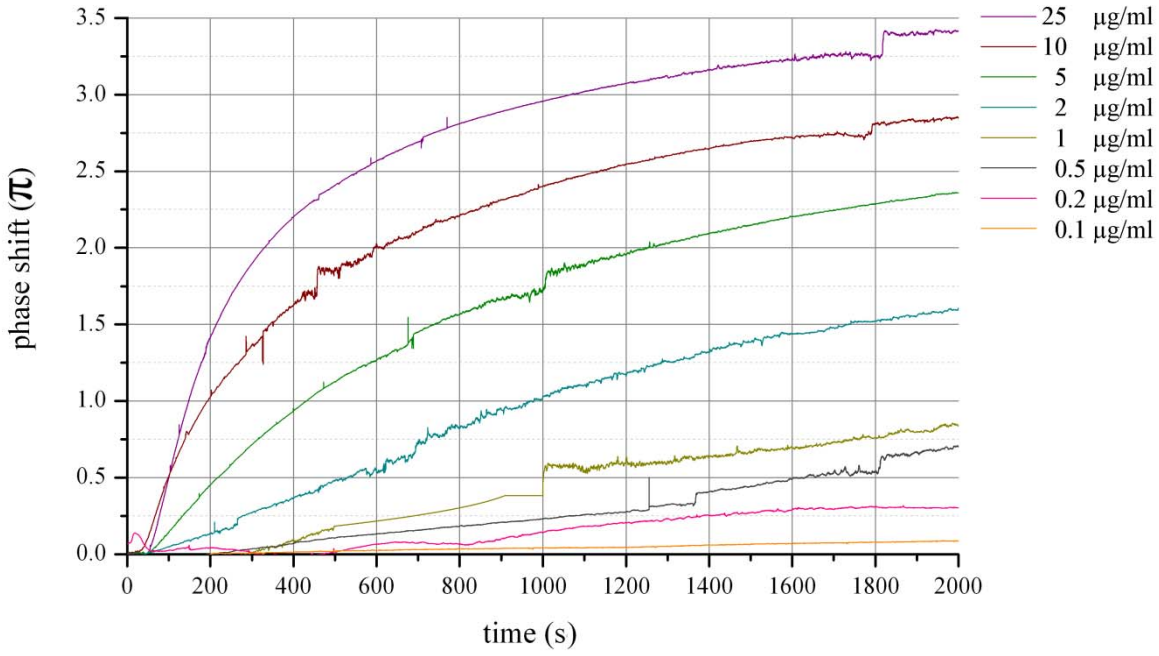


**Figure 14: Phase shift versus time, calculated from the transmitted optical power during the real-time measurements of Chromeon 642-streptavidin on BSA blocked PI-MZI sensors. After 25 µg/ml no significant further increase of the phase shift proportional to the increase of the concentrations occurs Therefore, the measurement of the 50 µg/ml concentration is not shown.**

At low concentrations, up to 2 µg/ml Chromeon 642-streptavidin, the phase shift increased almost constant with the concentration. For higher concentrations a saturation effect, comparable to the saturation effect found in the real-real time measurements with a-Si:H-MZI sensors, is obvious. In Fig. 15 and Table 8, the phase shift versus measured concentration of Chromeon 642-streptavidin is plotted for two different times. At 300 s a linear behavior between 1 and 10 µg/ml (16-166 nM) could be found. By analyzing the slope of the linear range, a chemical sensitivity of 0.14π per µg/ml or 0.008π per nM could be found.
The lowest concentration measured is 0.1 µg/ml Chromeon streptavidin, which causes a phase shift of 0.1π at 2500 s.

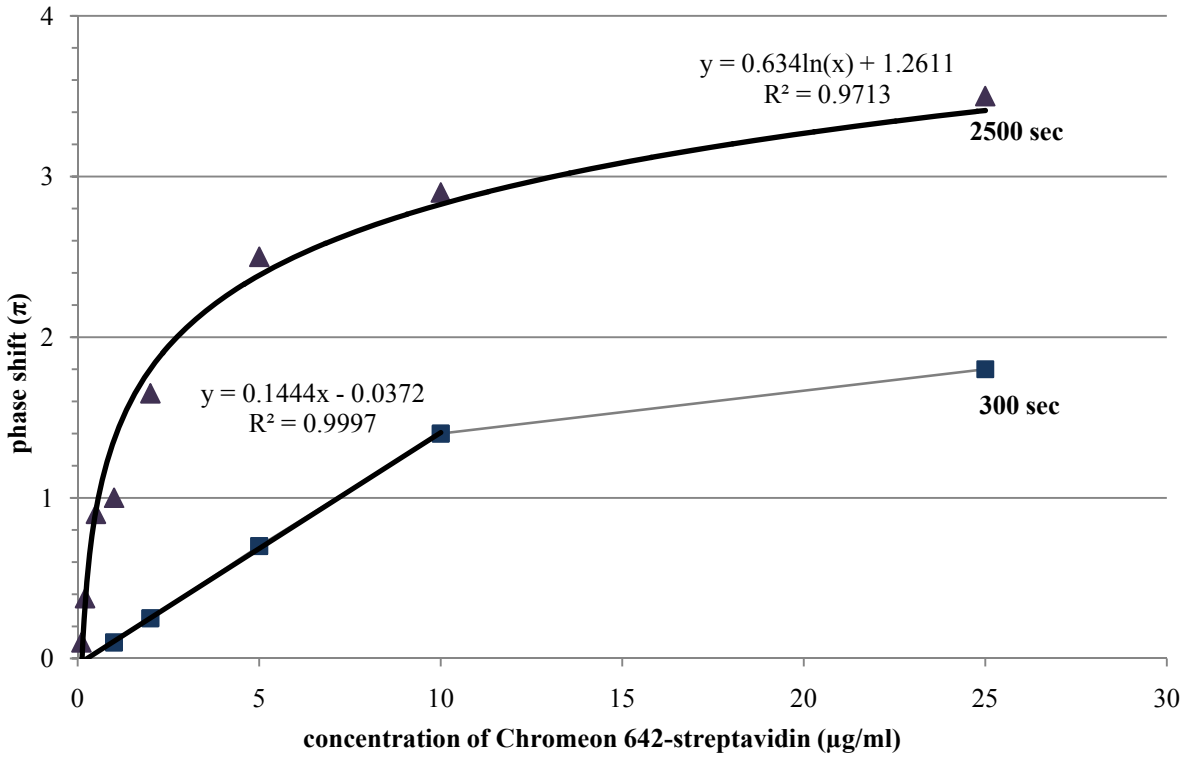


**Figure 15: Phase shifts gained from the surface sensing measurements plotted against the concentration of Chromeon 642-streptavidin, at 2500 s and 300 s. At 300 s, a linear behavior between 1-10 µg/ml can be found, while at 2500 s, the curve shows a logarithmic behavior for the whole measurement range from 0.1-25 µg/ml**

**Table 8: Phase shift gained from the surface sensing measurement plotted against the concentration of Chromeon 642-streptavidin, at 300 s and 2500 s measurement time**

| Concentration of Chromeon 642-Streptavidin (µg/ml) | Concentration of Chromeon 642-Streptavidin (nM) | phase shift (π) after 300 s | phase shift (π) after 2500 s |
|---|---|---|---|
| 0.10 | 1.6 | - | 0.10 |
| 0.20 | 3.3 | - | 0.38 |
| 0.50 | 8.3 | - | 0.85 |
| 1.00 | 16.6 | 0.10 | 1.00 |
| 2.00 | 33.3 | 0.25 | 1.65 |
| 5.00 | 83.3 | 0.7 | 2.50 |
| 10.00 | 166.6 | 1.40 | 2.90 |
| 25.00 | 416.6 | 1.8 | 3.50 |

Similar measurements were performed on unblocked PI-MZI sensors. The results of the BSA blocked and unblocked measurements are compared in Fig. 16, where the phase shifts are plotted against the concentration of Chromeon 642-streptavidin at 1000 s.
For high concentrations it is obvious that unblocked PI-MZI sensors show higher phase shifts, which indicate a higher concentration of Chromeon 642-streptavidin bound to the surface.

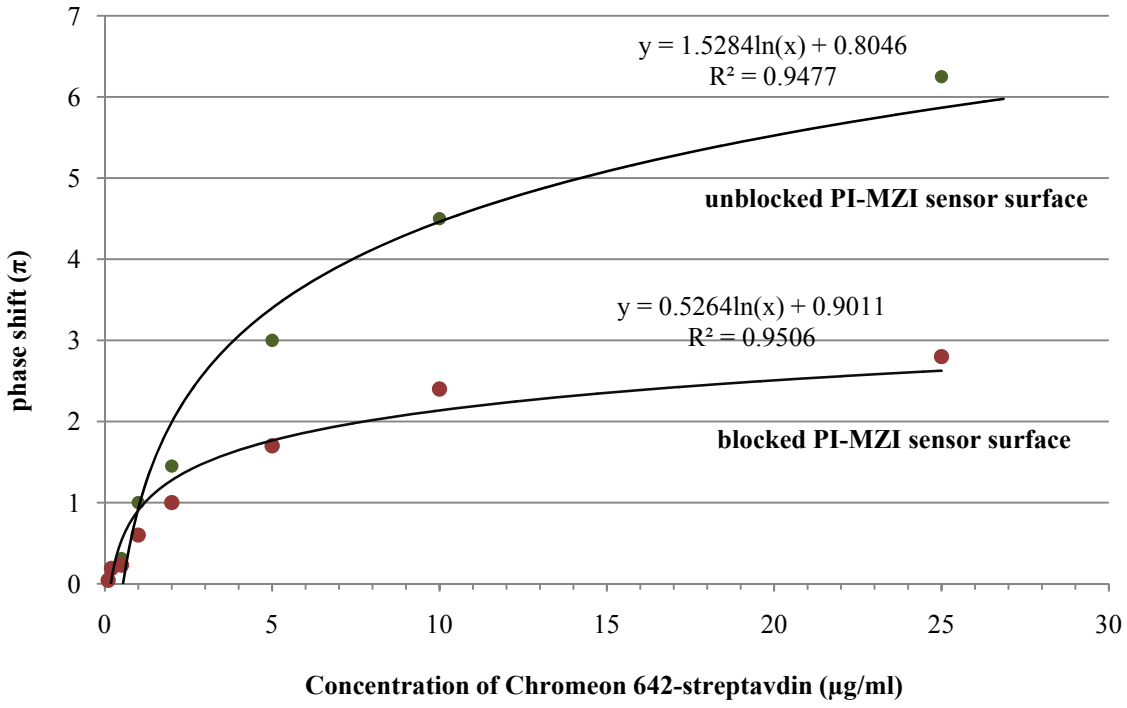


**Figure 16: Phase shifts of measurements of different concentrations of Chromeon 642-streptaividin at 1000 s for blocked and unblocked PI-MZI sensors**

With the Langmuir curve fitting (detail information is given in appendix B) done via StatGraph software, a value of the dissociation constant ($K_d$) of biotin-Chromeon 642-

streptavidin interaction of 87.8 ± (33.6762) x $10^{-9}$ M for the blocked PI-MZI sensors and of 49.3± (15.9842) x $10^{-9}$ M for the unblocked PI-MZI sensors could be found.

## 4 DNA hybridization experiments on PI-MZI sensors

For the DNA hybridization experiments the biotinylated PI-MZI sensors was mounted in the measurement setup with the fluidic system on top, which was filled with ultra pure water.
In the next step the water was exchanged against 150 mM PBS buffer and once the sensor response was stable, unlabelled streptavidin (200 µg/ml) dissolved in 150 mM PBS buffer was rinsed over the sensor surface. (See Table 2)
After approximately 2 min, the MZI sensor response became stable again, which indicates that the maximum streptavidin density on the surface was reached. Then, the streptavidin dissolved in PBS buffer was exchanged against pure PBS buffer again. The PBS buffer was rinsed over the surface for about 2 min to clean the streptavidin functionalized surface from non-bonded residues.
The described procedure was done every time on a new MZI sensor for the DNA experiments. The DNA concentration dissolved in 150 mM PBS buffer was kept constant at 1 µM.

### 4.1 Reference measurements for DNA experiments

To exclude unspecific binding of the complementary and non complementary DNA strands to the streptavidin functionalized PI-MZI surface and to analyze the binding of the biotin tagged DNA strands to the named surface, different reference measurements were performed.
The reference measurements with complementary and non complementary DNA showed no phase shift for the complementary and a very low phase shift (0.022π, see Fig. 19) for the non complementary ssDNA strands, which proves that no significant unspecific interactions of these DNA stands with the streptavidin functionalized surface exists. In contrast, the rinsing of biotin tagged DNA strands (1µM, dissolved in 150 mM PBS buffer) over the MZI surface has lead to a phase shift of approximately 0.30π (see Fig. 17), according to the binding of the biotin tag to the streptavidin layer.

### 4.2 DNA Hybridization

The hybridization occurs between the biotin tagged ssDNA and their complementary ssDNA strands. To monitor the hybridization, first the biotin tagged ssDNA was rinsed for

approximately 2 min over surface until the signal was stable and the streptavidin surface was saturated with this ssDNA strands. Then, the fluidic system was cleaned by rinsing with 150 mM PBS buffer for approximately 10 min. Afterwards, the PBS buffer was exchanged against the complementary ssDNA strand (1 µM) dissolved in PBS buffer and the signal was monitored. The hybridization between the immobilized biotin tagged ssDNA strand and their complementary ssDNA strand were measured two times and gave a phase shift of 0.26 ± 0.02π. (see Fig. 17)

## 4.3 Selectivity

To ensure selectivity of the hybridization the same experiment as described before, was performed with the non complementary ssDNA strands. In this experiment only a very low phase shift (0.015π) occurs during the rinsing of the non complementary ssDNA strands over the PI-MZI sensor surface functionalized with the biotin tagged ssDNA strand. (See Fig. 17)

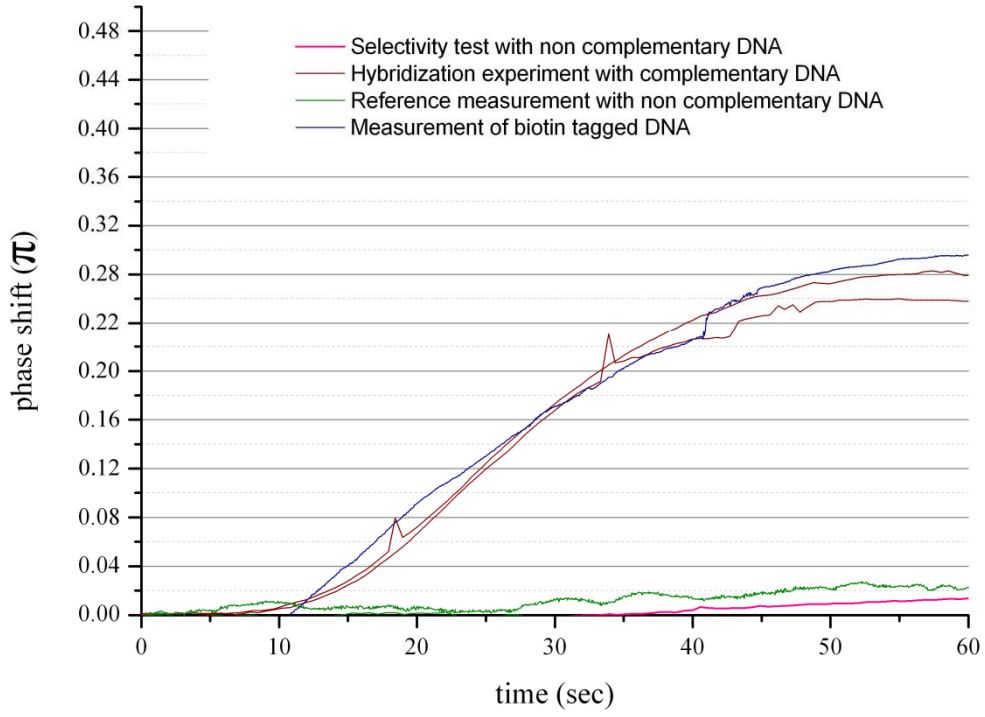


**Figure 17: Surface sensing DNA experiments on PI-MZI sensors**

The fluorescence scans of the different PI-MZI sensors showed the appearance of the fluorescence intensity after the hybridization step and supported the results of the surface sensing DNA hybridization experiments.

## 5 Summary

The first measurements in this chapter on a-Si:H and PI-MZI sensors evaluate the functionalization for the real-time measurements of streptavidin and show that the established protocols do not destroy the sensor layers.

It could be proven, employing MZI measurements with the fluorescence marker tetrametyl rhodamine 5-maleimide (TMR5M), that the maleimide moiety binds only to the MPTMS layer and do not bind nonspecific to the a-Si:H waveguide layer. For the PI-MZI sensors, the binding of the fluorescence marker TMR5M could not be validated using MZI measurements, because the phase shifts were too small to allow for conclusive results. Nevertheless, the control fluorescence scans verified that the maleimide moiety binds only to MPTMS functionalized PI and a-Si:H sensor surfaces.

The reference measurements to analyze the Chromeon 642-streptavidin binding to the MPTMS functionalized and biotinylated sensor surface on BSA blocked and unblocked samples confirm that a blocking strategy is necessary to suppress unspecific interactions on PI and a-Si:H sensors.

In addition, during these tests it was found that the untreated polyimide layer is not resistant against 150 mM PBS buffer. However, the functionalization with MPTMS makes the PI layer stable in the measurement environment, and therefore, overcomes this disadvantage.

The unspecific interactions of the Chromeon 642-streptavidin are completely blocked by the use of BSA. This blocking strategy leads to a reduction of the phase shifts in measurement of 10 µg/ml Chromeon 642-streptavidin by about 40% for PI and by about 26% for a-Si:H sensors. This shows that there is still some room to improve the surface functionalization or the blocking strategy.

Measurements of Chromeon 642-streptavidin were performed on the biotinylated BSA blocked PI and a-Si:H MZI sensors for different concentrations.

As predicted, these concentration dependent measurements reveal the higher sensitivity of the a-Si:H sensors (see Fig. 18).

The lowest measured concentration on both platforms is 1.6 nM (0.1 µg/ml) Chromeon 642-streptavidin, which gives a phase shift of 0.5π and 0.1π at 2500 s for the a-Si:H and the PI-MZI sensors, respectively. The linear range of the measurements depends on the time of the measurement and is at 300 s between 1.6 and 416 nM with a chemical sensitivity ($S_C$) of

0.029 π/nM for a-Si:H-MZI sensors and between 16 and 166 nM with a chemical sensitivity ($S_C$) of 0.008 π/nM for PI-MZI sensors. So the $S_C$ of the a-Si:H-MZI for the Chromeon 642-streptavidin measurement is 3.6 times higher than for the PI-MZI sensor. In Table 9 and in Fig. 16 the results of the Chromeon 642-streptavidin measurements on a-Si:H- and PI-MZI sensors are shown for comparison.

The Langmuir curve fitting shows almost similar results of the dissociation constant ($K_d$) between the biotin and Chormeon 642-streptavidin on PI- and a-Si:H-MZI sensors, with a $K_d$ of 87.8 ± (33.6762) x $10^{-9}$ and 79.1 ± (33.9118) x $10^{-9}$ M, respectively.

**Table 9: Comparison of phase shifts from the a-Si:H- and PI-MZI sensors obtained from measurements of different concentrations of Chromeon 642-streptavidin.**

| | phase shift (π) after 2500 s | |
|---|---|---|
| **Concentration of Chromeon 642-Streptavidin (µg/ml)** | **a-Si:H MZI sensor** | **PI-MZI sensor** |
| 0.10 | 0.50 | 0.10 |
| 0.50 | 2.20 | 0.85 |
| 1.00 | 4.30 | 1.00 |
| 2.00 | - | 1.65 |
| 5.00 | - | 2.50 |
| 10.00 | 13.39 | 3.29 |
| 25.00 | 17.90 | 3.50 |

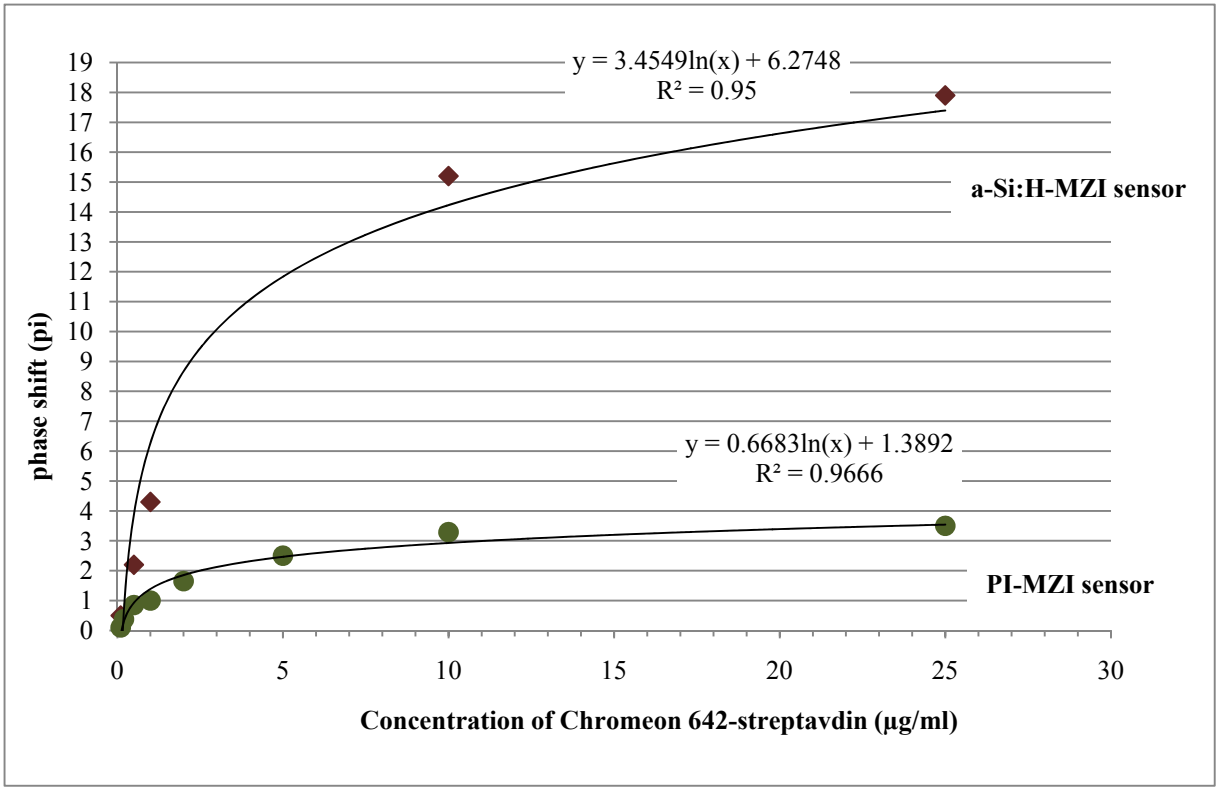


**Figure 18: Comparison of the a-Si:H- and PI-MZI sensor performance for the measurement of different concentrations of Chromeon 642-streptavidin. In measurement of 10 µg/ml Chromeon streptavidin, the PI-MZI sensor gives a phase shift of 3.29π, and the a-Si:H-MZI sensor a phase shift of 15.2π.**

In the surface sensing DNA experiments the a-Si:H-MZI sensor ($2.3 \pm 0.2\pi$ phase shift during hybridization) has a 10 times higher signal than the PI-MZI sensor ($0.26 \pm 0.02\pi$. phase shift during hybridization), but the main statements are for both sensors the same.

In both cases the complementary and non complementary single stranded DNA (ssDNA) did not undergo significant unspecific interactions with the streptavidin layer. Moreover, it was found that the biotin tagged ssDNA strands bound specifically to the sensor surfaces. The hybridization of the complementary DNA with the biotin tagged ssDNA functionalized sensor surfaces remained selective and binding with non complementary ssDNA could be excluded.

These results opens up the way for different ssDNA hybridization experiments on a-Si:H-MZI sensors (*e.g.* measurement of DNA melting curves).

For the PI-MZI sensors the remaining phase shifts are too low for such advanced experiments and the sensors have to be improved, for example by the increase of the number of surface bound single stranded DNA or by the use of oligonucleotides with a higher number of base pairs (e.g. 70 instead of 25) in order to obtain larger phase shifts.

# Abstract/Zusammenfassung

## Abstract

In this diploma thesis, the surface functionalization of amorphous hydrogenated silicon (a-Si:H) and polyimide (PI) evanescent waveguide based Mach-Zehnder interferometers (MZIs) was realized and verified with the model of streptavidin-biotin binding. In addition, a biosensing platform for DNA experiments was established.

Important for the successful realization of this project was the implementation of several surface characterization methods, such as the X-ray photoelectron spectroscopy (XPS), the surface fluorescence scans and atomic force microscopy (AFM). These methods enable the analysis of the progress of the functionalization and the monitoring of vital layer characteristics such as layer thickness or surface roughness. The XPS allowed to characterize the PI and a-Si:H substrates with respect to their atom composition. Surface modifications with different chemical groups (i.e. carboxyl-, amine- and sulfhydryl-groups) could be realized. The protocol of the sulfhydryl functionalization followed by the biotinylation was then chosen for the streptavidin immobilization. The use of Chromeon 642-streptavidin allowed for fluorescence scans in order to measure the surface concentration.

It was found that on unblocked biotinylated PI control samples 144 ± 20 fmol/mm$^2$ Chromeon 642-streptavidin and on unblocked biotinylated a-Si:H control samples 27 ± 2 fmol/mm$^2$ Chromeon 642-streptavidin can bind to the surface. Blocking with bovine serum albumin (BSA) hinders the binding of the Chromeon 642-streptavidin to unspecific binding sites. The specific binding of streptavidin on the biotinylated BSA blocked PI and a-Si:H surfaces amounts to approximately 80 ± 20 fmol/mm$^2$ and 20 ± 2 fmol/mm$^2$ respectively.

Atomic force microscopy (AFM) measurements indicated that the thin PI and a-Si:H layers are not damaged in course of the surface reactions and that the surface roughness stays below a mean roughness of $R_a$ =0.60 nm. XPS measurements provided further information, such as the atom composition at the layer surfaces before and after several functionalization steps. These analysis support the results from previous fluorescence scans and indicate possible reaction paths. The progress of the surface modification was analyzed on control samples, and after their successful functionalization, surface sensing real-time measurements on the MZI sensors were performed.

These measurements were planned as experiments that provide additional information about the sensor stability, reproducibility and sensitivity of sensors as well as the selectivity of the chemical binding.

These measurements showed that the characteristics of a-Si:H- and the PI-MZI sensors were not influenced by chemical treatments during the functionalization and it could be proven that the BSA blocking completely suppresses unspecific interactions of Chromeon 642-streptavidin with the sensor surfaces. As a consequence of the BSA blocking a reduction of the phase shifts by about 40% for PI-MZI sensors and by about 26% for a-Si:H-MZI sensors

was found. These results were supported by fluorescence measurements on blocked and unblocked samples, where the bound Chromeon 642-streptavidin concentration was reduced by about 44% on PI and 26% on a-Si:H surfaces. The lowest measured Chromeon 642-streptavidin concentration on the PI- and a-Si:H-MZI sensors was 1.6 nM (0.1 µg/ml), which caused a phase shift of 0.1π and 0.5π on PI and a-Si:H-MZI sensors. The linear range for a-Si:H-MZIs is between 1.6 and 416 nM with a chemical sensitivity ($S_C$) of 0.026 π/nM and for PI-MZI sensors between 16 and 166 nM with a chemical sensitivity 0.008 π/nM. Therefore, a-Si:H-MZI sensors have a 3.6 higher $S_C$ than PI-MZI sensors for the measurement of Chromeon 642-streptavidin.

Beside characterization of the MZI sensors by the Chromeon 642-streptavidin measurements, preliminary surface sensing DNA experiments on MZI sensor were performed. For this purpose unblocked biotinylated MZI sensors got functionalized with unlabeled streptavidin. The first DNA binding experiments, referred to as reference measurements, indicated that the biotin tagged single stranded DNA (ssDNA) bound to the streptavidin surface, because a phase shift corresponding to the binding process could be detected. On contrary, no unspecific interaction of the complementary and non complementary ssDNA strands to the streptavidin sensor surface could be found, which proves that the binding of the biotin tagged ssDNA was selective. The hybridization experiments showed that the complementary ssDNA strands bind to the surface bound biotin tagged ssDNA strand. The resulting phase shifts during hybridization were 2.3 π ± 0.2 for a-Si:H-MZI sensors and 0.26 ± 0.02 π for PI-MZI sensors respectively. In experiments with non complementary DNA no phase shift, and therefore, no unselective binding of non complementary DNA was detected, and that proves that the complementary DNA strands binds selective to the surface bound biotin tagged ssDNA strand.

These results open up the way for different DNA hybridization experiments on a-Si:H-MZI sensors.

For the PI-MZI sensors the remaining phase shifts are too low for advanced experiments and the sensors have to be improved, for example by the increase of the amount of surface bound single stranded DNA. Also the use of oligonucleotides with a higher number of base pairs (e.g. 70 instead of 25) may be possible in order to obtain larger phase shifts. For increasing the numbers of surface bound single stranded DNA, 3D-matrixes or dendrimers could be attached to the sensor surfaces.

However, this diploma thesis gives a limited number of possible surface modification ways for the used sensor surfaces, but opens the door to an almost infinite number of surface chemistries, which can be used to create application-orientated biosensors.

## Zusammenfassung

In dieser Diplomarbeit wurde die Funktionalisierung von auf amorphen hydrogenierten Silizium (a-Si:H) und Polyimid (PI) evanszenten Wellenleitern basierenden Mach-Zehnder Interferometern (MZI) realisiert und mittels Streptavidin-Biotin Model verifiziert. Weiters wurde eine biosensorische Plattform für DNA Experimente etabliert.

Für die Realisierung dieses Projektes war vor allem die Etablierung von verschieden Oberflächencharakterisierungsmethoden entscheidend, mithilfe deren die Überwachung des Fortschritts der Funktionalisierung möglich wurde. Ebenso konnte sichergestellt werden, dass das empfindliche MZI Schichtsystem (a-Si:H-SU-8 und PI-Ormoclad) nicht angegriffen oder zerstört wurde.

Die Anwendung der Photoelektronenspektroskopie (engl.: X-ray photoelectron spectrometer, XPS) ermöglichte die Charakterisierung der PI und a-Si:H Schichten. Nach dieser Charakterisierung wurden die Schichten mit verschieden chemischen Gruppen (Carboxyl-, Amino- und Sulfhydryl Gruppen) versehen. Das Protokoll für die Funktionalisierung mit Sulfhydryl-Gruppen, gefolgt von einer Biotinylierung der PI und a-Si:H Substrate wurde schließlich gewählt, um das Protein Streptavidin zu immobilisieren. Dabei wurde das fluoreszenzmarkierte Chromeon 642-Streptavidin verwendet, das es erlaubt durch Fluoreszenzscans zusätzliche Informationen zur Oberflächenkonzentration zu erhalten.

Dadurch war es möglich auf nicht geblockten biotinylierten PI Kontrollproben 144 ± 20 fmol/mm$^2$ und auf nicht geblockten biotinylierten a-Si:H Kontrollproben 27 ± 2 fmol/mm$^2$ Chromeon 642-Streptavidin nachzuweisen. Das blocken der biotinylierten Oberflächen mit Bovine Serum Albumin (BSA) verhinderte eine nicht spezifische Bindung und reduzierte die Konzentration von nun ausschließlich selektiv zu Biotin gebundenem Chromeon 642-Streptavidin auf 80 ± 20 fmol/mm$^2$ auf PI und 20 ± 2 fmol/mm$^2$ auf a-Si:H Kontrollproben.

Analysen mithilfe von Rasterkraftmikroskopie (engl.: Atomic force microscopy, AFM) auf Kontrollproben zeigte, dass die dünnen PI und a-Si:H Schichten durch die einzelnen Funktionalisierungsschritte nicht angegriffen wurden und die mittlere Rauigkeit nicht über den Wert von $R_a$=0.60 stieg. Zusätzliche XPS Messungen der Proben erbrachten weitere Informationen bezüglich der Atomkomposition von oberflächennahen Regionen nach unterschiedlichen Funktionalisierungsschritten. Die Resultate der XPS-Messungen stützten die Resultate der Fluoreszenzscans und zeigten mögliche Reaktionswege auf.

Nachdem erfolgreich ein Funktionalisierungsprotokoll auf Kontrollproben etabliert wurde, konnten oberflächensensitive MZI-Echtzeitmessungen durchgeführt werden. Diese Messungen wurden als Experimente so geplant, dass zusätzliche Informationen über die Sensorstabilität und Reproduzierbarkeit, sowie die Sensitivität und die Selektivität der chemischen Bindung erhalten wurden. Dabei konnte gezeigt werden das BSA blocken alle nicht spezifischen Interaktionen mit den PI und a-Si:H Oberflächen verhindert und das

Chromeon 642-Streptavidin selektiv angebunden werden kann. Allerdings wird dadurch auch das Sensorsignal bei PI-MZI Sensoren um 40% und bei a-Si:H MZI Sensoren um 26% verringert. Diese Resultate entsprechen den Ergebnissen aus den Fluoreszenzmessungen an geblockten und nicht geblockten biotinylierten Kontrollproben, bei denen die Änderung der Oberflächenkonzentration des Chromeon 642-Streptavidins 44% bei PI und 26% bei a-Si:H Substraten betrug.

Die kleinste gemessene Konzentration von Chromeon 642-Streptavidin mit den MZI Sensoren war 1,6 nM (0,1 μg/ml), was eine Phasenverschiebung von 0,1π auf PI und 0,5π auf a-Si:H-MZI Sensoren erzeugte. Der linearen Bereich liegt bei a-Si:H-MZI Sensoren zwischen 1,6 und 416 nM mit einer chemischen Sensitivität von 0,0026π/nM und bei PI-MZI Sensoren zwischen 16 und 166 nM mit einer chemischen Sensitivität von 0,0008π/nM. Dieses Verhalten zeigt, dass für die Messung von Chromeon 642-Streptavidin a-Si:H-MZI Sensoren 3.6 mal sensitiver sind als PI-MZI Sensoren.

Neben diesen Messungen wurde auch oberflächensensitive DNA Experimente durchgeführt. Dazu wurden die biotinylierten Sensoren mit einem nicht markierten Streptavidin beschichtet. Die ersten DNA Bindungsexperimente wurden als Referenzmessungen deklariert und zeigten dass der an die Streptavidinoberfläche bindet. Eine nicht spezifische Bindung des komplementären und nicht komplementären DNA Einzelstrangs konnte ausgeschlossen werden, da während den Messungen keinerlei signifikante Signaländerung auftrat. Dies zeigt, dass der Biotin getagte DNA Einzelstrang spezifisch an die Streptavidinoberfläche bindet. Die Hybridisierungsversuche zeigten, dass der komplementäre DNA Einzelstrang an den oberflächengebunden Biotin getagten DNA Einzelstrang bindet. Die resultierende Phasenverschiebung während der Hybridisierung war 2,3 $\pi \pm 0{,}2$ bei a-Si:H-MZI Sensoren und $0.26 \pm 0.02\ \pi$ für PI-MZI Sensoren. Zusätzlich wurde während eines vergleichbaren Versuches mit nicht komplementären DNA keine Phasenverschiebung und daraus folgend keine Bindung gemessen. Das zeigte wiederum die Selektivität der Bindung des komplementären DNA Einzelstrangs an den oberflächengebundenen DNA Einzelstrang.

Diese Resultate ermöglichen nun verschiedene DNA Hybridisierungsexperimente auf a-Si:H-MZI Sensoren. Die Phasenverschiebung auf PI-MZI Sensoren ist für weiterführende DNA Experimente zu gering und muss über andere Strategien erhöht werden. Dies kann beispielsweise über eine Erhöhung der Oberflächenkonzentration an gebundener Einzelstrang DNA mit einer anderen Funktionalisierungsstrategie oder durch Verwendung von DNA Oligonukleotiden mit einer höheren Anzahl an Basen (z.B. 70 statt 25) erreicht werden.

Zusammenfassend kann gesagt werden, dass diese Diplomarbeit zwar nur eine limitierte Zahl an möglichen Oberflächenmodifikationen wieder gibt, im Gegenzug jedoch eine große Zahl an weiteren die Möglichkeiten der Oberflächenchemie eröffnet, die zur Entwicklung einer Vielzahl von anwendungsorientierten Biosensoren führen kann.

# APPENDIX

# APPENDIX A

Chemical lists

**Chemicals for Functionalization and other tests**

| Name | Use | Chemicals | CAS-Nr. | Protocol |
|---|---|---|---|---|
| **ultrapure water** | Cleaning | ultrapure water | | Is taken form the SG ultra pure water system, which produces 18.2 MΩ/cm ultrapure water, that is filtered over a 0.2 µm sterile filter |
| **Isopropyl alcohol** | Cleaning | isopropyl alcohol, purchased from Sigma-Aldrich | 67-63-0 | |
| **Methanol** | Functionalization | methanol p.a. purchased from Sigma-Aldrich | 67-56-1 | |
| **Ethanol** | Chemical resistivity test | ethanol p.a. purchased from Carl Roth, | 64-17-5 | |
| **Nitric acid 10%** | Chemical resistivity test | Nitric acid 65 % | 7697-37-2 | |
| **1 M NaOH** | Activation | sodium hydroxide (NaOH) | 1310-73-2 | 4 g NaOH solved in 100 ml ultrapure water |
| **1 M and 0.2 M HCl** | Activation | hydrochloric acid (HCl) | 7647-01-0 | Diluted from conc.. HCl (37%, ~12 M) |
| **Acetate buffer 0.07 M pH 5.5** | Functionalization | sodium acetate trihydrate | 6131-90-4 | 2g sodium acetate trihydrate solved in 200 ml ultrapure water and adjusted to pH 5.5 with 10% acetic acid (~1.0 ml) |
| | | ultrapure water | | |
| | | acetic acid | 64-19-7 | |
| **Acetate buffer with Triton X-100** | Functionalization | acetate buffer 0.07 M pH 5.5 | | To 25 ml acetate buffer 0.07 M pH 5.5 add 5 ml 10 % tritonX-100 solved in Methanol |
| | | Triton X-100 | 9002-93-1 | |
| **Acid aqueous MPTMS solution** | Functionalization | acetate buffer with TritonX-100 | | To 30 ml acetate buffer with triton X-100 add 0.9 ml (3%) MTPMS 95%, stirrer for 3 h |
| | | (3-Mercaptopropyl) trimethoxy silane (MPTMS) 95% | 4420-74-0 | |
| **Acdic aqueous APTMS solution + ISO 50%v** | Functionalization | acetate buffer | | To 15 ml acetate buffer and 15 ml Isopropyl alcohol, 0.9 ml (3%) ATPMS 97% are added. |
| | | Isopropyl alcohol | 67-63-0 | |
| | | (3-Aminopropyl) trimethoxy silane (APTMS) 97% | 13822-56-5 | |
| **Acidic aqueous APTMS solution** | Functionalization | acetate buffer | | To 30 ml acetate buffer add 0.9 ml (3%) ATPMS 97% |
| | | (3-Aminopropyl) trimethoxy silane (APTMS) 97% | 13822-56-6 | |
| **Acidic aqueous APTMS solution with TritonX-100** | Functionalization | acetate buffer with TritonX-100 | | To 30 ml acetate buffer with triton X-100 add 0.9 ml (3%) ATPMS 97% |
| | | (3-Aminopropyl) trimethoxy silane (APTMS) 97% | 13822-56-5 | |
| **MES Buffer with Ethylendiamine pH 4.70** | Functionalization | 2-(N-Morpholino)ethanesulfonic acid | 4432-31-9 | 1.95 g (0.1 M) MES solved in 100 ml ultrapure water and than 6.65 g (0.5 M) ethylendiamin dihydrochloride is added. The solution is stirred till a clear solution occurs. The pH is adjusted to pH 4.7 with a few trops of 1 M NaOH |
| | | ethylendiamine dihydrochloride | 333-18-6 | |
| **EDC-Diamine solution** | Functionalization | MES buffer with Ethylendiamine pH 4.7 | | In 25 ml MES buffer with ethylendiamine 100 mg (0.025 M) EDC is solved. This solution is prepared before use. |
| | | 3-(ethyliminomethyleneamino)-N,N-dimethyl-propan-1-amine, (EDC) | 1892-57-5 | |
| **Toluene APTMS Solution** | Functionalization | (3-Aminopropyl) trimethoxy silane (APTMS) 97% | 13822-56-5 | To 30 ml Toluene 1 ml ultra pure water is added. The two phases are stirred and 0.9 ml (3 %v) APTMS is added |
| | | Toluene | 108-88-3 | |
| **MPTMS in Toluene** | Functionalization | (3-Mercaptopropyl) trimethoxy silane (MPTMS) 95% | 4420-74-0 | To 30 ml Toluene 1 ml ultra pure water is added. The two phases are stirred and 0.9 ml (3 %v) MPTMS is added |
| | | Toluene | 108-88-4 | |

| Name | Use | Chemicals | CAS-Nr. | Protocol |
|---|---|---|---|---|
| **MPTMS in Toluene with DMAP** | Functionalization | (3-Mercaptopropyl) trimethoxy silane (MPTMS) 95% | 4420-74-1 | To 30 ml Toluene with 100 mg DMAP 0.9 ml (3 %v) MPTMS is added |
| | | Toluene | 108-88-5 | |
| | | 4-dimethylaminopyridine (DMAP) | 1122-58-3 | |
| **THF MPTMS solution** | Functionalization | (3-Mercaptopropyl) trimethoxy silane (MPTMS) 95% | 4420-74-2 | To 34 ml of THF 165 µl (0.3 %v) hydrochloric acid (>37 %) is added under stirring and than 6 ml (15 %v) MPTMS is added. |
| | | Tetrahydrofuran | 109-99-9 | |
| | | conc. Hydrochloric acid | 7647-01-0 | |
| **Phosphate buffer pH 7.0, 0.05 M** | Binding Buffer | Sodium dihydrogen phosphate dihydrate | 13472-35-0 | 0.780g Sodium dihydrogen phosphate dihydrate solved in ultrapure water and adjusted on pH 7.0 with 1 M sodium hydroxide solution |
| | | 1 M sodium hydroxide solution | | |
| | | ultrapure water | | |
| **Binding buffer, pH 7.30** | Labelling with TMR5M or Binding of M-PEG2-Biotion to the sulfhydryl functionalized surface | phosphate buffer pH 7.0, 0.05 M | | To 8 ml ultrapure water 1 ml (10 %v) Isopropyl alcohol and 1 ml phosphate buffer pH 7.0, 0.05 M is added. Final pH: 7.30 |
| | | isopropyl alcohol | 67-63-0 | |
| **40% ammonium fluoride (NH4F) solution** | To create a fresh Si-H surface on the a-Si:H sample | 40% ammonium fluoride (NH4F) solution, purchased from Sigma Aldrich | 12125-01-8 | |
| **Glacial acetic acid** | Functionalization | glacical acetic acid, purchased from Sigma Aldrich | 64-19-7 | |
| **Undecylenic acid solution in Methanol** | Functionalization | Undecylenic acid, purchased from Sigma Aldrich | 112-38-9 | In 27 ml methanol 3 ml (10%) Undecylenic acid is solved |
| | | methanol | 67-56-1 | |
| **TMR5M stock solution** | Labelling of TMR5M | tetramethylrhodamine-5-maleimide (TMR5M) purchased from Sigma Aldrich | 174568-67-3 | 1 mg TMR5M solved in 1 ml methanol. |
| | | methanol | 67-56-1 | |
| **Labelling TMR5M solution:** | Labelling with TMR5M | TMR5M stock solution | | Different amounts of TMR5M stock solution is added to labelling buffer pH 7.3, to get final concentraions of 0.1 -10 µM of TMR5M. |
| | | Binding buffer pH 7.3 | | |
| **Triphenyl phosphin solution** | Labelling of TMR5M | triphenyl phosphin | 603-35-0 | 0.4 mg Triphenyl phosphin solved in 100 ml isopropyl alcohol |
| | | isopropyl alcohol | 67-63-0 | |
| **Carbonate buffer 0.2 M pH 9.0** | Labelling of DyLight N-hydroxysuccinimide (NHS) Ester | disodium carbonate | 497-19-8 | 0.518 g disodium carbonate and 0.711 g sodium hydrgencarbonate are solved in 50 ml ultrapure water, with 1 M HCl adjusted on pH 9.0 |
| | | sodium hydrgencarbonate | 144-55-8 | |
| | | ultrapure water | | |
| | | 1 M hydrochloric acid | | |
| **NHS-DyLight stock solution** | Labelling of DyLight N-hydroxysuccinimide (NHS) Ester | DyLight 649 N-hydroxysuccinimide (NHS) Ester, purchased from Fischer Scientific | non | 50 µg NHS-DyLight is solved in 1 ml carbonate buffer pH 9.0, final concentration 50 µM |
| | | carbonate buffer 0.2 M pH 9.0 | | |
| **Labelling NHS-DyLight solution** | Labelling of DyLight N-hydroxysuccinimide (NHS) Ester | DyLight N-hydroxysuccinimide (NHS) Ester, purchased from Fischer Scientific | non | Differentn amounts of NHS-DyLight stock solution is solved in carbonate buffer, to get final concentarions of 5-25 µM |
| | | carbonate buffer 0.2 M pH 9.0 | | |

## Chemicals for Biotinylation of the surface

| Name | Use | Chemicals | CAS-Nr. | Protocol |
|---|---|---|---|---|
| **Phosphate buffer pH 7.0, 0.05 M** | Binding of Maleimide-$PEG_2$-Biotin to thiol functional Group | Sodium dihydrogen phosphate dihydrate | 13472-35-0 | 0.780g Sodium dihydrogen phosphate dihydrate solved in 100 ml ultrapure water and adjusted on pH 7.0 with 1 M sodium hydroxide solution |
| | | 1 M sodium hydroxide solution | | |
| | | ultrapure water | | |
| **Binding Buffer pH 7.3** | Binding of Maleimide-$PEG_2$-Biotin to thiol functional Group | phosphate buffer pH 7.0, 0.05 M | | To 8 ml ultrapure water 1 ml (10 %v) Isopropyl alcohol and 1 ml phosphate buffer pH 7.0, 0.05 M is added. Final pH: 7.3 |
| | | isopropyl alcohol | 67-63-0 | |
| **Maleimide-$PEG_2$-Biotin stock solution** | Binding of Maleimide-$PEG_2$-Biotin to thiol functional Group | Maleimide-$PEG_2$-Biotin (M-$PEG_2$-Biotion) purchased from Fischer Scientific | | 2 mg of M-$PEG_2$-Biotin solved in 2 ml DMSO (99.9%), storage at -18°C |
| | | Dimethyl sulfoxide (DMSO) | 67-68-5 | |
| **M-$PEG_2$-Biotin solution** | Binding of Maleimide-$PEG_2$-Biotin to thiol functional Group | Maleimide-$PEG_2$-Biotin stock solution | | 250 µl of Maleimide-$PEG_2$-Biotin stock soluition is added to 10 ml binding buffer pH 7.3 |
| | | Buffer pH 7.3 | | |

## Chemicals for Streptavidin immobilization

| Name | Use | Chemicals | CAS-Nr. | Protocol |
|---|---|---|---|---|
| **Phosphate buffer saline** | Binding of streptavidin to Biotin | phosphate buffer saline (150 mM sodium phosphate, 150 mM sodium chloride) purchased from Fluka | | |
| **Chromeon 642-Streptavidin** | labelled streptavidin | Chromeon 642-Streptavidin purchased from Sigma | | |
| **Chromeon 642-Streptavidin standards** | | Chromeon 642-Streptavidin purchased from Sigma | | Different concentrations are produced by dilution of Chromeon 642-streptavidin stock solution in PBS buffer |
| | | phosphate buffer saline | | |

## Chemicals for Blocking of the unspecific binding sites

| Name | Use | Chemicals | CAS-Nr. | Protocol |
|---|---|---|---|---|
| **N-Ethyl-Malemide stock solution** | Blocking of thiol functional groups of MPTMS | N-Ethyl-Maleimide purchased form Fluka | 128-53-0 | 20 mg of N-Ethylmaleimide is solved in 2 ml DMSO (99.9%), storage at -18°C |
| | | Dimethyl sulfoxide (DMSO) | 67-68-5 | |
| **N-Ethyl-Malemide solution** | Blocking of thiol groups of MPTMS | N-Ethyl-Maleimide stock solution | | 25 µl of N-Ethyl-Maleimide is added to 10 ml labelling buffer pH 7.3 |
| | | Binding Buffer | | |
| **BSA stock soltution** | Blocking of unspecific binding sites on the PI and blocking of the thiol groups | Bovine serum albumin (BSA) purcased from Sigma | 9048-46-8 | 20 mg of BSA is solved in 2 ml PBS, storage at 4°C |
| | | Phosphate buffer Saline | | |
| **BSA solution** | Blocking of unspecific binding sites | BSA stock solution | | 10 µl of BSA stock solution is added to 990 µg Phosphate buffer saline, final Concentration 100 µg/ml |
| | | Phosphate buffer Saline | | |
| **Iodoacetamide** | Blocking of thiol groups of MPTMS | Iodacetamide purchased form Sigma | 144-48-9 | |
| **Iodoacetmide solution** | Blocking of thiol groups of MPTMS | Iodacetamide purchased form Sigma | 144-48-9 | 20 mg of Iodoacetamide is solved in 20 ml Binding buffer pH 8.0 |
| | | Binding Buffer, adjusted to pH 8.0 with 0.1 M Sodium hydoxide solution | | |

**Chemicals for surface sensing DNA experiments**

| Name | Modifiaction | Sequence | Use | Chemicals | Protocol |
|---|---|---|---|---|---|
| Phosphate buffer saline | | | Binding of biotin-tagged DNA to Strepavidin and Hybridisationbuffer | Phosphate buffer saline (150 mM sodium phosphate, 150 mM sodium chloride) purchased from Fluka | |
| Biotin-tagged DNA | 3´-Biotin | 5´-TCG CCA TTC GTT GAC TAC TTC TTA T -3´ | Functionalization with ssDNA | The 25-mer ssDNA purchased from VBC Biotech GmbH, Campus Vienna | Stock solution is prepared by dissolving in 150 mM PBS buffer, stored at -20°C |
| Complenary DNA | 5´-Cy3 | 3´-AGC GGT AAG CAA CTG ATG AAG AAT A-5´ | Hybridization | The 25-mer ssDNA purchased from VBC Biotech GmbH, Campus Vienna | Stock solution is prepared by dissolving in 150 mM PBS buffer, stored at -20°C |
| non binding DNA | 5´-Cy5 | 3´-TTG CTC TGA GGC AGA GTT T- 5` | Selectivitiy test | The 19-mer ssDNA purchased from VBC Biotech GmbH, Campus Vienna | Stock solution is prepared by dissolving in 150 mM PBS buffer, stored at -20°C |

# APPENDIX B

Statistical Data

## 1 Langmuir curve fit to gain the value of the dissociation constant $K_d$

### 1.1 Langmuir curve fit for the interaction of PI-MZI surface bounded biotin with Chromeon 642-Streptavidin

**Table 1: Values of the concentrations and the on the PI-MZI observed phase shift (π)**

| **Concentration of Chromeon 642-Streptavidin (nM)** *In calculation referred as LnM* | **Phase shift (π) after 2500 sec on unblocked PI-MZI** *In calculation referred as πunblocked* | **Phase shift (π) after 2500sec on blocked PI-MZI** *In calculation referred as πblocked* |
|---|---|---|
| 1.67 | 0.14 | 0.10 |
| 8.33 | 0.94 | 0.38 |
| 16.67 | 1.86 | 0.85 |
| 33.33 | 3.50 | 1.00 |
| 83.33 | 4.66 | 1.65 |
| 166.67 | 5.31 | 2.50 |
| 416.67 | 6.88 | 2.90 |
| 833.33 | 7.26 | 3.50 |

**a) Calculation for the blocked PI**

Nonlinear Regression

---

Dependent variable: πblocked

Independent variables:

LnM

Function to be estimated: (πmax*LnM)/(Kd+LnM)

Initial parameter estimates:

πmax = 7.0

$K_d$ = 1.0

Estimation method: Marquardt

Estimation stopped due to convergence of residual sum of squares.

Number of iterations: 9

Number of function calls: 29

Estimation Results

| Parameter | Estimate | Asymptotic Standard Error | Asymptotic 95.0% Confidence Interval Lower | Upper |
|---|---|---|---|---|
| pimax | 3.71245 | 0.175023 | 3.28418 | 4.14072 |
| $K_d$ (nM) | 87.8255 | 13.7627 | 54.1493 | 121.502 |

Analysis of Variance

| Source | Sum of Squares | Df | Mean Square |
|---|---|---|---|
| Model | 31.361 | 2 | 15.6805 |
| Residual | 0.148398 | 6 | 0.024733 |
| Total | 31.5094 | 8 | |
| Total (Corr.) | 10.7726 | 7 | |

R-Squared = 98.6224 percent

R-Squared (adjusted for d.f.) = 98.3929 percent

Standard Error of Est. = 0.157267

Mean absolute error = 0.112752

Durbin-Watson statistic = 2.27704

Residual Analysis

---

| | Estimation | Validation |
|---|---|---|
| n | 8 | |
| MSE | 0.024733 | |
| MAE | 0.112752 | |
| MAPE | 12.5762 | |
| ME | 0.0265195 | |
| MPE | 8.22543 | |

The StatAdvisor

---

The output shows the results of fitting a nonlinear regression model to describe the relationship between πblocked and 1 independent variables. The equation of the fitted model is

(3.71245*LnM)/(87.8255+LnM)

In performing the fit, the estimation process terminated successfully after 9 iterations, at which point the estimated coefficients appeared to converge to the current estimates.

The R-Squared statistic indicates that the model as fitted explains 98.6224% of the variability in πblocked. The adjusted R-Squared statistic, which is more suitable for comparing models with different numbers of independent variables, is 98.3929%. The standard error of the estimate shows the standard deviation of the residuals to be 0.157267. This value can be used to construct prediction limits for new observations by selecting the Forecasts

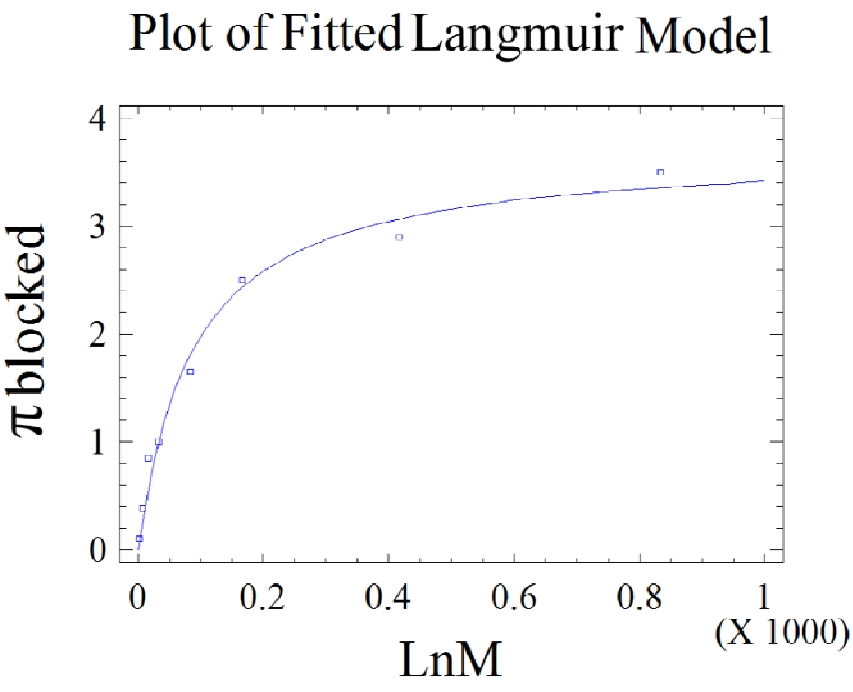

option from the text menu. The mean absolute error (MAE) of 0.112752 is the average value of the residuals. The Durbin-Watson (DW) statistic tests the residuals to determine if there is any significant correlation based on the order
in which they occur in your data file. Because the DW value is greater than 1.4, there is probably not any serious autocorrelation in the residuals.
The output also shows aymptotic 95.0% confidence intervals for each of the unknown parameters. These intervals are approximate and most accurate for large sample sizes. You can determine whether or not an estimate is statistically significant by examining each interval to see whether it contains the value 0.0. Intervals covering 0.0
correspond to coefficients which may well be removed form the model without hurting the fit substantially.

**a) Calculation for the blocked PI**

Nonlinear Regression

---

Dependent variable: πunblocked

Independent variables:

LnM

Function to be estimated: (πmax*LnM)/(Kd+LnM)

Initial parameter estimates:

πmax = 7.0

$K_d$ = 1.0

Estimation method: Marquardt

Estimation stopped due to convergence of residual sum of squares.

Number of iterations: 7

Number of function calls: 23

Estimation Results

---

| | | Asymptotic | Asymptotic 95.0% Confidence Interval | |
|---|---|---|---|---|
| Parameter | Estimate | Standard Error | Lower | Upper |

---

| | | | | |
|---|---|---|---|---|
| pimax | 7.52776 | 0.265256 | 6.8787 | 8.17682 |
| $K_d$(nM | 49.3062 | 6.53251 | 33.3217 | 65.2908 |

---

Analysis of Variance

---

| Source | Sum of Squares | Df | Mean Square |
|---|---|---|---|
| Model | 166.017 | 2 | 83.0084 |
| Residual | 0.549631 | 6 | 0.0916051 |
| Total | 166.566 | 8 | |
| Total (Corr.) | 49.9037 | 7 | |

R-Squared = 98.8986 percent

R-Squared (adjusted for d.f.) = 98.7151 percent

Standard Error of Est. = 0.302663

Mean absolute error = 0.203816

Durbin-Watson statistic = 2.10636

Residual Analysis

---

| Estimation | Validation |
|---|---|
| n | 8 |
| MSE | 0.0916051 |
| MAE | 0.203816 |
| MAPE | 15.32 |
| ME | -0.0124811 |
| MPE | -10.9404 |

The StatAdvisor

---

The output shows the results of fitting a nonlinear regression model to describe the relationship between πunblocked and 1 independent variables. The equation of the fitted model is

(7.52776*LnM)/(49.3062+LnM)

In performing the fit, the estimation process terminated successfully after 7 iterations, at which point the estimated coefficients appeared to converge to the current estimates. The R-Squared statistic indicates that the model as fitted explains 98.8986% of the variability in πunblocked. The adjusted R-Squared statistic, which is more suitable for comparing models with different numbers of independent variables, is 98.7151%. The standard error of the estimate shows the standard deviation of the residuals to be 0.302663. This value can be used to construct prediction limits for new observations by selecting the Forecasts option from the text menu. The mean absolute error (MAE) of 0.203816 is the average value of the residuals. The Durbin-Watson (DW) statistic tests the residuals to determine if there is any significant correlation based on the order in which they occur in your data file. Because the DW value is greater than 1.4, there is probably not any serious autocorrelation in the residuals.

The output also shows aymptotic 95.0% confidence intervals for each of the unknown parameters. These intervals are approximate and most accurate for large sample sizes. You can determine whether or not an estimate is statistically significant by examining each interval to see whether it contains the value 0.0. Intervals covering 0.0 correspond to coefficients which may well be removed form the model without hurting the fit substantially.

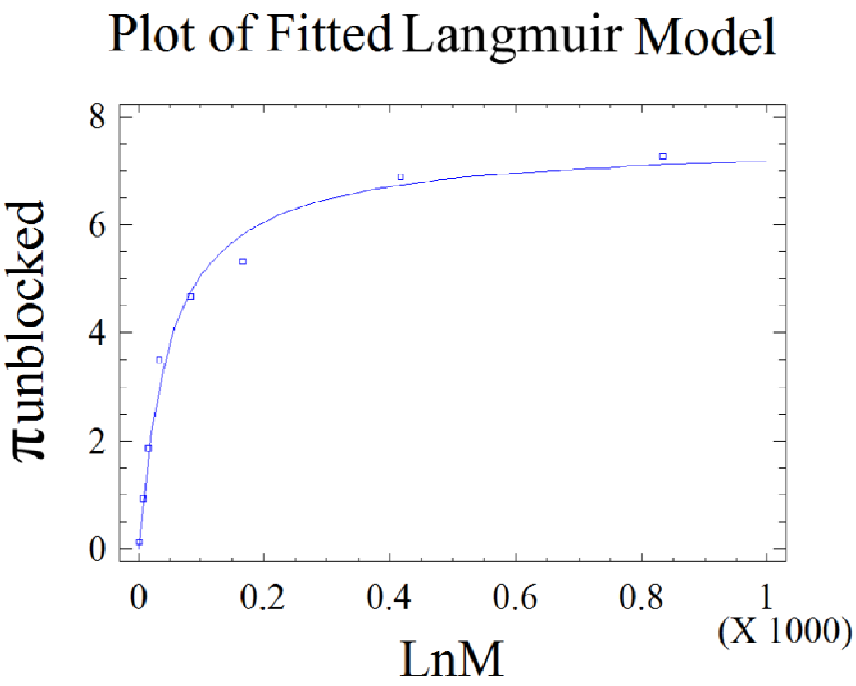

## 1.2 Langmuir curve fit for the interaction of a-Si:H-MZI surface bounded biotin with Chromeon 642-Streptavidin

**Table 2: Values of the concentrations and the on the a-Si:H-MZI observed phase shift (π)**

| **Concentration of Chromeon 642-Streptavidin (nM)** *In calculation referred as* **L**nanomolar | **phase shift (π) after 2500s on blocked a-Si:H-MZI surface** *In calculation referred as πblocked* |
|---|---|
| 1.67 | 0.5 |
| 8.33 | 2.2 |
| 16.67 | 4.3 |
| 83.33 | |
| 166.67 | 15.2 |
| 416.67 | 17.9 |
| 833.33 | 21.25 |

Nonlinear Regression

---

Dependent variable: πblocked

Independent variables:

Lnanomolar

Function to be estimated: (pimax*Lnanomolar)/(Kd+Lnanomolar)

Initial parameter estimates:

πmax = 7.0

$K_d$ = 1.0

Estimation method: Marquardt

Estimation stopped due to convergence of residual sum of squares.

Number of iterations: 8

Number of function calls: 26

Estimation Results

---

| | | Asymptotic | Asymptotic 95.0% Confidence Interval | |
|---|---|---|---|---|
| Parameter | Estimate | Standard Error | Lower | Upper |
| pimax | 22.4162 | 0.767559 | 20.2851 | 24.5472 |
| $K_d$ (nM) | 79.147 | 12.2141 | 45.2352 | 113.059 |

---

Analysis of Variance

---

| Source | Sum of Squares | Df | Mean Square |
|---|---|---|---|
| Model | 1024.94 | 2 | 512.471 |
| Residual | 1.6509 | 4 | 0.412726 |
| Total | 1026.59 | 6 | |
| Total (Corr.) | 399.289 | 5 | |

R-Squared = 99.5865 percent

R-Squared (adjusted for d.f.) = 99.4832 percent

Standard Error of Est. = 0.642438

Mean absolute error = 0.369945

Durbin-Watson statistic = 2.48276

Residual Analysis

---

| | Estimation | Validation |
|---|---|---|
| n | | 6 |
| MSE | | 0.412726 |
| MAE | | 0.369945 |
| MAPE | | 4.75784 |
| ME | | 0.0573192 |
| MPE | | 3.01133 |

The StatAdvisor

---

The output shows the results of fitting a nonlinear regression model to describe the relationship between πblocked and 1 independent variables. The equation of the fitted model is

(22.4162*Lnanomolar)/(79.147+Lnanomolar).

In performing the fit, the estimation process terminated successfully after 8 iterations, at which point the estimated coefficients appeared to converge to the current estimates.

The R-Squared statistic indicates that the model as fitted explains 99.5865% of the variability in πblocked. The adjusted R-Squared statistic, which is more suitable for comparing models with different numbers of independent variables, is 99.4832%. The standard error of the estimate shows the standard deviation of the residuals to be 0.642438. This value can be used to construct prediction limits for new observations by selecting the Forecasts option from the text menu. The mean absolute error (MAE) of 0.369945 is the average value of the residuals. The Durbin-Watson (DW) statistic tests the residuals to determine if there is any significant correlation based on the order in which they occur in your data file. Because the DW value is greater than 1.4, there is probably not any serious autocorrelation in the residuals.

The output also shows aymptotic 95.0% confidence intervals for each of the unknown parameters. These intervals are approximate and most accurate for large sample sizes. You can determine whether or not an estimate is statistically significant by examining each interval to see whether it contains the value 0.0. Intervals covering 0.0 correspond to coefficients which may well be removed form the model without hurting the fit substantially.

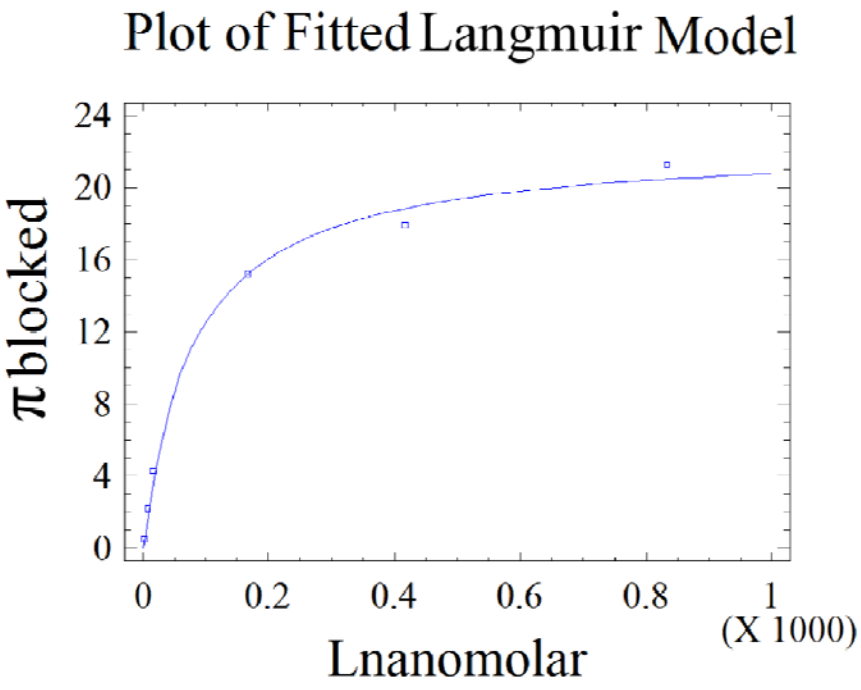

## Danksagung

Der erfolgreiche Abschluss meine Studiums ist an sehr viele verschiede Personen geknüpft, die mir ermöglichten zu Studieren und meinen Lebensunterhalt zu verdienen.

Zuerst möchte ich meiner ***Familie*** und vor allem meiner Mutter, Brigitte Melnik, danken, die mich immer in meinem Werdegang unterstütze und trotz vieler Ängste in die weite Welt reisen ließ.
Danke(!) an diesem Punkt für die vielen gereimten Worte in Brieflein und Kärtchen aus aller Welt, die mich aufmunterten.
Meinem Bruder, Stephan Melnik, und seiner Freundin, Brigitte Widermann, möchte ich danken, dass sie, obwohl sie nicht immer verstanden, was ich denn so in Wien treibe, mir immer mit Interesse an meinem Studium und an meiner Arbeit begegneten und mir die Besuche zu Hause in Salzburg so angenehm gestalteten.

Bei meinen ***Freunden*** möchte ich besonders bei Benedikt Nimmervoll und Roman Ferdinand Kreindl (und alle die sich an diesem Punkt angesprochen fühlen) für die vielen Diskussionen rund um die Naturwissenschaft bedanken.
Dank gilt auch meinen langjährigen Freunden/innen Martina Breitkreuz, Michael Löschel, James Osch, Rene Péschke, Seebacher Stefan und Josef Ruppert. Danken möchte ich euch für entspannende lustige Abende, aufgeregte Diskussionen über Gott und die Welt, dramatische Kurzfilme (leider noch nicht Oskar reif ☺) und die Unterstützung bei meinen Kurzgeschichten.

***Für den erfolgreichen Abschluss der Diplomarbeit***, möchte ich mich bei meinem Professor Dr. Michael Lämmerhofer und Dr. Rainer Hainberger am AIT für die Unterstützung und den tollen gemeinsamen Start bedanken.
Natürlich möchte ich auch den Kollegen am AIT, besonders Dr. Paul Müllner, Dr. Roman Bruck, Mag. Siefried Krainer, Mag. Michael Stierschneider und Dr. Nadezhda Kataeva, für die vielfältige Unterstützung danken.
Besonderer Dank gilt auch Dr. Stephan Abermann und Dr. Ole Bethge vom AIT bzw. vom FKE für die Unterstützung bei den XPS-Messungen im Reinraum der TU.

Falls ich an diesem Punkt jemanden vergessen haben sollte, hier noch ein besonders:

**„Danke!“**

Eva Melnik
Mobil: +43 676 56 43 993
e-mail: govina@gmx.at

# Curriculum Vitae

| | |
|---|---|
| Name | Eva Melnik |
| Adresse | Währinger Gürtel 168/3 |
| | A-1090 Wien |
| Geburtsdatum | 25.04.1981 |
| Geburtsort | Salzburg |
| Staatsbürgerschaft | Österreich |

**Ausbildung**

| | |
|---|---|
| 1987-1995 | Volks- und Hauptschule, Salzburg Liefering |
| 1995-2001 | Höhere Bundeslehranstalt für alpenländische Land- und Forstwirtschaft |
| Seit Oktober 2002 | Diplomstudium Chemie an der Universität Wien |
| Februar 2010 | Beginn der Diplomarbeit am Austrian Institute of Technology |

**Sprachkenntnisse**

| | |
|---|---|
| Deutsch | Muttersprache |
| Englisch | Fließend in Wort und Schrift |

**EDV – Kenntnisse**

| | |
|---|---|
| Mircrosoft Paket | Exel, Word, Powerpoint |
| Chemie | BKChem, Origin |
| Bildbearbeitung | Corel Draw |
| Literatursuche | Scopus, Scifinder |

**Fachbezogene Beschäftigung**

| | |
|---|---|
| 10.2005 - 02.2009 | Seibold Messtechnik<br>Diverse Tätigkeiten in der Forschung und Entwicklung von Online-Analysegeräten zur Abwasserkontrolle |